to

everyone
I
have
loved

Si l'on t'apportait la lune,
tout serait changé,
n'est-ce pas?

Ce qui est impossible
deviendrait possible...

[*Albert Camus*, 1945]

Index

Chapter 1

Introduction

The original millisecond pulsar PSR 1937+21 (1982: [1]) has a remarkable short spin period $P_{min} = 1.558$ ms. Since its discovery, about fourty millisecond pulsars (MSPs) has been detected in the field all spinning with periods longer than P_{min}. However, the search of MSPs requires a suitable apparatus and great computational capabilities (with which we will deal in Appendix A). Hence *the experiments were carried out with a very poor sensitivity to shorter spin periods*: the limits of the completed surveys are fully described in section [A.2.3]. As a consequence, it is not so surprising that the original millisecond pulsar is still the most rapidly rotating pulsar known so far.

Despite its smallness, the shortest pulsar spin period ever detected P_{min} is not a critical period for Neutron star (NS) rotation: NSs can indeed spin faster, as was indicated by Cook, Shapiro & Teukolsky (1994: [2]), regardless the details of the equation of state (EoS) for nuclear matter. In particular the period P_{min} is longer than the limiting period, P_{sh}, below which the star becomes unstable to centrifugal disruption at its equator. Only the discovery of a yet undetected ultra fast rotating millisecond radio pulsar would allow to set limits on the proposed EoSs; as an example (see Chapter 3), a very soft EoS permits pulsations at ~ 0.6 ms, whilst a very hard EoS only up to ~ 1.4 ms.

Besides the EoS, the most important processes which intervene in accelerating a NS up to P_{sh} are the evolution of the mass transfer (Chapter 2) from the low mass companion star ($\lesssim 1\mathrm{M}_{\odot}$) and the evolution of the NS magnetic moment μ (Chapter 4). In particular, a slowly decaying magnetic field favours only the re-acceleration of a NS to $P \gtrsim 5\div10$ ms. Conversely, if a rapid and substantial decay of the surface magnetic field takes place, a NS can attain $P < P_{min}$ (1999: [3]).

At present, there is no satisfactory theory for the origin of the magnetic field and consequently several avenues of field decay are possible: The field can either be a fossil remnant from the progenitor star or be generated soon after the formation of the NS. Thus, an unanswered question is where the bulk of the magnetic energy is stored [4]. If it resides mainly in the core (as in the case of a fossil field), the evolution of μ may be driven by variations in the rotational state of the NS, which affects the motion of the superfluid vortices and, in turn, of the fluxoids, carriers of the magnetic energy ([5] [6] [7] [8]). If the magnetic energy is generated and confined in the thin crust of the NS ([9] [10]), the surface magnetic field decay is guided by the ohmic diffusion and the dissipation of electric currents ([11]: see Chapter 4 for an updated set of references). The EoS valid for the core determines the thickness of the crust as well as the cooling history of the NS which both affect strongly the magnetic field decay. In the case of a crust field however, magnetic evolution is not univocal, depending sensitively on the properties of the nuclear matter at the crust–core boundary, where superfluid (SF) and superconductive (SC) phase transitions may occur. As crustal matter is progressively assimilated into the core due to accretion, the magnetic field at the crust-core boundary can either be expelled [12] or advected into the SC core where it no longer decays [13]. Thus, at the endpoint of evolution, the NS can either become non magnetic (on the long term), or preserve a relic field intense enough to shine again as MSP. These avenues are possible and the extent of the decay is intimately connected with the transfer rate and amount of matter accreted as heat released in the crust rises the electron and ion resistivity, accelerating the dissipation of the currents. Thus, field and mass transfer evolution couples strongly during the lifetime of the NS in a LMB.

Within the recycling scenario [14] [15] all schemes suggested for the origin and the evolution of μ allow accreting NSs to approach the magnetic moments and the periods that are characteristic of MSPs [12] [16].

In summary, the theory shows that the formation of MSPs in not an uncommon process, but reaching ultra short periods ($P \lesssim 1.5$ ms) requires rather extreme conditions, whose occurrence and efficiency can be quantified only on a statistical basis.

Therefore, in this Thesis, **we wish to determine** *whether a minimal but possibly physically consistent model for the recycling can provide* **indications on the relative period distribution** *of NSs in the millisecond and sub-millisecond ($P \leq 1.558$ ms) domain, as guide line for future searches.*

We used a population synthesis model (Chapter 5) that follows the evolution of the NSs in the μ-P plane within a scenario of recycling constructed using our knowledge of accretion in low mass X-ray binaries (LMXBs). We performed a statistical analysis on those objects evolving in the millisecond and submillisecond interval. The population synthesis calculation incorporates a detailed physical model (section [5.2]) for the evolution of a crustal magnetic field (using two boundary conditions to mimic expulsion or assimilation of the field by the SC core), adding further effects that might alter the statistical outcome. We also included the relativistic corrections (section [5.1]: also see Burderi, Possenti *et al.* 1999: [3]) necessary to describe the spinup process when the NS accretes matter from a disk, whose inner rim approaches the radius of the last quasi stable orbit.

This study is not aimed at correlating, on an evolutionary level, the observed population of LMXBs with the observed population of MSPs. MSPs may not be indeed the direct descendant of LMXBs: establishing this potential link or the link with LMBs forming through alternative evolutionary channels [17] [18] would require the complete statistical knowledge of the orbital parameters, of the mass ratios, of the hydrodynamical processes guiding mass transfer and ultimately of the internal evolution and structure of the donor star (see *e.g.* [19] or [20]). These are aspects of a complex statistical calculation that is beyond our purposes. Our aim is to address a number of questions that we are outlining below (Chapter 6).

1^{st} question *Are sub-millisecond pulsars a natural outcome of the evolution of neutron stars in low mass binary systems?*

In our population synthesis model we account for the evolution during the early phases when the NS in the LMB behaves as if isolated, and later when fed by wind accretion. The mass transfer during the Roche Lobe Overflow (RLO) phase is modeled considering a range of accretion rates which is close to the one observed in LMXBs [21] [22].

2^{nd} question *Is unsteady or transient accretion in LMBs a threat to the existence of sub-millisecond pulsars?*

In a number of models, the accretion rate is treated as a constant over the RLO phase: This is an approximation as its actual behaviour follows a complex evolutionary pattern depending on the orbital parameters and on the degree of mass and orbital angular momentum losses [19] [23]. The increasing evidence that NSs in LMXBs may suffer phases of transient accretion, due to thermal viscous instabilities in irradiation dominated disk (*e.g.* [24] [25] [26]), is suggestive that mass transfer onto a NS may not stop suddenly, at the end of the RLO: the star probably undergoes a progressive reduction of the mean accretion rate, modulated by alternate phases of higher and lower accretion. The effects of this transient behaviour on the evolution of the magnetic field is not known yet [27], but, if the magnetic field is not too weak, any drop in the accretion rate implies the growth of the typical dimension of the magnetosphere ([28]: see Chapter 2 for details). Dragged by the rapidly spinning NS, the magnetosphere can transform in a centrifugal barrier, accelerating the matter at the inner rim of the accretion disk to superkeplerian velocities (propeller effect [29]); this leads to the extraction of angular momentum from the compact object that spins down. Does unsteady accretion at the end of the RLO phase vanish the effect of the previous phases of spinup? Is the potential population of very rapidly spinning NSs reflected back to $P > P_{min}$? Many physical ingredients necessary to fully describe the propeller induced spindown are poorly known or difficult to assess (*e.g.* the exact law for the decrease of the mass transfer rate or the efficiency in the extraction of the angular momentum from the NS to the propelled matter). So, we studied the problem on a statistical basis, parametrizing the most uncertain quantities.

3^{rd} question *Are the millisecond pulsars a tool for discriminating the equation of state and/or the magnetic moment decay?*

The fastest rotating NSs detected so far have been discovered at radio frequencies, and statistical analyses based on current samples of MSPs (Cordes & Chernoff 1997 [30]) have revealed that the pulsar distribution is increasing toward short periods with best-fit minimum period slightly below P_{min}. Radio Searches for very rapidly spinning objects are now in progress. In particular the large scale survey at the Northern Cross Radiotelescope near Medicina (D'Amico *el al.* 1998 [31]), has a sensitivity profile relatively flat in the submillisecond period range. If successful, these searches can potentially provide information on the EoS for nuclear matter ([32] [33] [34] and the discussion of Chapter 3). If NSs can be recycled up to P_{sh}, the observed population can retain features of the EoS. Yet, many factors influence the recycling process, (magnetic moment evolution, total amount of mass disposable for the accretion, evolution of the mass transfer rate, propeller induced spin down and so on) likely spreading the observed distribution to slower spin rates and perhaps, in extreme cases, almost completely masking the effects of the EoS. Thus, can we determine, on a statistical basis, whether recycled rapidly rotating pulsars preserve signatures, in their μ-P diagram, for a distinction between the EoSs?

4^{th} question *Do weakly magnetized rapidly spinning neutron stars exist?*

Both types of evolution for a magnetic field of crustal origin allow, to a different degree, for the decay of μ at values lower than those typical of the observed MSPs sample, and probably below the threshold for radio emission [13] [35] [36] [37]. In view of the current searches an additional question is worth exploring: How significant is the production of weakly magnetized NSs during recycling? The statistical approach will help in clarifying whether the behaviour of highly condensed matter can be inferred from a close analysis of the recycled NS μ distribution.

5^{th} question *Which is the mimimum mass of a neutron star approaching the centrifugal disruption limit?*

Fast spinning neutron stars, recycled in low mass binaries, may have accreted a substantial amount of mass. The available relativistic measurements of neutron star masses, (all clustering around 1.4 $M_{\odot}$) however refer mostly to slowly rotating neutron stars which accreted a tiny amount of mass during evolution in a massive binary system. We develop a semi–analytical model for studying the evolution of the spin period P of a magnetic neutron star as a function of the baryonic mass load M_{ac}; evolution is followed down to submillisecond periods and the magnetic field is allowed to decay significantly before the end of recycling. We use different equations of state and include rotational deformation effects, the presence of a strong gravitational field and of a magnetosphere. For the non–magnetic case, comparison with numerical relativistic codes shows the accuracy of our description. With this model, we determined the *minimum* accreted mass requested to spin–up a *magnetized* 1.35 $M_{\odot}$–neutron star at a few millisecond and/or below 1 millisecond.

6^{th} question *Which is the typical mass of a neutron star recycled in a low mass X-ray binary?*

In the framework of the population synthesis code, we studied the mass distribution of the recycled NSs, investigating whether we can expect a significant fraction of objects more massive than the canonical value of 1.4 $M_{\odot}$.

7^{th} question *Which other effects could inhibit the formation of ultra fastly rotating neutron stars?*

We conclude our theoretical investigation reviewing possible mechanisms that could prevent the formation of ultra rapidly spinning neutron stars such as: highly non-conservative scenarios of mass transfer in low-mass binaries, angular momentum losses from the binary system, $r-$mode instabilities of the neutron star (Andersson 1998 [38]) and crustal deformations induced by accretion (Bildsten 1998 [39]).

Bibliography

[1] **Backer, D.C., Kulkarni, S.R., Heiles, C., Davis, M.M., Goss, W.M. 1982**, *Nature*, **300**, 615

[2] **Cook, G.B., Shapiro, S.L., Teukolsky, S.A. 1994a**, *ApJ*, **423**, L117 (CSTa)

[3] **Burderi, L., Possenti, A., Colpi, M., Di Salvo, T., D'Amico, N. 1999**, *ApJ*, **519**, 285

[4] **Bhattacharya, D. & Srinivasan, G. 1995**, *X-ray Binaries*, eds. Lewin W.H.G., van Paradijs J., van den Heuvel E.P.J., Cambridge University Press, 495

[5] **Srinivasan, G.,** *et al.* **1990**, *Curr.Sci.*, **59**, 31

[6] **Ding, K.J., Chen, K.S., & Chau, H.F. 1993**, *ApJ*, **408**, 167

[7] **Miri, M.J., & Bhattacharya, D. 1994**, *MNRAS*, **269**, 455

[8] **Ruderman, M.A., Zhu, T.,& Chen, K 1998**, *ApJ*, **492**, 267

[9] **Blandford, R.D., Appelgate, J.H. & Hernquist, L. 1983**, *MNRAS*, **204**, 1025

[10] **Urpin, V.A., Levshakov, S.A., & Yakovlev, D.G. 1986**, *MNRAS* **219**, 703

[11] **Sang, Y., & Chunmugam, G. 1987**, *ApJ*, **323**, L61

[12] **Urpin, V.A., Geppert U., & Konenkov, D. 1998**, *MNRAS*, **295**, 907

[13] **Konar, S., & Bhattacharya, D., 1999**, *MNRAS*, **303**, 588

[14] **Alpar, M.A., Cheng, A.F., Ruderman, M.A., & Shaham, J. 1982**, *Nature*, **300**, 728

[15] **Bhattacharya, D. 1995**, in *X-ray Binaries*, ed. W.H.G. Lewin, J. van Paradijs & E.P.J. van den Heuvel (Cambridge Univ. Press), 5

[16] **Konar, S., & Bhattacharya, D., 1999b**, *MNRAS*, **308**, 795

[17] **Kalogera, W., & Webbink, R.F. 1996**, *ApJ*, **458**, 301

[18] **Kalogera, W., & Webbink, R.F. 1998**, *ApJ*, **493**, 351

[19] **Ergma, E., Sarna, M.J. & Antipova, J. 1998**, *MNRAS*, **300**, 352

[20] **Muslimov, A.G. & Sarna, M.J. 1993**, *MNRAS*, **262**, 164

[21] **Frank, J., King, A.R., & Raine, D. 1992**, *Accretion Power in Astrophysics*, Cambridge University Press

[22] **Webbink, R.F., Rappaport, S.A., & Savonije, G.J. 1983**, *ApJ*, **270**, 678

[23] **Ergma, E., & Sarna, M.J. 1996**, *MNRAS*, **280**, 1000

[24] **van Paradijs, J. 1996**, *A&A*, **464**, L139

[25] **King, A.R., Kolb, U., & Szuszkiewicz, E. 1997**, *ApJ*, **488**, 89

[26] **King, A.R., Frank, J., Kolb, U., Ritter, H. 1997**, *ApJ*, **484**, 844

[27] **Page, D., Colpi, M., Geppert, U. & Possenti, A. 2000**, in preparation

[28] **Bhattacharya, D. & van den Heuvel, E.P.J. 1991**, *Phys.Rep.*, **203**, 1

[29] **Illarionov, A., & Sunyaev R. 1975**, *A&A*, **39**, 185

[30] **Cordes, J.M. & Chernoff, D.F. 1997**, *ApJ*, **482**, 971

[31] **D'Amico, N., et al., 1998**, Proc. Symp. *Neutron Stars and Pulsars*, Tokyo, Japan, Ed. N. Shibazaki, N. Kawai, S. Shibata, T. Kifune, Universal Academy Press, Inc., 235

[32] **Burderi, L., & D'Amico, N. 1997**, *ApJ*, **490**, 343

[33] **Phinney, E.S., Kulkarni, S.R. 1994**, *Ann.Rev.Astron.Astrophys.*, **32**, 591

[34] **Stergioulas, N., & Friedman, J. 1995**, *ApJ*, **444**, 306

[35] **Geppert, U., & Konenkov, D., 1998**, Proc. Symp. *Neutron Stars and Pulsars*, Tokyo, Ed. N. Shibazaki, N. Kawai, S. Shibata, T. Kifune, Universal Academy Press, Inc.

[36] **Sturrock, P.A. 1971**, *ApJ*, **164**, 529

[37] **Ruderman, M.A.& Sutherland, P.G., 1975**, *ApJ*, **196**, 51

[38] **Andersson, N. 1998**, *ApJ*, in press, gr-qc/9706075

[39] **Bildsten, L. 1998**, *ApJ*, **501**, L89

Chapter 2

Normal & recycled pulsars

The so-called $\mu - P$ diagram (section [2.2.1]) proved useful for studying the pulsars as the color-magnitude diagram proved for the stars. In this Chapter 2 we will refer to this diagram for shortly overviewing on the classification (section [2.2.2]) and the evolution (section [2.2.3]) of the ~ 1300 pulsars detected so far. We will deserve a more extended discussion to the recycling process (section [2.3]), the fundamental evolutionary model applied in this *Thesis*.

2.1 Neutron stars & pulsars

Stars with typical initial mass ranging in the interval $5 \div 8$ $M_\odot \longrightarrow 20 \div 25$ $M_\odot$ [1] (the exact boundary values being still subject of scientific debate) end up their life with a gravitational collapse of their core. The dynamics of the event is not yet fully understood, but the current scenario (*Core collapse* model) suggests that the collapse originates a Type II supernova explosion, whose remnants are an expanding gaseous envelope (SuperNova Remnant: SNR) and a neutron star (NS). The latter being [2]:

$\longmapsto$ a ultracompact object (mean density $<\rho> \gtrsim 10^{14}$ gcm^{-3}),

$\longmapsto$ rotating at high spin rate (typical periods at the birth in the range $P_{ini} \sim 10^{-3} \longrightarrow 1$ sec),

$\longmapsto$ having an high magnetic moment ($\mu \sim 10^{28}$ Gcm^3 $\longrightarrow 10^{32}$ Gcm^3),

$\longmapsto$ and large spatial motion (median 3-dimensional speed of $\sim$ 460 km/sec).

This event takes place in our Galaxy once every $\sim 50 \div 100$ yr.
Another proposed [3] [4] avenue for the formation of a neutron stars is via the accretion of matter from a companion star onto a massive white dwarf, bringing it beyond the Chandrasekar limit (*Accretion induced collapse* model: AIC [5]).

Ultra high magnetic moments (corresponding to surface magnetic fields $B_S \sim 10^{10}$ Gauss $\longrightarrow 10^{14}$ Gauss) and fast spinning rates allow the young neutron stars to be sources of radioemission, thus appearing as *Pulsars* (PSRs). Many models (see for example Melrose [6] for a review) have been proposed whose basic mechanism is the creation of a pair cascade [7]. In the original Ruderman & Sutherland's model [8] a gap of thickness h develops above the magnetic caps of the neutron star. A potential drop $\Delta V \sim (\Omega B_S h^2)/2c$ establishes along the gap, accelerating electrons up to a Lorentz factor $\gamma_{max} \lesssim (e\Delta V)/(m_e c^2)$. Moving in the neutron star magnetic field, these electrons emit curvature photons of frequency $\nu_{curv} \sim (c/r_{curv})\gamma^3_{max}$ where r_{curv} is the curvature radius of the magnetic field lines. The photons are able to pair create (thus sustaining the cascade) only if

$$\frac{\pi\hbar\nu_{curv}}{m_e c^2}\,\frac{B_\perp}{B_q} > \frac{1}{14} \tag{2.1}$$

with $B_q = 4.4\times10^{13}$ Gauss. The equation (2.1) translates into a relation between the surface magnetic field B_S and the angular velocity Ω of the neutron star. For a given value of B_S [9], only the neutron stars spinning with periods shorter than a predicted value $P_{death}(B_S)$ can radiate.

2.2 The $\mu - P$ diagram

The *"magnetic moment"* versus *"rotational period"* diagram (abbreviated $\mu - P$ diagram) offers a convenient graphic representation for classifying the pulsars and tracing their evolution. Thus in sections [2.2.1] and [2.2.2] we will describe how it is built and where different classes of sources are distributed in it.

2.2.1 *Filling the diagram*

The $\mu - P$ diagram reports the rotational period and the magnetic moment of all the pulsars for which these two values are known.

The pulsing period (along with the dispersion measure DM, see Appendix A) is usually the first measured quantity when a new pulsar is detected. Unless for some misinterpreted cases (*e.g.* PSR J2144-3933, whose rotational period showed up three times longer than estimated at the discovery [10]) it corresponds to the rotational period P of the star, *i.e.* to the abscissa coordinate in the $\mu - P$ plane.

The measurement of μ relies on the assumed correlation between the rotational energy loss of the pulsar and its magnetodipole emitted power:

$$\frac{d}{dt}\left(\frac{1}{2}I\,\Omega^2\right) = -\frac{2}{3c^3}\,\mu^2\,\Omega^4 \tag{2.2}$$

where I is the moment of inertia of the neutron star and it has been implicitly assumed that the magnetic moment is perpendicular to the rotational axis of the star, that is $\mu \equiv \mu_\perp$. With a little algebra, from (2.2) one gets

$$\mu = \sqrt{\frac{3c^3}{8\pi^2}} \sqrt{I} \sqrt{P\dot{P}} = 3.2 \times 10^{37} \sqrt{P\dot{P}} \text{ Gauss cm}^3 \qquad (2.3)$$

where the coefficient at the third member has been calculated assuming $I = 10^{45}$ gcm^2: this value satisfactorily approximates the moment of inertia calculated with different equations of state (see section [3.1]) for a 1.4 $M_\odot$ neutron star. In order to obtain a reliable value for the period derivative a pulsar must be usually timed for about $1 \div 2$ yr. Once measured $\dot{P}$, the equation (2.3) allow μ to be determined and the pulsar included in the $\mu - P$ diagram.

Adopting a specific value for the neutron star radius R (in general dependent on the assumed mass and on the equation of state for the nuclear matter), one can also estimate the surface magnetic field intensity B_S using the relation $\mu \sim B_S R^3$. In *c.g.s gaussian* units there are typically ~ 18 orders of magnitude between μ and B_S. However, due to the steep power in R, the determination of B_S is in principle more uncertain than that of μ.

So far (15 January 2000) 1317 radiopulsars have been discovered [11], but for only 720 galactic field pulsars both P and μ are known: as reported in section [B.1], these numbers are still quickly increasing mainly due to the so-called *PM-Survey*, running at the Parkes radiotelescope [12]. We acknowledge the *PM-Survey* people for the possibility of displaying the unpublished updated $\mu - P$ plot in Figure 2.1. The pulsars found in globular clusters are not included since the gravitational potential of the cluster can deeply affect the values of $\dot{P}$, in turn making the μ-values extremely uncertain.

Besides the representative points for 720 objects, four lines appear in Figure 2.1. They are:

- the DEATH LINE of Chen & Ruderman [9], drawn as a *solid line*. It divides the plane in two regions: in the upper part the radioemission is allowed, whereas below the line it is inhibited (see section [2.1]). This line accounts for the lacking of pulsars in the right lower part of the diagram, the so-called *pulsar graveyard*: this region should host many neutron stars, none of which is detectable in the radiowave band. The exception is represented by the pulsar PSR J2144-3933 [10], with $P = 8.5$ sec and $\mu = 2.1 \times 10^{30}$ Gcm^3.

- the HUBBLE LINE drawn as the *lower dot-dashed line*. It marks where the characterist age $\tau_c = P/(2\dot{P})$ of a pulsar is equal to the Hubble time $t_H = 10^{10}$ yr. Assuming (i) a magnetodipole emission as in the equation (2.2), (ii) a constant magnetic moment for the star and (iii) a initial rotational period much shorter than the current period, the value of τ_c can be interpreted as the lifetime of the neutron star since the beginning of its radioemission. Thus the Hubble line discriminates objects (those on the right of the line, having $\tau_c > t_H$) that certainly must violate some of the three hypotheses.

⇀ the YOUNG PULSAR LINE (drawn as the *upper dot-dashed line*) is similar to the Hubble Line, despite it selects the pulsars younger than 10^3 yr (those on the left of the line, having $\tau_c < 10^3$ yr: none detected up to now).

⇀ the SPIN-UP LINE, drawn as a *dotted line*. It concerns only the so-called *recycled pulsars* (see section [2.3]). Neutron stars with long rotational periods and low values of μ (mostly located in the *pulsar graveyard*) can be spun up via the accretion of matter from a companion in a binary system. For each value of μ and of the accretion rate $\dot{M}_{acc}$ the spin-up line defines the minimum period $P \propto \mu^{6/7}\dot{M}_{acc}^{-3/7}$ attainable during the spin up process.

2.2.2 *Normal and millisecond pulsars*

Figure 2.1 shows that the known pulsars span almost 4 orders of magnitude in rotational period [$P_{min} = 1.558$ ms and $P_{max} = 8509.827$ ms are the two extreme values, observed respectively in J1939+2134 [13] and in J2144-3933 [10]] and almost 6 orders of magnitude in magnetic moment [$\mu_{min} = 7.3 \times 10^{25}$ Gcm^3 and $\mu_{max} = 5.5 \times 10^{31}$ Gcm^3 are the minimum and maximum values, inferred for the pulsars PSR J2317+1439 [14] and PSR J1814-1744 [15]]. However the pulsars are not uniformly distributed in the plot and we can easily distinguish 2 main clusters of objects:

▷ the so-called **"normal pulsars"**, with high magnetic moments and long spin periods;

▷ the **"millisecond pulsars"**, with low magnetic moments and fast rotational rates.

The young newly born pulsars belong to the former group whose main features we listed in section [2.1]. In contrast, the observational properties of the population of the millisecond pulsars (MSPs) can be summarized as follows:

⋆ short periods $P < 10 \div 20$ ms (a bit conventional choice);

⋆ magnetic moments in the range $10^{25.8} \rightarrow 10^{27}$ Gcm^3;

⋆ high fraction of binarity ($\gtrsim 70\%$ in contrast with the $\sim 1\%$ of the normal pulsars);

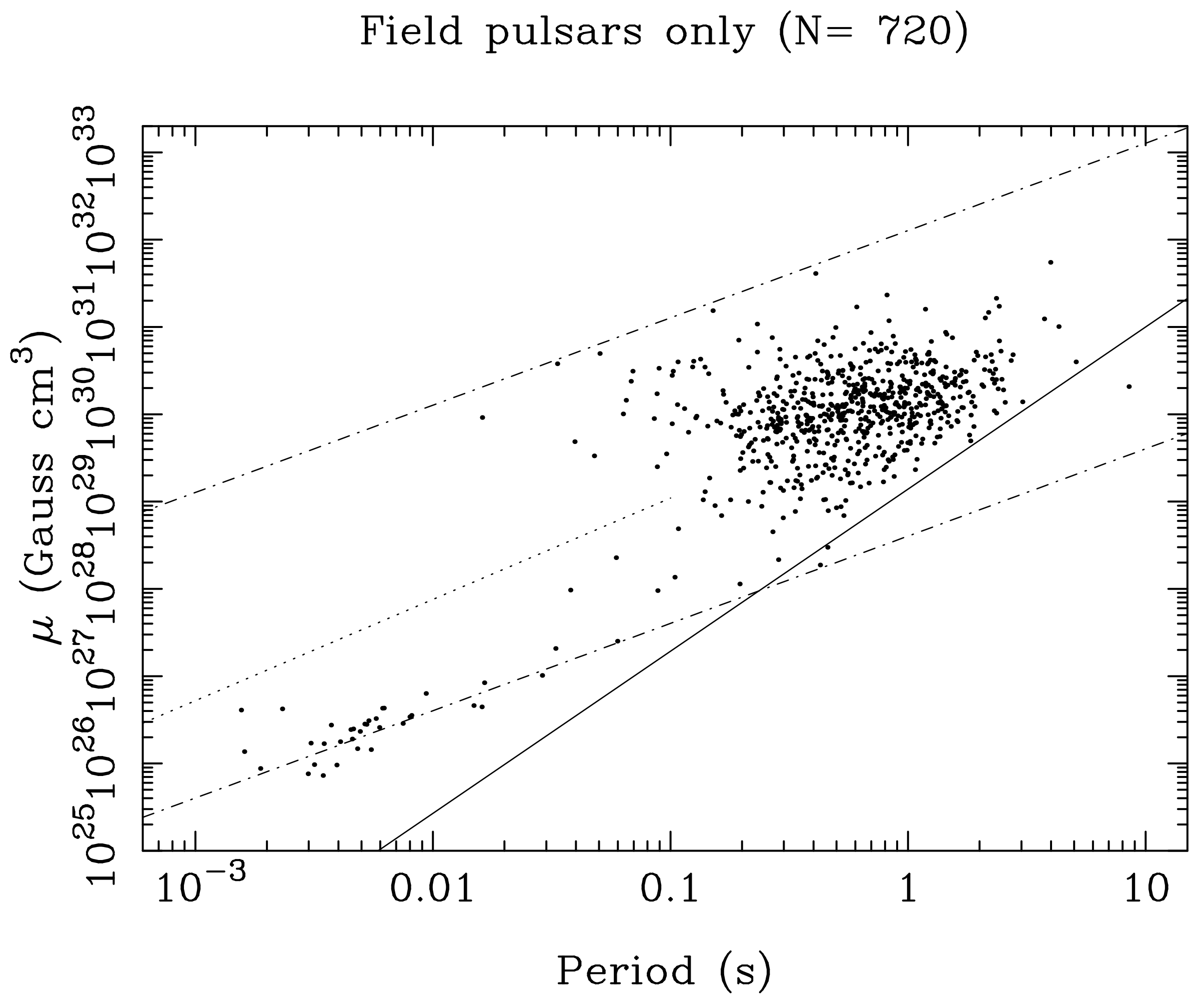

Figure 2.1: "magnetic moment" μ versus "rotational period" P diagram updated at the 15 January 2000. The *solid line* represents the Chen & Ruderman's "death line" [9], below which the radio emission should be inhibited. The *dotted line* is the "spin-up" line for Eddington accretion rate, whereas the *lower dot-dashed line* is the "Hubble line" (both explained in the text). Unpublished plot from the *PM-Survey* group.

- $\star$ mean 3-dimensional velocity of $\sim$ 130 km/sec, about four times slower than that of the normal pulsars [14]; moreover the isolated objects appears slightly slower than the millisecond pulsars enclosed in binaries [16];
- $\star$ almost as many objects moving away from the galactic plane as toward [14], a clear signature for a dynamically old population (the bulk motion of the ordinary pulsars is directed away from the galactic disk);
- $\star$ large characteristic ages $\tau_c = P/(2\dot{P})$, with more than 10 objects showing τ_c greater than the Hubble time $\sim 10^{10}$ yr;
- $\star$ slightly less average radio luminosities with respect to the normal pulsar population [17];
- $\star$ wider duty cycles (see section [A.1]) with respect to the ordinary pulsars (in average 21% versus 3% [17]);
- $\star$ mean spectral indexes identical to those of the normal population (-1.6 ± 0.1 versus -1.7 ± 0.1) [17];
- $\star$ higher degree of polarization and abnormal frequency development of the pulse profile with respect to the ordinary pulsars [18].

2.2.3 *From ordinary to MSPs: tracks in the $\mu - P$ plane*

Given the observational facts of section [2.2.2], a question arises: which is (if any) the linkage between the two different classes of pulsars? The current answer is a paradigm known as *Recycling scenario*:

> **The millisecond pulsars are old neutron stars spun up by the accretion of matter from a companion in a multiple stellar system.**

The different stages of the rotational evolution of a recycled neutron star will be fully discussed in section [2.3], whereas we will deal with the magnetic evolution of the star in Chapter 4. Here we only sketch the general framework of the aforementioned scenario.

The model (see for example [19] for subtleties) describes the millisecond pulsars as the final outcome of **binaries having a primary star of $M_{G,1} \gtrsim 8$ M$_\odot$ and a secondary star with mass $M_{G,2} \lesssim 1 \div 2$ M$_\odot$**. The evolution and expansion of the more massive star leads to a unstable mass loss from its outer layers, thus engulfing the binary system. As a consequence, the secondary lighter star is forced to spiral-in toward the centre of mass of the system and eventually a compact binary is formed. It consists of the secondary star (whose gravitational mass $M_{G,2}$ is practically unchanged) and the Helium core of the swelled primary. The first part of this binary evolution ends up with the explosion of the He core as a supernova and the formation of a neutron star.

If the supernova event disrupts the system, the newly born neutron star (located somewhere in the upper left part of the $\mu - P$ plane) behaves as a young isolated pulsar. It spins down by magnetodipole radiation, first moving through the region of the "normal" pulsars and then crossing (from left to right) the *death line* in the $\mu - P$ plane. After that moment the radioemission would cease forever and (was the magnetic moment spontaneously decaying; see Chapter 4) the radio quiet neutron star simply would follow an almost vertical path in the diagram.

The history is completely different if the binary survives the supernova explosion. Due to the high mass of the He core ($M_{G,1}^{He} \gtrsim 2.2 \div 4$ $M_\odot$ [20] [21]) the mass expelled from the system during the explosion could exceed half of the total pre-supernova mass of the binary. This circumstance should unbind the system, but recent calculation [22] showed up that a suitable natal kick applied to the neutron star can indeed stabilize the binary. In particular we are left with a neutron star of $M_{G,n} \sim 1.4$ $M_\odot$ orbiting a normal star of similar mass.

At the beginning (*ejector phase*), the neutron star could appear as a ordinary pulsar (unless the radiowaves being absorbed by the plasma wind from the companion: see section [2.3.1]), but later the matter from the secondary star can directly interact with the neutron star magnetic field, making the radioemission impossible. First (*propeller phase*) the infalling matter extracts angular momentum *FROM* the neutron star and thus the compact object moves toward far right in the $\mu - P$ plane. Conversely, when the rotational period reaches $100 \div 10000$ sec, the angular momentum of the plasma wind can be transferred *TO* the neutron star (*wind accretion phase*), allowing a slight spin up of the compact object. During this very long phase (few billions years) a decreasing of the neutron star magnetic moment can occur (about two orders of magnitude from the original value of $10^{29} \div 10^{31}$ Gcm^3). An example of such evolution is depicted in Figure 7 of Chapter 4.

The system undergoes another fundamental change when the secondary evolves off the main sequence and a heavy mass transfer sets in (*Roche-lobe overflow phase*): in fact it becomes a Low Mass X-ray Binary. Three mechanisms allows the mass exchange to keep on: for long orbital periods ($P_b \gtrsim 2$ days) the mass transfer is driven by the nuclear evolution of the secondary. For intermediate periods ($0.1 \lesssim P_b \lesssim 2$ days) the magnetic braking [23] basically dominates, whereas the gravitational radiation emission [24] sustains the mass transfer for extremely tight systems ($P_b \lesssim 2$ hours). Different values of the initial orbital periods $P_{b,i}$ and of the mass ratios $q_i = M_{G,2}/M_{G,n}$ lead to strongly different final systems. A complete classification is quite difficult; as a general trend [25]:

◇ systems having $P_{b,i} \gtrsim 2$ days and $q_i < 5/6$ should terminate their evolution as long orbital period ($\gtrsim 50$ days) Low Mass Binary Pulsars (LMBPs) formed by a radiopulsar and a white dwarf in a circular orbit;

- ◇ systems having $P_{b,i} \gtrsim 2$ days and $q_i > 5/6$ should undergo a second spiral-in, thus ending up as a radiopulsar+white dwarf in a tight circular orbit ($\gtrsim 10$ hours);

- ◇ systems having $P_{b,i} \lesssim 0.5$ days should become near permanent faint Low Mass X-ray Binaries (LMXBs), formed by a radio quiet neutron star and a main sequence very light star;

- ◇ systems having $0.5 \lesssim P_{b,i} \lesssim 2$ days are much more sensitive to the interplay between q_i and $P_{b,i}$. They can end up as radiopulsar+white dwarf systems having either ultrashort orbital periods (≤ 2 hours) or intermediate orbital periods ($1 \div 50$ days).

Besides the orbital evolution, the Roche Lobe Overflow phase implies a relevant spin-up of the neutron star. In most cases the compact object accretes matter and angular momentum from a keplerian disk, thus horizontally moving toward left in the $\mu - P$ plane. However this re-acceleration process cannot proceed unlimited. When the neutron star reaches the *spin-up line* (see Figure 2.1 and the more detailed discussion of section [2.3.4]) it cannot spin up further unless its magnetic moment decays. Here it is evident the *tight connection between the rotational and the magnetic evolution of a recycled neutron star*: only if the magnetic moment weakens down to 10^{27} Gcm^3 (corresponding to surface field of $\sim 10^9$ Gauss), an accreting compact object can attain rotational periods shorter than 10 ms, typical of the millisecond pulsars. It is usually assumed that, once reached the spin-up line, a neutron star evolves sliding down it until the mass transfer from the secondary switches off.

In summary **we are eventually left with a spun-up neutron star circularly orbiting a low mass white dwarf** ($M_{G,wd} \sim 0.1 \div 0.3$ M$_\odot$). Its position is often in the left lower corner of the $\mu - P$ plane. In particular, if it resides above the *death line*, **the neutron star can appear** (or re-appear) **as a rapidly pulsing radiopulsar**, slowly horizontally moving toward right in the diagram. For special parameters of the system, the recycled pulsar could later ablate [26] or even evaporate the light companion [27], thus accounting also for the small subset of isolated fastly spinning objects (for other mechanisms see [28] [29]).

In this picture, the LMXBs are seen as the progenitors of the millisecond pulsars. Indeed, such connection is not yet completely demonstrated. However, the discovery in 1998 of rapid (2.49 ms) coherent pulsations from a transient LMXB (SAXJ1808.4-3658 [30]) gave strong support to the model. It is nowaday observed a discrepancy between the birthrate B_{LMXB} of the progenitors (the LMXBs in the Galaxy) and that of the descendants B_{LMBP} (the LMBPs in the Galaxy): $B_{LMBP} \gtrsim 10\ B_{LMXB}$ [2]. First White & Ghosh [31] tried to interpret this discrepancy as a consequence of a cosmic star formation rate peaking at $z \simeq 1.5$.

In fact, due to the different evolutionary timescales, the LMXB population peaks at $z \sim 0.5 \div 1$, whereas the millisecond pulsar population reaches its maximum much later, only for $z \lesssim 0.5$. It seems questionable to apply their estimates to the Milky Way, but their work pointed out the key-role of a detailed star formation history in exploring the relation between B_{LMXB} and B_{LMBP}.

An alternative scenario calls for the *Accretion Induced Collapse* of a white dwarf embedded in a binary system with a mass-losing companion [3]. The different neutron star formation mechanism (with respect to the *Core Collapse* model) would account for the much shorter rotational periods and the lower surface magnetic fields of the millisecond pulsars [5]. However, many aspects of the AIC are still very unclear; in addition, the recent consideration of the so-called r-mode instabilities (see section [3.4.3] for a discussion) seems to indicate that the accretion induced collapse of a white dwarf cannot produce neutron stars rotating at periods shorter than ~ 10 ms [32]. Thus the *recycling scenario* currently shows up the best theoretical framework for explaining the high-spin low-magnetic moment population of pulsars.

2.3 The standard recycling scenario

According to the recycling scenario (see *e.g.* Pringle & Rees 1972 [33] or Lipunov 1992 [34]), the neutron stars in low mass binaries (LMBs) may experience several evolutionary phases

I. **EJECTOR**

II. **PROPELLER**

III. **WIND ACCRETION**

IV. **ROCHE LOBE OVERFLOW**

V. **MILLISECOND PULSAR**

2.3.1 *Ejector*

In this phase the *ejected* relativistic wind (and/or the radiation) from the young neutron star is strong enough to sweep the plasma wind of the companion away, thus creating a cavern around the compact object. The neutron star does not practically feel any influence from its companion, evolving as an isolated object. In particular, provided the light-cylinder of the neutron star (see later) is well inside the swept cavern, magnetodipole emission occurs [35] and the **neutron star spins down** according to the simple law:

$$\dot{P} = 3.15 \times 10^{-16} \frac{\mu_{26}^2}{P} \text{ s yr}^{-1} \tag{2.4}$$

where μ_{26} is the magnetic moment in units of 10^{26} Gcm^3. This radioemission could be partly or even completely absorbed by the plasma cloud surrounding the cavern, mainly by free-free absorption.

Quantitatively, this phase lasts while the pressure P_m of the energy outflow from the new born neutron star is sufficient to stop the plasma wind from the companion at a radius R_{st} larger than the radius R_G for the gravitational capture of the infalling matter. The latter lengthscale is given by:

$$R_G = \frac{2GM_G}{v_{wind}^2} \tag{2.5}$$

where v_{wind} is the speed of the wind plasma relative to the neutron star. The stopping radius R_{st} is determined balancing the pressure due to the neutron star energetic outflow L_m

$$P_m = \frac{L_m}{4\pi R_{st}^2 c} \sim \frac{\mu^2\Omega^4}{6c^3}\frac{1}{4\pi R_{st}^2 c} \tag{2.6}$$

with the dynamical pressure of the plasma P_a

$$P_a = \rho_{wind}\, v_{wind}^2 \tag{2.7}$$

where the density of the plasma wind ρ_{wind} must be evaluated at the stopping radius R_{st}. Assuming a spherical symmetry for the plasma wind, one can just get

$$R_{st} = a\left[1 + 4a\left(\frac{3c^4 v_{wind}\dot{M}_{capt}}{2\mu^2\Omega^4 R_G^2}\right)^{1/2}\right]^{-1} \tag{2.8}$$

where a is the binary separation and $\dot{M}_{capt}$ is the rate of gravitational capture of the wind plasma, defined as $\dot{M}_{capt} = \dot{M}_{comp}(R_G/2a)^2$ with $\dot{M}_{comp}$ the mass loss rate from the companion star.
The radius of the light-cylinder R_{lcy} assigns the typical distance from the neutron star at which the velocity of its corotating magnetosphere $v_{co}(R_{lcy}) = \Omega R_{lcy}$ would reach the speed of the light c, that is

$$R_{lcy} = \frac{c}{\Omega} \tag{2.9}$$

In summary, the ejector stage occurs until

$$R_{st} \ > \ \max(R_G; R_{lcy}) \tag{2.10}$$

2.3.2 *Propeller*

The spin down of the neutron star (and perhaps its magnetic field decay; see Chapter 4) leads to a progressive decreasing of the pressure exerted on the binary plasma cloud either by the radiation and by the relativistic particles released from the neutron star. Thus a second phase occurs (propeller), when a fraction of the plasma matter from the companion star can be captured by the compact object and penetrates down to its magnetosphere. However, the rotational rate of the neutron star is still rapid enough to prevent the accretion of the infalling matter; indeed the magnetosphere acts as a centrifugal barrier [36]: the captured plasma is forced into super keplerian rotation and is *propelled* away, extracting angular momentum from the compact object. Hence, in this stage, the **neutron star loses angular momentum and spins down**. Conversely, the thermal and the magnetic evolution of the neutron star do not differ from that of an isolated object.

A quantitative study of this stage calls for the introduction of another characterist lengthscale, namely the so-called *magnetospheric radius* R_{mag}, defined balancing the dynamic pressure of the captured matter $P_{dyn} = \rho_{capt}(R_{mag}) \cdot v^2_{capt}(R_{mag})$ with the typical pressure of the neutron star magnetic field $P_{mag} \sim B^2(R_{mag})/(8\pi)$. It turns out for example [21]:

$$R_{mag} = 9.8 \times 10^5 \ \phi \ \mu_{26}^{4/7} \ \dot{M}_{capt,EDD}^{-2/7} M_1^{-1/7} R_6^{-2/7} \mathrm{cm} \tag{2.11}$$

where $\phi \sim 1$ (a recent estimate of ϕ can be found in [37]); in the equation (2.11) M_1 is the neutron star mass in solar masses, R_6 the static equatorial radius in units of 10^6 cm and $\dot{M}_{capt,EDD}$ the capture rate in units of Eddington, i.e. $1.5 \times 10^{-8}\ R_6 \mathrm{M}_\odot\ \mathrm{yr}^{-1}$. Basically this magnetospheric radius divides the space in two regions: where the distance d from the neutron star is much greater than R_{mag} the effects of the neutron star magnetic field are negligible, whilst where $d \lesssim R_{mag}$ the magnetic field governs the matter flow. During the propeller phase

$$R_{st} \ < \ R_G \tag{2.12}$$

and the plasma reaches the magnetospheric boundaries, that is $d \sim R_{mag}$. Hence, if the corotation velocity $v_{co}(R_{mag}) = \Omega R_{mag}$ of the magnetosphere at R_{mag} is greater than the keplerian velocity $v_{kepl}(R_{mag})$ at the same radius, the infalling matter must be accelerated by the local magnetic field just up to $v_{co}(R_{mag})$, in principle being expelled. The related rate of extraction of angular momentum from the system "neutron star + magnetosphere" may be estimated as

$$\dot{L} \ = \ \xi \ [\ v_{co}(R_{mag}) \ - \ v_{kepl}(R_{mag}) \ ] \ R_{mag} \ \dot{M}_{capt} \tag{2.13}$$

where ξ is an uncertain efficiency factor $(0.01 \rightarrow 1)$ [38] accounting for the detailed physics of the interaction between the plasma and the magnetic field. As a consequence the neutron star spins down with a rate:

$$\dot{P} \ = \ \xi \ \beta \ P^2 \ \mu^{2/7} \ \dot{M}_{capt}^{6/7} \tag{2.14}$$

with $\beta = [(GM_G/8)^{3/7}]/\pi I$, where I is the moment of inertia of the neutron star. The spin-down ends up when the decreasing $v_{co}(R_{mag})$ becomes equal to $v_{kepl}(R_{mag})$ at the magnetospheric radius, whose position could be meanwhile changed due either to a decay of the magnetic moment or to a variation in the mass transfer from the evolving companion star. This phase can usually last up to $\sim 10^9$ yr (dependent on the main sequence lifetime of the companion star) braking the rotation of the neutron star down to $P = 10^2 \div 10^4$ sec (according with the efficiency factor ξ).

2.3.3 *Wind accretion*

The accretion phase sets in everytime the magnetosphere does not act as a barrier to matter approaching the magnetospheric radius. Most of the Low Mass Binary systems experience two phases of accretion, a first long living (a few 10^9 yr) phase of *wind accretion* and a subsequent shorter phase of enhanced accretion from a disk. In the former phase, a fraction of the plasma wind from the companion falls onto the neutron star surface and the nuclear burning of the accreted material warms up the neutron star. Therefore the thermal (and probably the magnetic) evolution of the object starts differing from that of an isolated neutron star. Moreover at least a fraction of the angular momentum carried by the accreting matter can be transferred to the compact object and the **neutron star slowly spins up**.

This stage can be described by the same formulae as the propeller phase; the main difference is the sign of the parenthesis $[v_{co}(R_{mag}) - v_{kepl}(R_{mag})]$ which in this case is negative, in turn making $\dot{P}$ negative too (see equation (2.14)). Since the accretion from a wind is more or less spherical, the efficiency ξ is much smaller than unity and so only a modest spin-up takes place. Simulations show that P can hardly be reduced by more of one order of magnitude.

2.3.4 *Roche Lobe Overflow*

This phase begins when the companion star leaves the main sequence, filling its Roche-lobe. As a consequence, the mass transfer is strongly enhanced, and the accreted matter likely forms a keplerian disc rotating around a shrunk magnetosphere. The accretion torque **spins the neutron star up to rapid rotational rates** ($P \lesssim 0.01 \div 0.1$ sec), whereas the infalling matter heats the neutron star surface up to $10^8 \div 10^{8.5}$ K (perhaps significantly weakening also the magnetic moment of the star). The gravitational energy released during the accretion can transform these objects into sources of X-ray radiation (X-ray Low Mass Binaries). In low mass binaries this RLO-phase can probably last as long as $10^7 \longrightarrow \sim 5 \times 10^8$ yr.

In the statistical analysis of the *Thesis*, we assume (section [5.3.2]) that during this stage all the neutron stars are fed through a keplerian disk whose inner radius r_{in} depends on the magnetic and rotational parameters of the neutron star. In general

$$r_{in} = \max(R_{mag}; R_\Omega; r_{ms}) \tag{2.15}$$

where R_{mag} is defined in (2.11), R_Ω is the physical equatorial radius of the neutron star (accounting for the inflation due to very fast rotation, see section [3.2]) and r_{ms} is the radius of the last stable orbit (section [3.3]).

- For high enough μ, the magnetic coupling between the disk and the star determines the extent of the angular momentum transfer: the corresponding value of r_{in} is R_{mag}.

- If the magnetic field is very low ($\mu \lesssim 10^{26.5}$Gcm^3), R_{mag} is smaller than R_Ω (or r_{ms}) and the accretion disk is truncated directly at the NS surface ($r_{in} = R_\Omega$) or at the last stable orbit ($r_{in} = r_{ms}$).

The period evolution of the neutron star can be followed using the quite general angular momentum balance relation

$$\frac{d(I_\Omega \Omega)}{dt} = g\ \dot{M}_{acc}\ l_{in} \tag{2.16}$$

where I_Ω is the moment of inertia of the rotating star, Ω its angular velocity and l_{in} the specific angular momentum of the accreting matter at the relevant inner radius r_{in} of the disk. The torque function $g = g(\Omega)$ accounts for the details of the angular momentum transfer between the neutron star magnetosphere and the accretion disk and various authors proposed different models for it [39] [40]. When $r_{in} = R_{mag}$ and $g = 0.0$ the NS is on the so–called *spinup line*, where it can accrete mass without modifying its angular momentum $I_\Omega \Omega$. If an effective magnetic field decay occurs, the neutron star should evolve just sliding down on the spin-up line competing to its accretion rate (in Figure 2.1 the spin-up line for an Eddington accretion rate is plotted).

Though g has been properly calculated only for the case $r_{in} = R_{mag}$, the equation (2.16) can be used (just setting $g = 1.0$) even when the magnetospheric radius is inside the marginally stable radius r_{ms} or inside the star's radius.

The evolution of the accretion rate $\dot{M}_{acc}$ during the Roche Lobe Overflow stage is difficult to assess. A constant $\dot{M}_{acc}$ is only a first order approximation, perhaps acceptable for a subset of wide-orbit binary systems whose mass transfer is driven by the nuclear evolution of the secondary [41]. In general, many authors (see for example Muslimov & Sarna [42] and Ergma *et al.* [43]) showed how $\dot{M}_{acc}$ can vary in LMXBs under different hypotheses for the evolution of the system: conservative or non conservative mass transfer, orbital angular momentum losses, initial orbital period and/or secondary evolutionary stage.

In particular transient accretion due to thermal viscous instabilities in irradiation dominated disks (*e.g.* [44] [45]) suggest that the mass transfer onto a neutron star is not suddenly switched off. The star likely undergoes an overall reduction of the mean accretion rate, modulated by alternate phases of higher and lower accretion. If the magnetic moment is not too weak, any drop in the accretion rate implies the growth of the magnetospheric radius (look at the equation (2.11)). Since the neutron stars is now rapidly spinning, the corotation velocity at the magnetospheric radius $v_{co} = \Omega R_{mag}$ can overcome the local keplerian velocity v_{kepl} (decreasing for increasing R_{mag}) and a new *second phase of propeller* may set in. In the formalism of this section [2.3.4] it implies $g < 0$. The main consequence would be a spin down of the neutron star in the final part of the RLO-stage.

Comparing the observation with their model, Burderi, King & Wynn [25] concluded that this *second propeller phase* should be ineffective in significantly braking the rotational rate of the neutron star; however many physical ingredients necessary to fully describe the phenomenon are yet poorly known, mainly the efficiency factor ξ and the evolutionary law $\dot{M}_{acc} = \dot{M}_{acc}(t)$. Since the *second propeller phase* could in principle modify the period distribution of the recycled objects, it will be subject of a particular investigation in this *Thesis.*

2.3.5 *Millisecond pulsar*

If the position of the neutron star in the $\mu - P$ plane at the end of the mass transfer is above the "death line" [7] [8] [9] the neutron star shines as a *millisecond pulsar* and suffers secular spin down by magnetic dipole torques (equation (2.4)). In this terminal phase, the pulsar migrates to the right of the $\mu - P$ diagram, but its drifting towards longer periods is extremely slow due to the low magnetic moment. Therefore the detected rotational period P should be close to the period P_0 at the beginning of this stage. The age t of a pulsar can be related to its characteristic age $\tau_c = P/(2\dot{P})$, using the magnetic dipole spin-down model with a braking index $n = 3$ and constant magnetic moment:

$$t = \tau_c \left[1 - \left(\frac{P_0}{P} \right)^2 \right] \tag{2.17}$$

For ordinary pulsars one usually assumes $P_0 \ll P$ thus approximating $t \sim \tau_c$. In the case of a millisecond pulsar this assumption is no more justified and so

$$t < \tau_c \tag{2.18}$$

This account for the extremely long values of τ_c measured in a subset of the millisecond pulsar population [14].

Bibliography

[1] **Fryer, C.L 1999**, *ApJ*, **522**, 413

[2] **Phinney, E.S., Kulkarni, S.R. 1994**, *Ann.Rev.Astron.Astrophys.*, **32**, 591

[3] **Michel, F.C. 1987**, *Naure*, bf 329, 310

[4] **Canal, R. & Isern, J. & Labaj J. 1990**, *Ann.Rev.Astron.Astroph.*, **28**, 183

[5] **Yi, I. & Grindlay E. 1998**, *ApJ*, **505**, 828

[6] **Melrose, D. 2000**, in *Pulsar Astronomy - 2000 and beyond*, Proc. of IAU Colloquium 177, ASP Conf.Series, in press

[7] **Sturrock, P.A. 1971**, *ApJ*, **164**, 529

[8] **Ruderman, M.A.& Sutherland, P.G., 1975**, *ApJ*, **196**, 51

[9] **Chen, K. & Ruderman, M. 1993**, *ApJ*, **402**, 264

[10] **Young, M.D., Manchester, R.N. & Johnston, S. 1999**, *Nature*, in press

[11] **D'Amico, N. 2000**, in *Pulsar Astronomy - 2000 and beyond*, Proc. of IAU Colloquium 177, ASP Conf.Series, in press

[12] **Camilo, F.** *et al.* **2000**, in *Pulsar Astronomy - 2000 and beyond*, Proc. of IAU Colloquium 177, ASP Conf.Series, in press

[13] **Backer, D.C., Kulkarni, S.R., Heiles, C., Davis, M.M., Goss, W.M. 1982**, *Nature*,**300**, 615

[14] **Toscano, M.** *et al.* **1999**, *MNRAS*, **307**, 924

[15] **Kaspi, V.M.** *et al.* **2000**, in *Pulsar Astronomy - 2000 and beyond*, Proc. of IAU Colloquium 177, ASP Conf.Series, in press

[16] **Johnston, S., Nicastro, L. & Koribalski, B. 1998**, *MNRAS*, **297**, 108

[17] **Kramer M.** *et al.* **1998**, *ApJ*, **501**, 270

[18] **Xilouris, K.M.** *et al.* **1998**, *ApJ*, **501**, 286

[19] **Verbunt, F. 1993**, *Ann.Rev.Astron.Astrophys.*, **31**, 93

[20] **Habets, G.M.H.J. 1985**, *Ph.D. Thesis*, University of Amsterdam

[21] **Bhattacharya, D. & van den Heuvel, E.P.J. 1991**, *Phys.Rep.*, **203**, 1

[22] **Kalogera, V. 1998**, *ApJ*, **493**, 368

[23] **Pylyser, E. & Savonije, G.J. 1988**, *A&A*, **208**, 52

[24] **Landau, L.D. & Lifshitz, E. 1959**, in *The Classical Theory of Fields*, (Oxford: Pergamon)

[25] **Burderi, L., King, A. R., Wynn, G. A. 1996**, *ApJ*, **457**, 348

[26] **van den Heuvel, E.P.J. & van Paradijs, J.A. 1988**, *Nature*, **334**, 227

[27] **Levinson, A. & Eichler, D. 1991**, *ApJ*, **379**, 359

[28] **Phinney, E.S. & Hansen, B.M.S. 1993**, in *Caltech*, pag. 371

[29] **Leonard, P.J.T., Hillis, J.G. & Dewey, R.J. 1994**, *ApJL*, **423**, L19

[30] **Wijnands & van der Klijs, M. 1998**, *Nature*, **394**, 344

[31] **White, N.E. & Ghosh, P. 1998**, *ApJ*, **504**, 31

[32] **Kokkotas, K.D. & Stergioulas, N. 1998**, *A&A*, **341**, 110

[33] **Pringle, J.E. & Rees, M.J. 1972**, *A&A*, **21**, 1

[34] **Lipunov, V.M. 1992**, in *Astrophysics od Neutron Stars*, (Springer-Verlag: Heidelberg)

[35] **Shvartsman, V.F. 1970**, *Radiofizika*, **13**, 1852

[36] **Illarionov, A., & Sunyaev R. 1975**, *A&A*, **39**, 185

[37] **Burderi, L., Di Salvo, T., Robba, N.R., Del Sordo, S., Santangelo, A., Segreto, A., 1998**, *ApJ*, **498**, 831

[38] **Miri, M.J., & Bhattacharya, D. 1994**, *MNRAS*, **269**, 455

[39] **Ghosh, P., & Lamb, F.K. 1991**, in Proc. NATO/ASI Ser **344**, *Neutron Stars: Theory and Observations*, ed. J.Ventura & D.Pines (Dordrecht: Kluwer), 363

[40] **Wang, Y. 1996**, *ApJ*, **465**, L111

[41] **Webbink, R.F., Rappaport, S.A., & Savonije, G.J. 1983**, *ApJ*, **270**, 678

[42] **Muslimov, A.G. & Sarna, M.J. 1993**, *MNRAS*, **262**, 164

[43] **Ergma, E., Sarna, M.J. & Antipova, J. 1998**, *MNRAS*, **300**, 352

[44] **King, A.R., Kolb, U., & Szuszkiewicz, E. 1997**, *ApJ*, **488**, 89

[45] **King, A.R., Frank, J., Kolb, U., Ritter, H. 1997**, *ApJ*, **484**, 844

Chapter 3

The role of the Equation of State

The search for ultra rapid rotating pulsars is a valuable tool for investigating the physics of the ultra highly condensed state: in particular the detection of the shortest rotational period of a neutron star can put constraints to the equation of state (EoS) of the nuclear matter. In this Chapter 3, after a short summary of the general results ([3.1] and [3.2]), we will focus on the case of the recycled neutron stars, reviewing about the predictions of different equations of state [3.3]. Eventually, we will highlight some effects (from [3.4.1] to [3.4.4]) that could modify the predictions.

3.1 Static neutron stars

At the equilibrium, all the non-rotating neutron star models must satisfy the general relativistic equation of hydrostatic balance (the Tolman-Oppenheimer-Volkoff equation [1]):

$$\frac{dP}{dr} = -\, G\, \frac{[\,\rho(r) + P(r)/c^2\,][\,m(r) + 4\pi r^3 P(r)/c^2\,]}{r^2\,[\,1 - 2Gm(r)/(rc^2)\,]} \tag{3.1}$$

where $P(r)$, $\rho(r)$, $m(r)$ are the proper pressure and mass-energy density at radius r and the proper mass contained within that radius. The pressure-dependent addends in the two parentheses at the numerator show that in the case of general relativity pressure contributes to the mass-energy, steepening the gradient of the pressure with respect to the newtonian case. Once adopted an equation of state for the neutron star matter (in turn determining the dependence of P on ρ), the first order differential equation (3.1) and the mass continuity equation

$$m(r) = \int_0^r 4\pi\, r^2\, \rho\, dr \tag{3.2}$$

can be numerically solved for different values of the constant of integration, producing a *mono-parametric series of neutron star models*, usually *labeled by their total gravitational mass.*

Requiring only microstability and causality within general relativity, in 1974 Rhoades and Ruffini [2] placed a **firm upper limit on the mass of a static neutron star** $\lesssim 3.2(\rho_0/\rho_m)^{1/2}\mathrm{M}_\odot$, where $\rho_0 = 4.6 \times 10^{14}$ gcm^{-3} and ρ_m is the maximum density for which the equation of state is satisfactorily known [3] [4].

Since then, many investigations have been devoted to the determination of the exact equation of state for ultra highly condensed matter, but no general agreement has been reached so far. At densities in excess of several times 2×10^{14} gcm^{-3} even the composition of the nuclear matter is subject of scientific debate. The bulk of the neutron star core should be composed of a mixture of neutrons, protons, electrons and muons in equilibrium with respect to the weak interaction, but at even higher densities, a variety of new and exotic particles (*e.g.* hyperons, kaons) could become important. Moreover, the nuclear matter might undergo phase transitions (*e.g.* boson condensate, kaon condensate, quark deconfinement) deeply affecting its physical properties. In summary, during the last 30 years many tens of different equations of state for the highest nuclear densities have been suggested (see for example [5] [6] [7] [8]): being these densities far beyond the experimental possibilities of the terrestrial laboratories, *one would hopefully like to discriminate between them on the basis of astronomical observations.*

In Table 3.1 we list the values of the maximum gravitational mass for static neutron star models obtained integrating the (3.1) for a set of representative equations of state. Since the pulsar PSR 1913+16 has a gravitational mass of 1.44 $\mathrm{M}_\odot$ [9], only EoSs with maximum static mass greater than that value have been considered.

As a guideline, the whole set of EoSs can be grouped into two main classes, the **soft-EoSs** and the **stiff-EoSs**. Roughly, their characteristics affect the neutron star models as follows:

$\Longrightarrow$ SOFT EQUATIONS OF STATE

1. smaller radii;
2. higher central density;
3. thinner crust.

$\Longrightarrow$ STIFF EQUATIONS OF STATE

1. greater radii;
2. lower central density;
3. more extended crust.

Table 3.1: Physical characterists of static and max-rotating models

	max static		max rotating		1.4 $M_\odot$-star		
EoS	$M_{G,max}$	R_{static}	$M_{G,max}$	P^{abs}_{min}	R_{static}	$R_{\Omega-max}$	$P^{1.4\ M_\odot-star}_{min}$
F	1.46	7.9	1.67	0.47	9.2	14.6	0.80
A	1.66	8.4	1.95	0.47	9.6	13.7	0.73
E	1.75	8.6	2.05	0.48	10.0	14.3	0.78
AU	2.13	9.4	2.55	0.47	10.4	14.4	0.80
FP	1.90	9.4	n.a.	n.a.	10.6	n.a.	0.86
D	1.65	9.3	1.95	0.57	10.7	15.3	0.86
FPS	1.80	9.3	2.12	0.53	10.9	15.5	0.87
UT	1.84	9.5	2.19	0.54	10.9	15.5	0.87
BBB1†	1.79	9.6	2.14	0.57	11.0	15.8	0.89
BBB2†	1.92	9.5	2.27	0.52	11.0	15.9	0.90
UU	2.20	9.8	2.61	0.50	11.2	15.7	0.89
BPAL21†	1.69	9.3	1.97	0.56	11.4	n.a.	n.a.
C	1.86	9.9	2.17	0.59	12.1	17.6	1.06
N*	2.64	12.7	3.22	0.68	13.6	19.1	1.20
BPAL32†	1.95	10.5	2.30	0.63	13.8	n.a.	n.a.
L	2.70	13.7	3.27	0.76	15.0	21.3	1.40
PS	2.28	16.0	n.a	n.a.	16.4	n.a.	1.67
M	1.80	11.6	2.10	0.81	16.7	24.6	1.75

Table 3.1: The 2^{nd} and the 3^{rd} columns list the maximum gravitational mass ($M_\odot$) and the circumferential radius (in km) for static models. The 4^{th} and the 5^{th} columns report the maximum mass and the minimum period (in ms) for rotating models. The last 3 columns refer to models of constant $M_G = 1.4\ M_\odot$. The EoSs marked with (†) are from [8], all the other ones from [7], except FP-EoS [10] and PS-EoS [11]. Some values are not available ($n.a.$) in literature. FP and PS's values are partly from the model of Chapter 5.

The neutron star radius is a key-parameter for the next discussion: thus we sorted the EoSs in Table 3.1 in order of increasing radius for the canonical 1.4 $M_\odot$ star. Going from up to down in the list, we move from very soft EoSs to intermediate EoSs and then to ultra stiff EoSs. Using this sorting criterion, the correlation of the maximum static mass $M_{G,max}$ with the *stiffness* of the EoS is only grossly verified, with some remarkable exceptions (*e.g.* the AU-EoS, the UU-EoS and the M-Eos).

3.2 Rapidly rotating neutron stars

Equilibrium models of rapidly rotating neutron stars in general relativity are solution of the Einstein's equation for the stationary gravitational field in axisymmetry, coupled to the equation of the hydrostatic equilibrium. The metric may be expressed as:

$$ds^2 \;=\; g_{\mu\nu}\, dx^\mu dx^\nu \;=\; -e^{\gamma+\rho}\, dt^2 + e^{2\alpha}\left(r^2 d\theta^2 + dr^2\right) + e^{\gamma-\rho}\, r^2 \sin^2\theta\,(d\phi - \omega dt)^2 \tag{3.3}$$

where $g_{\mu\nu}$ is the metric tensor. The metric potentials γ, ρ, α and the angular velocity ω of the stellar fluid relative to the local inertial frame are functions only of r and θ. The stress-energy tensor of the matter source is assumed to be that of a perfect fluid:

$$T^{\mu\nu} \;=\; (\epsilon \;+\; P)\; u^\mu u^\nu \;+\; P g^{\mu\nu} \tag{3.4}$$

where ϵ is the total energy density and u^μ is the matter four-velocity, satisfying $u^\mu u_\mu = -1$. It can be expressed in the more transparent form [12]:

$$u^\mu \;=\; f(\gamma;\rho;\omega;\Omega)\;[\,1, 0, 0, \Omega\,] \tag{3.5}$$

where $\Omega = u^3/u^0$ is the angular velocity of the fluid element, measured by a distant observer in an asymptotically flat space-time. Once specified an EoS (that is the function $P(\epsilon)$) the relevant equations can be integrated. Of course in this case we haven't a mono-parametric set of solutions, but the *equilibrium models depends on two physical quantities*: a possible choice is *baryonic mass* M_B and *angular velocity* Ω of the star.

Indeed, analytical solutions are impossible and also the numerical approach is time consuming. After some early attempts [13] [14], only in 1986 first Friedman, Ipser & Parker [6] were able to implement realistic equations of state in their code. Major improvements were later introduced by Bonazzola *et al.* (1993: [15]) and by Cook, Shapiro & Teukolsky (1994: [7]). These authors (CST) constructed equilibrium sequences of rotating neutron stars with constant baryonic mass using a formalism developed by Komatsu *et al.* in 1989 [17].

For describing shortly the main results of the CST's calculation, we focus on an intermediate equation of state (the FPS-EoS) and refer to Figure 3.1. In the "gravitational mass" versus "circumferential radius" plot, the equilibrium models occupy only an allowed region, bounded by four limits, namely [7]:

i. STATIC LIMIT, where the neutron star does not rotate. It is represented by the solid curve on the left of the plot, whose coordinates M_G and R are derived solving for the Tolman-Oppenheimer-Volkoff's equation;

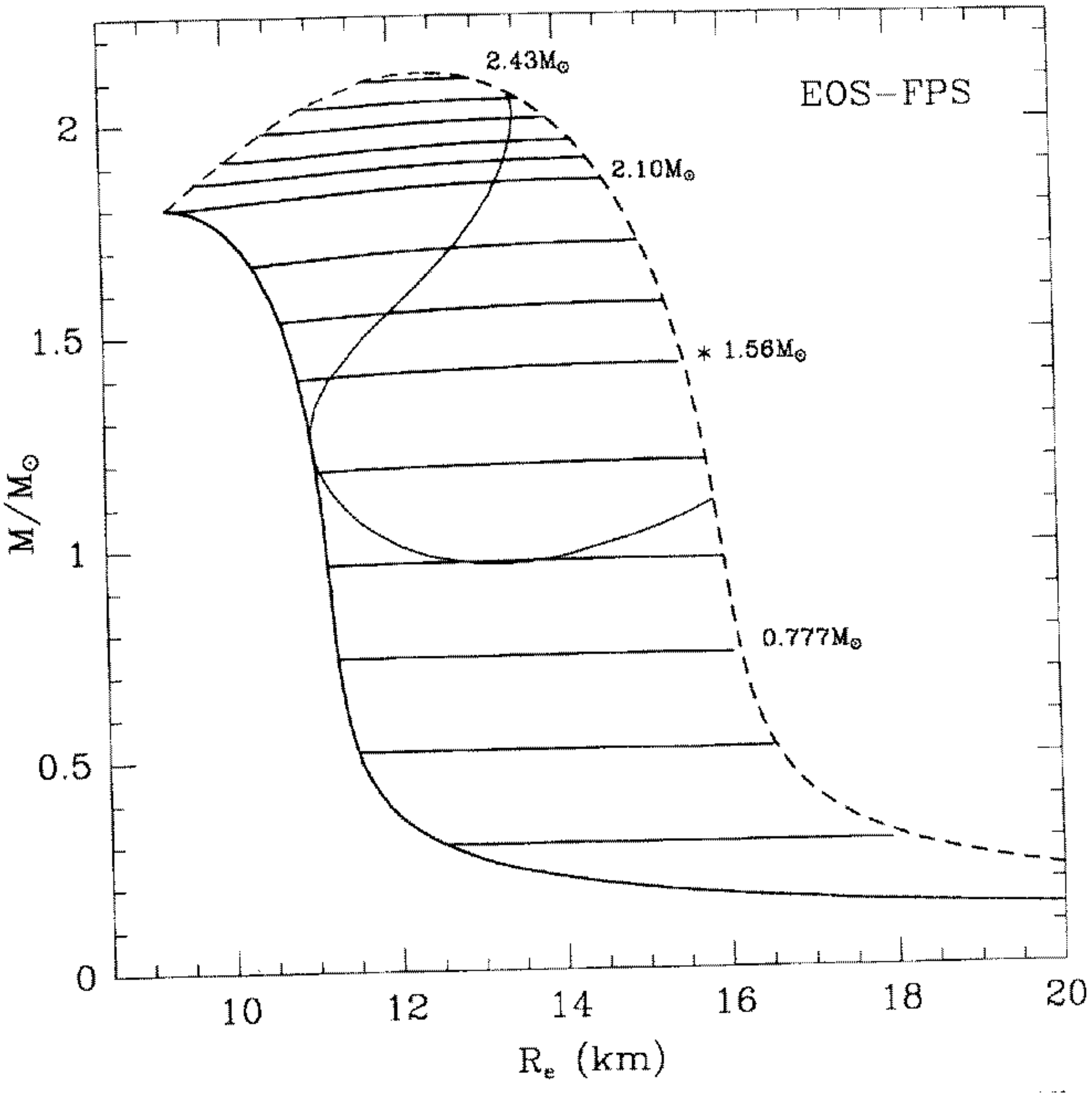

Figure 3.1: Constant baryonic mass sequences in the gravitational mass versus circumferential radius plane. Selected sequencies (*solid horizontal lines*) are labeled by the values of the baryonic mass. The other curves are explained in the text [7].

ii. MASS SHEDDING LIMIT, where the compact object rotates as fast as to prevent the gravitational attraction to keep matter bound to the neutron star surface. It appears as dotted line on the right of the plot;

iii. RADIAL STABILITY LIMIT, where a model is marginally stable to quasi-radial perturbations. It shows up as the dotted line (in the upper left part of the plot) joining the maximum static mass (on the static limit) with the absolute maximum mass; the loci of this line mark the onset of the collapse of the neutron star to a black hole. The calculation of CST did not account for non-axisymmetric perturbations, whose discussion we defer to section [3.4.2];

iv. LOW MASS LIMIT, below which a neutron star cannot form mainly due to the onset of β decay instabilities [16]; it is located far on the lower right corner of the plot.

Constant rest mass sequencies appear as horizontal solid lines in the plot; moving from right to left they report the gravitational mass and the radius of a neutron star of fixed baryonic mass which loses angular momentum for example via magnetodipole or gravitational radiation emission. In particular these sequencies can be grouped in two classes:

I. **Normal sequencies**, terminating at the left end with a non rotating ($\Omega = 0$) model; they are bounded by the static and the mass shedding limits;

II. **Supramassive sequencies**, which do not contain any static solution; in this case, when a neutron star slows down, it can approach the radial stability limit and eventually collapses.

In summary, as one would expect, the centrifugal forces act against collapse allowing for a given EoS to support a **maximum rotating mass greater than the maximum static mass**. For example, looking at Figure 3.1 we see that the maximum gravitational mass for the FPS-EoS is 2.12 $M_{\odot}$, whilst from Table 3.1 we get a maximum *static* mass of 1.80 $M_{\odot}$. Of course, also the circumferential equatorial radius R_{Ω} of the rotating configurations differs from the static radius reported in Table 3.1: in particular, for a given baryonic mass, **the quicker the star spins, the larger its equatorial radius**. In Figure 5.1 of Chapter 5 we can see the increasing of R_{Ω} as a function of Ω for an handful of EoSs. In the case of a baryonic mass of $M_B = 1.40$ $M_{\odot}$, Table 3.1 reports the circumferential equatorial radii at the mass shedding limit for various EoSs: for example, the mass shedding configuration of an FPS model has a radius $R_{\Omega} = 15.5$ km, to be compared with $R = 10.9$ km of the static model.

Table 3.1 reports also the minimum spin periods attainable by neutron star models with different EoSs. In particular we have listed two values: the absolute minimum period P_{min}^{abs} and the minimum period $P_{min}^{1.4\ M_{\odot}}$ for a 1.4 $M_{\odot}$ neutron star.

The former is mostly related to the case of *supramassive sequencies*, whereas the second could represent the minimum period at the birth of a neutron star having the *canonical mass*. We can interpret the results using a simple fitting formula proposed by Burderi & D'Amico [18] for estimating the minimum period before centrifugal disruption P_{shedd} of a rotating neutron star of baryonic mass M_B and a given equation of state:

$$P_{shedd} \;=\; 1.75\; P_K \;=\; 0.957\; (\; \frac{R_{static}}{10\ \mathrm{km}}\;)^{3/2}\; (\; \frac{\mathrm{M}_\odot}{M_{G,static}}\;)^{1/2}\ \mathrm{ms} \qquad (3.6)$$

where P_K stands for the classic keplerian centrifugal limit (obtained equating the gravitational and the centrifugal forces for a blob of matter orbiting just at the surface of the star). R_{static} and $M_{G,static}$ are the radius and the gravitational mass of a non spinning neutron star model with the baryonic mass M_B and the same EoS. One can check that the proposed formula reproduces the values in Table 3.1 with an accuracy better than 10%.

In the case of a fixed canonical mass, the expression (3.6) clearly shows the role of the radius in determining the minimum attainable period before the mass shedding sets in at the equator: **the larger the radius is, the longer the minimum period is**. If all the neutron stars would be born with the canonical mass, *the softest EoSs would allow initial maximum spin rates about twice higher than the stiffest EoSs.* A similar trend takes place for the absolute minimum period P^{abs}_{min}, but in this case the range of the predicted values is narrower due (see equation (3.6)) to the combined effects both of the radius (smaller for softer EoSs) and the maximum mass (fundamentally greater values for stiffer EoSs).

In principle, a neutron star could move even from left to right along a constant baryonic mass sequency (look at Figure 3.1), but studying such evolution sounds academic: at the moment the only known way for accreting angular momentum onto a quasi-static neutron star is to transfer mass to it, thus changing its baryonic number. Therefore one has to address the problem of calculating in general relativity the features of the so-called **Accreting sequencies**.

3.3 Recycled neutron stars

The equation of state for the nuclear matter determines the internal structure of a neutron star of given baryonic mass M_B and angular velocity Ω. Both these quantities vary during the recycling process in a binary system, along with changings in the radius, the moment of inertia, the central density, the kinetic energy, the gravitational mass and the internal structure of the neutron star.

In 1994, Cook, Shapiro & Teukolsky [19] used their relativistic code [7] for constructing evolutionary tracks for the recycling of neutron stars to millisecond periods. They began with a non rotating *bare neutron star of canonical grav-*

itational mass and assumed that the accretion occurs from the inner edge of a Keplerian disk (or directly onto the neutron star surface if the radius r_{ms} of the marginally stable orbit is smaller than the equatorial radius of the star). In each step, the accreted rest mass δM_0 entirely deposits the competing angular momentum δJ_{i+1} on the neutron star and the authors verify that the new model (with baryonic mass $M_i + \delta M_0$ and angular momentum $J_i + \delta J_{i+1}$) allows equilibrium. The typical results of this calculation are illustrated in Figure 3.2 for the case of the equation of state FPS.

This plot shows a representation in the plane M_G vs "central density" of the same results already discussed for Figure 3.1; the region of the equilibrium models is contained inside 4 boundaries: static limit (right solid line), mass shedding limit (left solid line), radial stability limit (dashed line in the upper right corner), low mass limit (lower left point at the intersection between static and mass shedding limit). The constant baryonic mass sequencies are represented as almost horizontal lines: normal sequencies up to $M_B = 2.10\mathrm{M}_\odot$, supramassive sequencies for $2.10\ \mathrm{M}_\odot < M_B < 2.43\ \mathrm{M}_\odot$. The standard **Accretion sequency** for a star having initial $M_G = 1.40\ \mathrm{M}_\odot$ is drawn as the thin dashed line labeled by (a). This track (followed upward) crosses many sequencies of constant baryonic mass and then ends up at the centrifugal disruption limit, when the gravitational mass is $M_G = 1.76\ \mathrm{M}_\odot$ (corresponding to a baryonic mass of $M_G = 1.97\ \mathrm{M}_\odot$) and the rotational period is equal to $P_{sh} = 0.747$ ms.
The relevant evolutionary quantities for various EoSs are collected in Table 3.2. Inspecting this Table, we note:

1. Except for the ultra soft F-EoS, all the evolutionary paths terminate at the mass shedding limit.

2. In order to attain the centrifugal disruption limit, the range of accreted baryonic mass is $\Delta M_B \sim 0.35 \div 0.50\ \mathrm{M}_\odot$.

3. For most among the softest EoSs, the gravitational mass at the mass shedding limit is greater than the competing maximum static mass (*e.g.* for A, E and D-EoS).

4. The ratio T/W (kinetic energy over gravitational energy) is always smaller than 0.13 even at the mass shedding limit.

5. The mass-shedding period depends on the specific equation of state: for the stiffest EoSs it is twice longer than for the softest ones.

6. All the minimum attainable periods are shorter than the minimum rotational period observed so far, $P_{obs} = 1.558$.

These results suggest two outstanding conclusions:

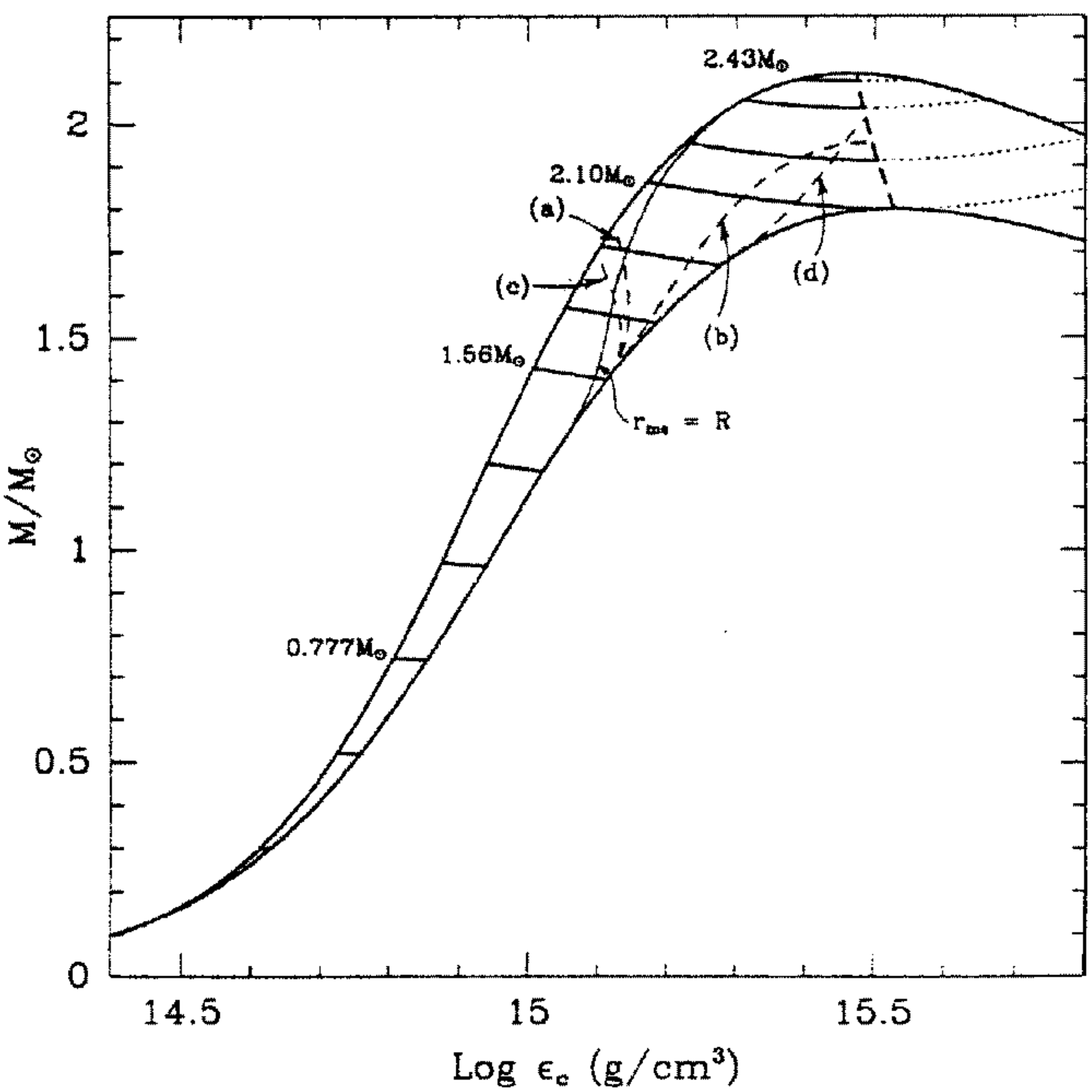

Figure 3.2: Accretion sequencies in the gravitational mass versus central density ϵ_c plane for the FPS-EoS. Constant baryonic mass sequences (*almost horizontal lines*) are labeled by the values of the baryonic mass. The thin solid line labeled by $r_{ms} = R$ marks the $(M_G;\epsilon_c)$-coordinates of the neutron stars whose marginally stable orbit skims the surface. The other curves are explained in the text [19].

Table 3.2: Disk accretion onto a 1.4 $M_\odot$ neutron star

EoS	Fate	T/W_{fin}	ΔM_B	$M_{G,fin}$	P_{fin}	$M^{static}_{G,max}$	$M^{rotating}_{G,max}$	P^{abs}_{min}
F	Collapse	0.034	0.172	1.52	0.72	1.46	1.67	0.47
A	MassShed	0.120	0.428	1.77	0.60	1.66	1.95	0.47
E	MassShed	0.115	0.414	1.76	0.66	1.75	2.05	0.48
AU	MassShed	0.126	0.446	1.79	0.70	2.13	2.55	0.47
D	MassShed	0.111	0.405	1.76	0.73	1.65	1.95	0.57
FPS	MassShed	0.114	0.416	1.76	0.75	1.80	2.12	0.53
UT	MassShed	0.119	0.429	1.78	0.75	1.84	2.19	0.54
UU	MassShed	0.121	0.436	1.78	0.78	2.20	2.61	0.50
C	MassShed	0.103	0.389	1.74	0.89	1.86	2.17	0.59
N*	MassShed	0.130	0.484	1.84	1.08	2.64	3.22	0.68
L	MassShed	0.116	0.443	1.80	1.25	2.70	3.27	0.76
M	MassShed	0.091	0.367	1.74	1.49	1.80	2.10	0.81

Table 3.2: The second and the third columns contain the fate of the neutron star at the end of the recycling and the related final ratio of kinetic energy over gravitational energy. The fourth and fifth columns report the total accreted baryonic mass and the final gravitational mass (in units of solar masses). The sixth column lists the final attained rotational periods. The last three columns displays values already reported in Table 3.1, here reported for comparison. All the values are from [19].

#1# **Provided an efficient transfer of angular momentum onto the neutron star is at work, all viable equations of state allow for recycling a 1.4 $M_\odot$ unmagnetized neutron star to ultra-rapid spinning rates**. The reason why recycling works is that *in general relativity the maximum mass of a star increases with rotation*. Thus, even taking into account item (3.) of the previous list, a spun up neutron star does not collapse to a black hole. Moreover, the accreted mass ΔM_B does not entirely go into increasing the total mass of the star because of the gravitational binding energy.

#2# In principle, **the detection of the minimum spin period of the recycled pulsars can discriminate between the proposed equations of state**. This result of the CST's calculation has been fully discussed by several authors (*e.g.* [20] [21] [18] and references therein). In view of these considerations and taking into account the items (5.) and (6.) of the list, in this *Thesis* we focus on two EoSs, as a representation of the two main classes: the **ultra-stiff PS-EoS** [11] and the **mild-soft FP-EoS** [10]. As inferred within the model presented in section [5.1], their limiting periods

$$\begin{aligned} P_{sh} &= 0.73 \text{ msec} \qquad \text{for FP} - \text{EoS} \ \ (\textit{mild soft}) \\ P_{sh} &= 1.40 \text{ msec} \qquad \text{for PS} - \text{EoS} \ \ (\textit{ultra stiff}) \end{aligned}$$

are close to the boundaries of the allowed range of the mass shedding periods for the EoSs explored by CST (see Table 3.2); thus they are suitable for investigating the effects of different kind of EoSs on the period distribution of synthesized population of recycled neutron stars.

3.4 Which threats for recycling up to ultra short periods?

Three variations to the standard recycling model were explored by CST: the track (c) in Figure 3.2 mimics the accretion onto a magnetized neutron star (for which an autoconsistent fully relativistic calculation is beyond the current computational capability): the evolution is studied helding fixed at $2.0 \cdot r_{ms}$ the radius of the inner rim of the accretion disk, thus simulating the presence of a magnetosphere. The *final outcomes are only slightly affected* with respect to the case (a). In section [5.1] we will develop a semi-analytical model just addressing the description of the rotational evolution of a magnetic neutron star undergoing accretion via a keplerian disk. The code reproduces satisfactorily the results of CST for bare neutron stars, requiring a much lighter computational effort and providing the opportunity of studying magnetized stars as well.

The track (d) in Figure 3.2 depicts the evolution of a neutron star with initial gravitational mass $M_G = 1.7\ M_\odot$. It demonstrates that for sufficiently massive stars the recycling can end up with a collapse to black hole instead than with the centrifugal disruption of the star at its equator. This could be relevant only if assuming a bimodal [22] or a continuum distribution of masses for the neutron stars at their birth.

On the contrary, in the following four sections we will discuss some physical phenomena which could more severely affect the predictions of section [3.3].

3.4.1 *Low efficiency of the angular momentum transfer*

In calculating the track (a) of Figure 3.2, CST assumed that all the angular momentum $j_K \delta M_0$ of the accreting blobs is deposited onto the neutron star, where j_K is the specific angular momentum of the matter at the inner edge of the keplerian disk. In general one could argue:

$$\delta J = f_J \cdot (j_K \delta M_0) \tag{3.7}$$

where δJ is the angular momentum accreted by the neutron star and f_J is a number ranging from $0 \longrightarrow 1$. The key-role of an efficient transfer of the angular momentum from the accreting disk matter to the star is displayed in the track (b) of Figure 3.2: in this case, CST assumed that only an half ($f_J = 1/2$) of the angular momentum of the infalling blobs ends up onto the neutron star. Starting with the same model as the case (a), the evolution does not terminate with the centrifugal disruption of the star, but at the radial stability limit, that is with a collapse. At the final point the rotational period is slightly shorter ($P = 0.66$ ms) than for the path (a), but this higher final spin rate is obtained at the price of a much larger loading of mass ($\Delta M_B = 0.71$ M$_\odot$ to be compared with $\Delta M_B = 0.41$ M$_\odot$). A further decreasing of the fraction f_J would strongly slow down the re-acceleration of the neutron star, either inhibiting the spinup to the centrifugal limit (in the case of the stiff EoSs), or leading the star to a sooner radial collapse (for the soft EoSs).

In 1993, Miller & Lamb [23] proposed a physical situation where small values of f_J could occur. They argued that for accretion luminosities greater than $\sim 0.2\ L_{EDD}$ ($\sim 3 \times 10^{37}$ erg/sec) the radiation drag forces could transfer most of $j_K \delta M_0$ to the radiation field instead of to the neutron star. In this situation, the neutron stars could be spun up to ultra fast periods, but their re-birth as radiopulsars would become highly improbable.

3.4.2 *Non-axisymmetric instabilities*

In general relativity no exact criterion for the onset of non-axisymmetric instabilities is known: therefore the spinup processes described in section [3.3] could halt before attaining the centrifugal limit.

A detailed analysis calls for the general functional form of the modes of oscillation of a fluid spheroid spinning at angular velocity Ω:

$$\exp\left[\, i\sigma_m(\Omega)t \;+\; im\phi\,\right] \;\cdot\; \exp\left[-\,\frac{t}{\tau_m(\Omega)}\right] \tag{3.8}$$

where t is the time, ϕ the azimuthal angle, $\sigma_m(\Omega)$ the m-th mode frequency, $\tau_m(\Omega)$ the m-th timescale-constant, m a relative number (labeling the mode) and i the imaginary unit. It is easy to check that an instability is damped on a timescale $\tau_m(\Omega)$ whether $\tau_m(\Omega) > 0$. Conversely, it grows whether $\tau_m(\Omega) < 0$. The transition between the two regimes takes place at a critical spinning frequency Ω_m of the spheroid, solution of the equation ${\tau_m}^{-1}(\Omega_m) = 0$. In particular there are two branches of instability:

$\Longrightarrow$ **$\mathbf{m \leq -2}$ modes** DRIVEN UNSTABLE BY THE VISCOSITY OF THE FLUID and damped by the gravitational radiation (GR). They were first studied in the XIX century [24].

$\Longrightarrow$ **m $\geq$ 2 modes** DRIVEN UNSTABLE BY THE GRAVITATIONAL RADIATION and damped by the viscosity. They were first investigated by Chandrasekar in 1970 [25] [26].

For fast rotating compact objects like millisecond pulsars, *only the modes with* $m \lesssim 5$ *showed up to be relevant* [27]. Many investigations were devoted to these modes in the framework of Newtonian polytropes or more realistic EoSs (see for example [28] for a review). We can summarize the results as follows:

- above 2×10^{10} K, the bulk viscosity damps all the modes;
- below 10^7 K, a neutron star reaches the mass shedding period before any $|m| \leq 5$-mode instabilities set in [29];
- for 10^7 K $< T < 2 \times 10^{10}$ K the situation is still under debate: in principle, the GR driven $m \geq 2$-modes should set in [30], but Mendell [31] argues that below the superfluid transition temperature of the core ($\lesssim 10^9$ K), the *mutual friction* between electrons and neutron vortices could prevent the instabilities to grow.

Burderi & D'Amico [18] plotted (see Figure 3.3) the shortest possible rotational periods of a neutron star vs its temperature for two extreme (either ultrasoft or ultrastiff) equations of state, accounting also for the current knowledge about non-axisymmetric instabilities. For realistic temperatures and baryonic masses of recycled neutron stars, **the periods at which axisymmetric instability would set in are remarkably close to the competing centrifugal disruption limits**.

A statement confirmed by more recent fully relativistic calculation: in 1999 Morsink, Stergioulas & Blattnig [32] obtained an empirical fitting formula (insensitive to the EoS to within 4–6%) for the critical value of the ratio T/W (kinetic over gravitational energy) at which the $m = l = 2$ *f*-mode (see section [3.4.3] for the labeling of the instability modes) becomes unstable:

$$(T/W)_{m=2} \;=\; 0.115 \;-\; 0.048\,\frac{M_G}{M^{static}_{G,max}} \tag{3.9}$$

where $M^{static}_{G,max}$ is the maximum allowed mass for a static star of a given EoS (for comparison Newtonian physics predicts that such perturbation sets in when $T/W > 0.14$ for an incompressible McLaurin spheroid). The equation (3.9) and the item (4.) of section [3.3] suggest that **non-axisymmetric instabilities should not be a severe obstacle to recycling**, unless for the extreme rotational rates within 7-15% from the mass shedding. Therefore, these kinds of instability could be relevant in the context of the gravitational radiation emission from astrophysical sources, but perhaps they do not affect the possibility of spinning the neutron star up to ultra fast rates.

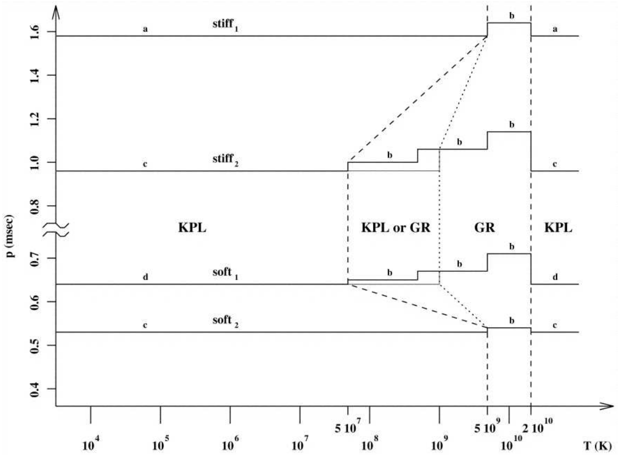

Figure 3.3: Schematic plot of the shortest rotational period (in ms) of a neutron star versus its temperature. Two EoSs (an ultrasoft and an ultrastiff) and two neutron star baryonic masses (the canonical 1.4 $M_\odot$ and the maximum mass, respectively 1.63 $M_\odot$ and 3.27 $M_\odot$) are used. KPL indicates the regions where the shortest periods are determined by the centrifugal disruption limit, whereas GR marks the zones where the gravitational radiation driven instabilities are relevant. From [18].

3.4.3 *r-modes*

The oscillations of a star can be expressed by the Lagrangian displacement vector $\vec{\xi}$, representing the displacement of a given fluid element due to the perturbation. Since $\vec{\xi}$ is a vector on a $(\theta,\ \phi)$ 2-sphere, in general it can be split into a sum of a *spheroidal* (also called polar) and a *toroidal* (also called axial) component. For a non rotating star the oscillation modes are either purely spheroidal or purely toroidal. In a rotating star the spherical symmetry is broken and a coupling of polar and axial terms occurs. Thus, a normal mode of oscillation in a spinning star is defined polar (=spherical) if it reduces to a purely spherical mode in the non-rotating limit. The previous section [3.4.2] mainly dealt just with the spheroidal perturbations of a rotating neutron star, characterized by the indexes of the spherical harmonic functions Y_l^m. They are also known as *f*-, *p*- and *g*-modes. Conversely, a normal mode for a rotating star is defined axial (=toroidal) if it is purely axial in the non-rotating limits. Such perturbations were classified as *r*-modes, but only in 1998 Andersson [33] discovered their relevance for the fast spinning neutron stars.

The *r*-modes belong to the large set of the Chandrasekar-Friedman-Schutz gravitational radiation driven instabilities [34] whose general mechanism is the following [35]: if the pattern velocity of the generic $(l\ , m)$ mode

- *counter-rotates* with respect to the frame rotating with the star,

- but appears *co-rotating* with the star to a distant inertial observer,

then when the perturbation radiates away angular momentum the star can find a rotational state both of lower angular momentum and lower energy, thus permitting the amplitude of the mode to grow. In particular at the first order in the star's angular speed Ω, the angular frequency of a $(l\ ,m)$ r-mode is [36]:

$$\Omega^{l,m}_{star} = \frac{2\ m\ \Omega}{l(l+1)} \tag{3.10}$$

as seen from the frame rotating with the star; conversely it becomes

$$\Omega^{l,m}_{inertial} = \Omega^{l,m}_{star} - m\ \Omega = -\frac{m\ \Omega}{l(l+1)}\ (\ l^2 - l - 2\ ) \tag{3.11}$$

if measured by an inertial observer. Hence, it is easy to verify that *all the r-modes with $l \geq 2$ are generically unstable to the emission of gravitational radiation* (the $l = 1$ mode being marginally stable). Of course, the *instability is active as long as its growth-time is shorter than the damping-time due to the viscosity* of the neutron star matter. Then in order to assess its effects on the rotational evolution of a neutron star, one must investigate these timescales. Earlier attempts were performed for example by Kokkotas & Stergioulas [36] and by Andersson, Kokkotas & Stergioulas [35]. The former authors argued that the $m = l = 2$ r-mode dominates the timescale of this instability. The latter authors estimated the gravitational radiation growth-time for this mode:

$$\tau_{gw} = 22\ \left(\frac{1.4\ \mathrm{M}\odot}{M_G}\right)\ \left(\frac{10\ \mathrm{km}}{R}\right)^4\ \left(\frac{P}{1.0\ \mathrm{ms}}\right)^6\ \mathrm{sec} \tag{3.12}$$

The damping timescales are much harder to calculate due to the many uncertainties about the microphysics of the neutron star matter. In the simplest scenario there should be two different regimes for the shear viscosity η: below the superfluid transition temperature ($\sim 10^9$ K) it is dominated by the electron-electron scattering [30], and the implied damping-time is [35]:

$$\tau_{sv} = 3600\ \left(\frac{1.4\ \mathrm{M}\odot}{M_G}\right)\ \left(\frac{R}{10\ \mathrm{km}}\right)^5\ \left(\frac{T}{10^7\ \mathrm{K}}\right)^2\ \mathrm{sec} \tag{3.13}$$

Above the superfluid transition, the shear viscosity should be governed by the neutron-neutron interactions, but, for this temperature range the bulk viscosity ζ becomes much more relevant. Using the available estimates [37] for ζ one can get

$$\tau_{bv} = 1.8 \times 10^{11} \left(\frac{1.4\ M\odot}{M_G}\right) \left(\frac{R}{10\ \mathrm{km}}\right)^5 \left(\frac{10^9\ \mathrm{K}}{T}\right)^6 \left(\frac{1.0\ \mathrm{ms}}{P}\right)^2 \mathrm{sec} \quad (3.14)$$

for the bulk-viscosity damping-time. At each value of the temperature of the star, the critical period below which the gravitational radiation instability sets in can be obtained solving the equation

$$\frac{1}{\tau_{gw}} + \frac{1}{\tau_{sv}} + \frac{1}{\tau_{bv}} = 0 \quad (3.15)$$

The result of a similar calculation is reported in Figure 3.4. It turns out that for young neutron stars with hot interiors these previously neglected oscillations could limit [38] the spin of the star to a small fraction ($\sim 0.2 - 0.3$) of its keplerian centrifugal limit. In particular for new born neutron stars this effect could spindown the star at $P > 10$ ms in a very short time (~ 1 yr), so accounting for the lacking of young NSs spinning at period of few milliseconds [39]. The effectiveness of the r-modes in the high temperature regime has been recently confirmed [40] by more refined calculations for rapidly rotating neutron stars.

Andersson, Kokkotas & Stergioulas [35] claimed that a similar mechanism could occur during the LMXB-phase, thus preventing the spinup of a old accreting neutron star below $\sim P_{min}^{obs} = 1.558$ ms. In particular, combining (3.12) and (3.13) they got the following value for the critical period:

$$P_{crit} = 2.3 \left(\frac{R}{10\ \mathrm{km}}\right)^{3/2} \left(\frac{T}{10^7\ \mathrm{K}}\right)^{1/3} \mathrm{ms} \quad (3.16)$$

However, the difficulties in the calculations of the values of the shear and bulk viscosities for superfluid nuclear matter at $T \sim 10^7 - 10^{8.5}$ K (relevant for the accretion phase) leave a large uncertainty in the role of this instability in the recycling process. For example the coupling between vorticity and shear viscosity [42] could modify the diagram of Figure 3.4, allowing cold stars to remain stable up to the centrifugal disruption limit. Also the role of the superfluid *mutual friction* is still unclear: Lindblom & Mendell [41] pointed out that the r-modes could be completely suppressed for acceptable (though not highly probable) choices of the superfluid transition parameters.

3.4.4 *Accretion induced quadrupole moments*

When a rotating neutron star develops a misaligned quadrupole moment Q, it becomes source of gravitational waves, loosing energy and angular momentum at a rate

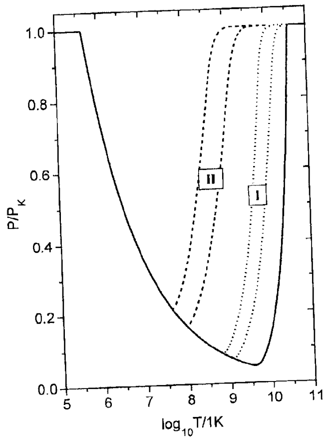

Figure 3.4: The *solid line* divides the plane in two regions: in the upper part the r-mode instabilities operate, in principle spinning down the star. Below the *solid line* they are damped either by the bulk (*right branch*) or by the shear (*left branch*) viscosity. The *dashed lines* report the period-temperature evolution for: (I) standard cooling with modified URCA process and (II) rapid cooling due to DURCA process. The adopted star model has a keplerian centrifugal limit $P_K = 0.8$ ms [35].

$$\dot{E}_{gr} = \frac{32G}{5c^5} \cdot Q^2 \cdot \Omega^6 \qquad ; \qquad N_{gr} = \dot{L}_{gr} = \frac{\dot{E}_{gr}}{\Omega} \tag{3.17}$$

where Ω is the angular speed of the star. If N_{gr} exactly balances the spin up torques, the neutron star accretes matter without shortening its rotational period. In 1998 Bildsten [43] suggested a mechanism for providing the accreting neutron stars of a quadrupole moment $Q \simeq 10^{-7}MR^2$. The basic phenomenon is the electron capture (EC) undergone by the nuclei in the crust of the star. In cold neutron stars, the EC is completely governed by the density in the crust, determining the Fermi energy of the electrons and thus their chance of overcoming the energy barrier against capture. On the contrary, in typical accreting neutron stars the temperature in the crust ($\simeq 10^8$ K) is hot enough to make the EC cross section sensitive to the local temperature. In particular, in hotter regions the EC occurs at lower local pressure and so the related *EC-density-jump* takes place at a smaller depth in the crust. Thus, any lateral temperature variation turns out into local density variations, eventually generating a quadrupole moment.

Bildsten argued that this accretion induced Q should be long-living, provided the accretion rate is larger than $\sim 2 \times 10^{-3}$ $\dot{\mathrm{M}}_{\mathrm{EDD}}$. In fact, in this case, the time for transporting heat around the upper crust ($\rho \sim 2 \div 3 \times 10^{11}$ gcm^{-3}) is longer than the time to locally heat the crust itself; as a consequence, any large scale thermal asymmetry can survive in the relevant crustal layer (and the lateral density disuniformities too). In summary, an X-ray bright accreting neutron star could easily develop and maintain a quadrupole moment $Q \simeq 10^{-7} MR^2$.

If so, no matter the EoS, **the gravitational waves emission would balance the spin up torques at rotational periods significantly longer than the centrifugal limit** of the neutron star, typically at $2\pi/\Omega \sim 2.5 \div 3.5$ ms. This model was prompted by the observation of the period distribution of the neutron stars currently undergoing the X-ray emitting Roche Lobe Overflow phase in Low Mass X-ray Binaries. Indeed, it could explain the apparent clustering of the rotational periods of these sources (~ 2.5 ms $\rightarrow \ \sim 4.0$ ms) as inferred from the standard interpretation of the kHz-QPOs detected in their X-ray power spectra [44].

Yet, many points in this scenario are still unexplored, *e.g.* the relative vertical motion of the density disuniformities in the crust, or the origin of great scale temperature asymmetries at the depths involved in the process.

Bibliography

[1] **Oppenheimer, J.R. & Volkoff, G. 1939**, *Phys.Rev.*, **55**, 374

[2] **Rhoades, C.E. & Ruffini, R. 1974**, *Phys.Rev.Lett*, **32**, 324

[3] **Hartle, J.B. & Sabbadini. A.G. 1977**, *ApJ*, **213**, 831

[4] **Celotti, A., Miller, J.C.& Sciama, D.W. 1999**, *Cl.Quantum Grav.*, Millenium Issue, **16**, A3

[5] **Arnett, W.D., & Bowers, R.L. 1977**, *ApJS*, **33**, 415

[6] **Friedman, J.L., Ipser, J.R. & Parker, L. 1986**, *ApJ*, **304**, 115

[7] **Cook, G.B., Shapiro, S.L., Teukolsky, S.A. 1994**, *ApJ*, **424**, 823

[8] **Datta, B., Thampan, A.V. & Bombaci, I. 1998**, *A&A*, **334**, 943

[9] **Taylor, J.H. 1992**, *Phil.Trans.R.Soc.London*, bf 341, 117

[10] **van Riper, K.A. 1988**. *ApJ*, **329**, 339

[11] **Pandharipande, V., & Smith, R. 1975**, *Nucl.Phys. A*, **237**, 507

[12] **Bardeen, J.M. 1970**, *ApJ*, **162**, 71

[13] **Bonazzola, S. & Schneider, J. 1974**, *ApJ*, **191**, 273

[14] **Butterworth, E.M. 1976**, *ApJ*, **204**, 561

[15] **Bonazzola, S., Goulgoulhon, E., Salgado, M. & Marck, J.A. 1993**, *A&A*, **278**, 421

[16] **Colpi, M., Shapiro, S.L. & Teukolsky, S.A. 1993**, *ApJ*, 414, 717

[17] **Komatsu, H., Eriguchi, Y. & Hachisu, I. 1989**, *MNRAS*, **237**, 355

[18] **Burderi, L., & D'Amico, N. 1997**, *ApJ*, **490**, 343

[19] **Cook, G.B., Shapiro, S.L., Teukolsky, S.A. 1994a**, *ApJ*, **423**, L117

[20] **Phinney, E.S., Kulkarni, S.R. 1994**, *Ann.Rev.Astron.Astrophys.*, **32**, 591

[21] **Stergioulas, N., & Friedman, J. 1995**, *ApJ*, **444**, 306

[22] **Woosley, S.E. & Timmes, F.X. 1996**, *Nucl.Phys. A*, **606**, 137

[23] **Miller, M.C. & Lamb, F.K. 1993**, *ApJ*, **413**, L43

[24] **Thomson, W. & Tait, P.G. 1883**, in *Principles of Natural Philosophy*, Oxford: Clarendon

[25] **Chandrasekar, S. 1970**, *Phys.Rew.Lett*, **24**, 611

[26] **Chandrasekar, S. 1970**, *ApJ*, **161**, 561

[27] **Ipser, J.R. & Lindblom, L. 1989**, *Phys.Rew.Lett*, **62**, 2777

[28] **Friedman, J.L. & Ipser, J.R. 1992**, *Phil.Trans.R.Soc.Lond.*, **340**, 391

[29] **Lindblom, L. 1987**, *ApJ*, **317**, 325

[30] **Cutler, C. & Lindblom, L. 1987**, *ApJ*, **314**, 234

[31] **Mendell, G. 1991**, *ApJ*, **390**, 530

[32] **Morsink, S.M., Stergioulas, N. & Blattnig, S.R. 1999**, *ApJ*, **510**, 854

[33] **Andersson, N. 1998**, *ApJ*, **502**, 708

[34] **Thorne, K.S. 1987**, in *300 years of gravitation*, eds. Hawking and Israel (Cambridge Univ. Press)

[35] **Andersson, N., Kokkotas, K.D., & Stergioulas, N. 1999**, *ApJ*, **516**, 307

[36] **Kokkotas, K.D. & Stergioulas, N. 1998**, *A&A*, **341**, 110

[37] **Sawyer, R.F. 1989**, *Phys.Rew.D*, **39**, 3804

[38] **Stergioulas, N. 1998**, *Rotating Stars in Relativity, Living Reviews in Relativity*, gr-qc/9805012

[39] **Lindblom, L., Owen, B.J., Morsink, S.M. 1998**, *Phys.Rev.Lett.*, **80**, 4843

[40] **Yoshida, Shin., Karino, S., Yoshida, Shij. & Eriguchi, Y. 1999**, astro-ph/9910532

[41] **Lindblom, L. & Mendell, G. 1999**, astro-ph/9909084

[42] **Rezania, V. & Maartens, R. 1999**, astro-ph/9909073

[43] **Bildsten, L. 1998**, *ApJ*, **501**, L89

[44] **van der Klijs, M. 1998**, in *The Many Faces of Neutron Stars*, eds. Alpar,Buccheri, van Paradijs, Dordrecht: Kluwer, 337

Chapter 4

Magnetic field evolution

Even a superficial inspection of the magnetic moment vs period ($\mu - P$) plane of pulsars shows two distinct groups of objects: a major population of sources with high values of μ and a smaller set of rapidly rotating pulsars with much lower magnetic moments. The origin of this dichotomy is one of the more puzzling issues in the physics of the neutron stars. After a short historical outline (section [4.1]), we will focus on the current ideas (section [4.2] and [4.3]) about the evolution of the surface magnetic field of a neutron star, highlighting the physical framework where this *Thesis* develops.

4.1 Historical and observational outline

Less than a couple of years after the discovery of the pulsars, Ostriker & Gunn (1969: [1]) proposed that the surface magnetic field of the pulsars should not be constant. With this assumption these authors were able to explain the absence of pulsars with periods much longer than 1 second (the decreasing of μ would bring the objects below the *death line*, switching off the radio emission [2]) and account for the claimed [3] decrease of the radio luminosity L_R as a function of the characteristic age τ_c (in the hypothesis $L_R \propto L_{bol} \propto \mu^2$). Their pioneeristic statistical studies suggested that the neutron stars at birth have very high magnetic moments $\mu \simeq 10^{29} \div 10^{31}$ Gcm^3, whose values decay exponentially in the subsequent evolution of the stars. In particular they interpreted the decay as due to ohmic dissipation of electrical currents in the neutron star interior, with a typical timescale [4]

$$\tau_\mu = 4\sigma R^2/\pi c^2 \ , \tag{4.1}$$

where R is the star radius and σ is the conductivity, supposed constant on time and uniform in the region of the star where the magnetic field resides.

Even with these simple considerations, the key-role played by the position where the magnetic energy is stored is evident.

- ⇝ Ostriker & Gunn adopted the value of the electrical conductivity for the crystallized crust of the star ($\sigma_{crust} \simeq 0.6 \times 10^{23}$ sec^{-1} [5]), thereby implicitly assuming that the magnetic field is mainly concentrated in the outer layers ($\rho < 10^{14}$ g cm^{-3}) of the compact object. In this case they obtained $\tau_\mu \sim 4 \times 10^6$ yr.

- ⇝ In the same year, Baym, Pethick and Pines (1969: [6]) argued that the magnetic field pervaded the entire star and so one had to adopt the much higher value of σ related to the core of the star, thus predicting decay timescale for the magnetic moment greatly exceeding the Hubble time. A result confirmed ($\tau_\mu > 10^{12}$ yr : [7]) in 1971 when different conductivities in the star interior were taken into account.

The hypothesis of an exponential μ-decay found its best apparent support a decade later from the measurements of the pulsar proper motions [8]. In 1982, Lyne, Anderson & Salter compared the characteristic ages τ_c with the kinematic ages $\tau_k = |z|/v_z$ for a sample of pulsars. The quantity z represents the height of the pulsar on the galactic plane, whereas v_z is the vertical component of the pulsar's speed. Since most pulsars are likely born in the galactic disk, and since they often switch off when crossing it again (the typical timescale for this process is $\sim 150 \times 10^6$ yr), we can satisfactorily conclude that $\tau_k \sim \tau_{true}$, being τ_{true} the true age of the pulsar. Lyne, Anderson & Salter found:

$$\tau_k = \frac{|z|}{v_z} < \frac{P}{2\dot{P}} = \tau_c \ . \tag{4.2}$$

Assuming that the initial spin period is much shorter than P, the ratio $P/2\dot{P}$ overestimates the true age τ_{true} of a source only if its magnetic moment decreases as the pulsar evolves: this is a model-independent confirmation of the decay of μ.

This scenario did not change until the early nineties, when a larger sample of objects and a better understanding of the distribution of the ionized component in the interstellar medium became available. The second item modified the estimations of the kinematic ages: in fact the values of $|z|$ are mostly obtained deriving the pulsar distance d from the observation of the dispersion measure DM (see section [A.1] for a more extended discussion about this quantity). The relation between d and DM depends on the volumetric density of free electron n_e along the line of sight from the antenna to the source. New results about the vertical distribution of n_e on the galactic plane implied that the previous values of $|z|$, hence τ_k, had been underestimated [9].

On the other hand, the larger number of known pulsars allowed for a refined statistical analysis of the population, including the finite scale height of the distribution of n_e and the selection effects in the pulsar surveys. Synthesized populations were produced with a Monte Carlo code assuming different hypotheses for the timescale of the magnetic moment decay. The resulting distribution functions of the many parameters (*i.e.* period, period derivative, flux, dispersion measure, galactic latitude, proper motions and so on) were compared with the observations. Different groups undertook this task: a first attempt by Narayan & Ostriker (1990: [10]) seemed to support evidence for a field decay, but later investigations [11] [12] [13] contrasted this result and the more recent calculations (see for example Hartman *et al.* 1997: [14]) appear to indicate that the observed pulsar population is compatible with a decay of the magnetic moment μ occurring on timescales $\tau_\mu > 10^8$ yr, that is longer than the typical active lifetime of these radiosources.

4.1.1 *Current observational facts*

Nowadays the results of the observations could be summarized as follows [15]:

(i) the isolated pulsars having high values of the magnetic moments ($\mu \sim 10^{29} \longrightarrow 10^{31}$ Gcm^3) do not show any significant decay of μ during their active life ($\lesssim 10^8$ yr) [11] [12] [13] [14];

(ii) the millisecond pulsars, the pulsars in globular clusters and most of the binary pulsars possess lower values of the magnetic moment, down to 7×10^{25} Gcm^3;

(iii) the low-μ objects do not undergo further significant field decay; this result is inferred from the old age of most among these still radioemitting sources ($\tau_{true} \gtrsim 10^9$ yr), implying that the timescale for the μ-decay is at least comparable with τ_{true} [16] [17] [18] [19].

4.2 The origin of the low values of the magnetic moment

4.2.1 *Low values of μ at birth?*

In order to understand the origin of magnetic moment values spanning an interval larger than 5 order of magnitude, the simpler option would be the assumption that high and low field objects form two branches of a bimodal distribution of magnetic moments at the birth of the neutron stars, *i.e.* the low μ pulsars are born just with low fields. The strong age distinction among the two groups, the high-μ stars being at least ten times younger than the low-μ ones (see item (i) and

(iii) of the section [4.1.1]), the different fraction of binarity and other contrasting characteristics of the two subpopulations (proper motions, velocities [20], rotational periods and so on) are very hard to reconcile with a unique mechanism of formation and evolution.

4.2.2 *Spontaneous decay?*

Another possibility would call for a spontaneous decay of the magnetic field over variable timescales: if at the beginning μ decreases very slowly and later the decay becomes much faster, hopefully one could explain both the point (i) and the point (iii) of section [4.1.1]. Indeed, many refined models for the evolution of μ flourished in the last decade. In section [4.3] we will report on the basic statements and the equations used for these calculations. Here we briefly discuss critically the results. A first improvement was to abandon the hypothesis of a uniform conductivity in the crust of the star; for example Yakovlev & Urpin in 1980 [21] calculated and showed a substantial increase of σ when moving from the outer liquid layers to the deeper crystallized crust. As a consequence, Sang & Chanmugam showed in 1987 [22] that the decay of a field residing only in the crust is not strictly exponential: the reason for this is that, in addition to the ohmic field decay, there is also an inward diffusion of the field towards region of higher σ and thus longer decay timescale. Due to the large uncertainties in the depth penetrated by the initial field, Sang & Chanmugam [22] pointed out that the magnetic moment can decay much more quickly if, at birth, it resides in the outer lower density regions of the crust. This result is clearly displayed in Figure 4.1.

The inclusion in the calculation of the cooling history of the neutron star was a second major improvement in modeling the evolution of a crustal magnetic field. Indeed, the conductivity σ at any depth in the crust is strongly affected by the local temperature, and in general is increasing as the star cools. Thus the calculation must adopt a time dependent value for the conductivity, which in general is a function both of the time t and of the radial position r inside the star $\sigma = \sigma(t, r)$. A first attempt to account for the thermal evolution of the neutron star was performed in 1990 [24], but a more extended investigation was that of Urpin & Muslimov (1992: [25]) and Urpin & Konenkov (1997: [26]). They confirmed the non exponential behaviour of the decay, showing that the slower the cooling of the star the faster the decrease of its magnetic moment. Figure 4.2 depicts the decay of the surface magnetic field B_S for different values of the impurity parameter Q (see section [5.2] for an extended discussion of this quantity) and various initial depths penetrated by the field.

Examining Figure 4.2, we see that the prescribed decay occurs in three different stages. A first short phase ($\lesssim 10^6$ yr) of comparatively rapid decay, during which μ could be reduced from the values $\sim 6 \div 30 \times 10^{30}$ Gcm^3, typical for pulsars in supernova remnants, to the standard values $\sim 1 \div 3 \times 10^{30}$ Gcm^3 of the bulk

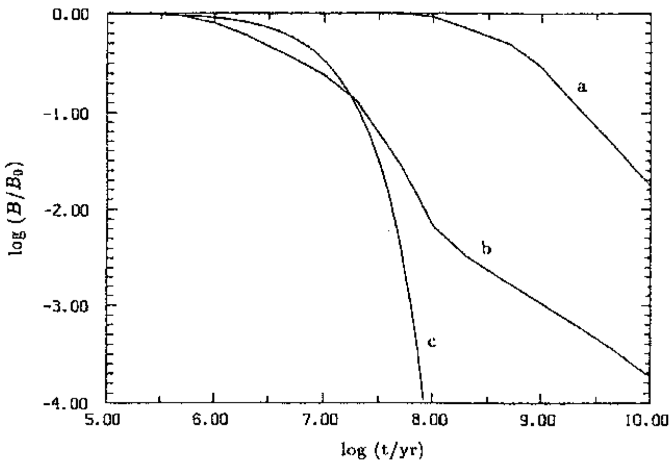

Figure 4.1: Ohmic field decay curves calculated by Sang & Chanmugam. Curve a represents the case of an initial magnetic field occupying the whole crust, whereas curve b refers to a field which initially penetrates the crust only down to the density $\rho \leq 4 \times 10^{13}$ gcm^3. An exponential decay with timescale of 9.1×10^6yr is plotted for comparison in curve c [23].

of the normal pulsars population. In the next $10 \div 300$ Myr the field decay curves flatten, implying a negligible reduction of μ during the active life of a pulsar. In the last stage of the evolution the curves assume a power-law shape. These different behaviours depend on changes in the conductivity regimes. At the beginning σ is determined by the electron-photon scattering in the region where the currents circulate. In the second phase the electron-impurity scattering (almost independent on the temperature) dominates, whereas in the last phase the decay is mainly governed by the diffusion of the field down to the crust-core boundary.

Since 1971, it is well known that the ohmic dissipation cannot produce a significant decay of the magnetic field of a pulsar if the bulk of the magnetic energy is stored in its core [7]. This result was extended by Pethick & Sahrling in 1995 [27]: if the field penetrates the inner region of the star, the ohmic decay timescale must be longer than the Hubble time, even in the most favourable situation of currents completely confined in a low conductive crust.Therefore an alternative scenario was proposed that allows for a reduction of μ in the hypothesis of a core magnetic field.

We will give details about this approach in the following section [4.3.2]; basically it assumes that the magnetic field in the core of a neutron star is stored in quantized fluxoids. They can be dragged by the movement of the vortices, quantized units carrying the angular momentum of the star.

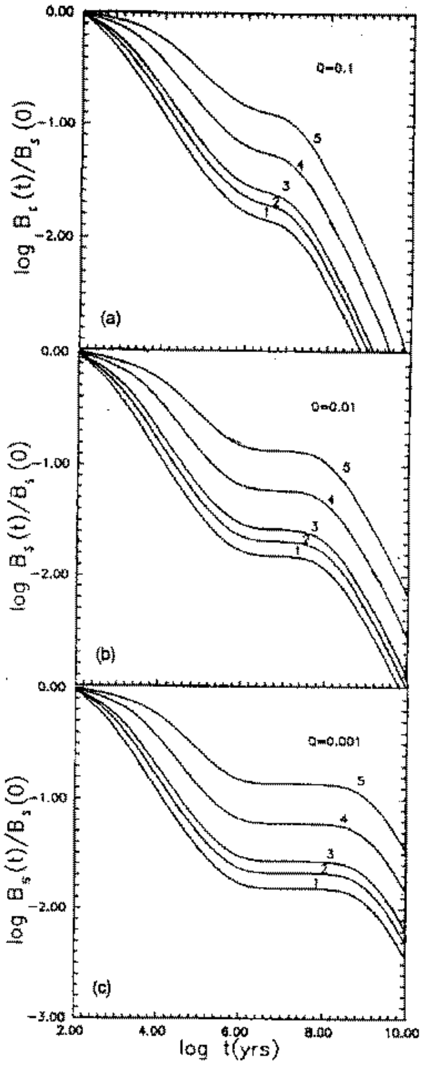

Figure 4.2: Ohmic field decay curves calculated by Urpin & Muslimov. The three panels refer to different values of the impurity content Q. The curves are labeled from 1 to 5 according to increasing initial depth penetrated by the magnetic field [25].

When the neutron star spins down (for example as a consequence of magnetodipole emission), the vortices shift away from the rotational axis of the star and the fluxoids are forced to follow them. Thus a fraction of the fluxoids approach the core-crust boundary, where they vanish due to the much lower local electrical conductivity [28]. In summary, in this framework the spin history of the star drives and controls the changes of the magnetic field. Assuming an almost instantaneous decay of the fluxoids when they reach the core-crust interface, one obtains just a linear relation between the fractional decrease of the magnetic moment and the fractional decrease of the angular velocity of the star. Introducing this dependence in the magnetodipole emission formula, the time evolution of μ can be simply expressed by a power-law with index $-1/4$ [29] [30]. Accounting also for the relaxation time of the fluxoids in the crust, Miri [31] obtained the paths, in the $B_S - P$ diagram, of isolated pulsars undergoing this *magnetodipole spin-down-induced* evolution. Figure 4.3 reports the results for different initial values of the surface magnetic field B_S (we remind that $\mu = 10^{30}$ Gcm^3 corresponds to $B_S \sim 10^{12}$ G, depending slightly on the neutron star model). The power law with index $-1/4$ is clearly visible for pulsars having low magnetic field at birth. So, in this model, they would experience a restricted slower decay with respect to the almost exponential evolution of the objects born with high fields.

Unfortunately, up to now it is not possible to perform a reliable statistical test of all the models presented in this section [4.2.2]. They predict clearly distinct evolutionary paths only during the early stage of the pulsar life, namely during the first 10^6 yr after the birth. Therefore a large sample of young neutron stars is requested to compare them. Up to now, the pulsar catalog lists only an handful of such objects, being the observed pulsar population dominated by elder sources, with characteristic time of few 10^7 yr. In such situation, there is no statistical clue for rejecting the hypotesis of a non decaying field. Some of the surveys in progress, namely the one running at Parkes [32], devoted to the search of young pulsars, could hopefully change this unpleasant situation in the next years.

However, **no one of the spontaneous decay models** proposed so far **can explain magnetic moments of** 10^{26} **Gcm**^{3}, which are typical of the millisecond pulsars. In order to attain these values of μ within a Hubble time, the crustal models would require that the currents are located only in a narrow outer part of the crust at $\rho < 6 \times 10^{10}$ gcm^{-3}, a very unlikely possibility. The spin-down-induced models predict a decrease in μ of at most two orders of magnitude with respect to the initial values, as illustrated in Figure 4.3.

4.2.3 *Decaying in binaries?*

In view of our current knowledge about pulsars, one major common characteristic allows to group the low field objects: **all the pulsars with low magnetic moment spent a part of their life in a multiple stellar system**. In section

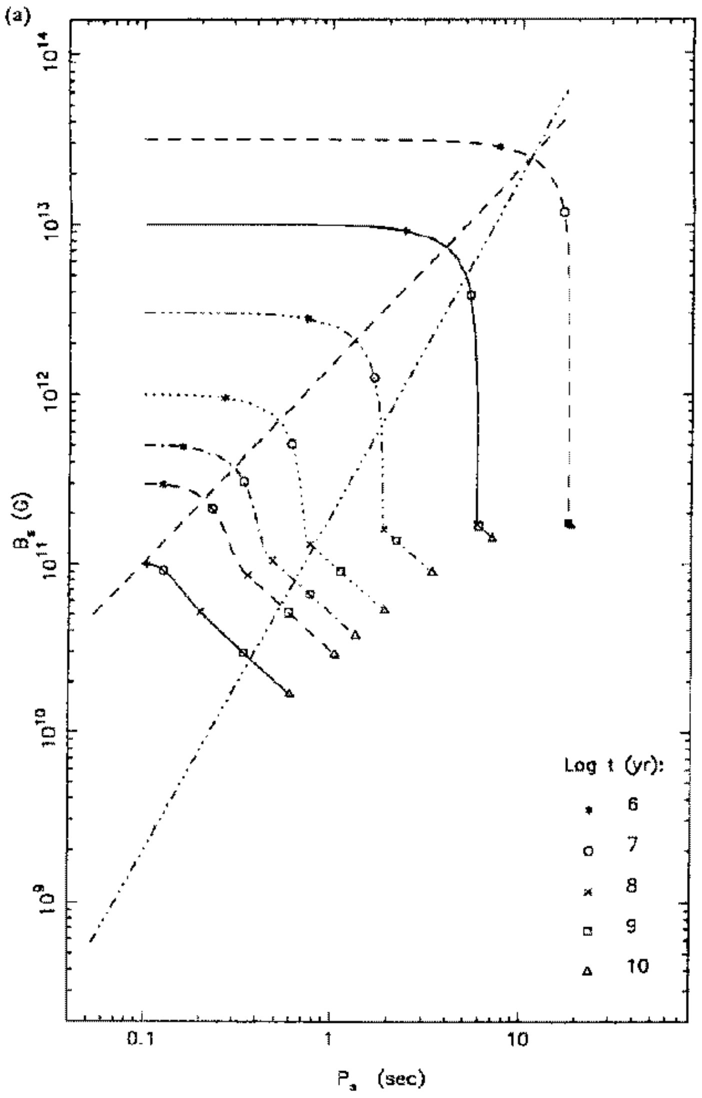

Figure 4.3: The evolutionary paths followed in the plane $B_S - P$ by the *isolated pulsars*, according to the spin-down induced magnetic field decay scenario. The power-law decay with index $-1/4$ involves only the neutron stars having at birth a surface magnetic field of the order $\lesssim 5 \times 10^{11}$ G. The *triple-dot-dashed line* is the *death line*: radio emission is allowed only on its left side. [31].

[2.2.3], we presented the current paradigm about the origin of the millisecond pulsars: they are old neutron stars recycled in binaries. Similar consideration are valid for the pulsars embedded in the globular clusters, where the chance of stellar encounters (with formation of binary systems) is much higher than in the galactic field, and a neutron star can be included in a binary system even after a long time spent as an isolated object. Guided by this fact, many authors have tried to relate the low values of μ with the interactions occurring between the neutron star and its companion star in a binary system. We will deal with these attempts in the next section [4.3].

4.3 μ-evolution in binaries: the current ideas

Unluckily, there is no comprehensive theory for the birth and for the evolution of the magnetic moment in a neutron star. Therefore two different classes of physical scenarios have been proposed up to now, according to where the bulk of the magnetic energy is stored.

I. CRUSTAL MAGNETIC FIELD $\Longrightarrow$ **accretion driven scenario**

II. CORE MAGNETIC FIELD $\Longrightarrow$ **spin driven scenario**

4.3.1 *Accretion driven decay*

The onset of a thermomagnetic instability, which transforms heat into magnetic energy during the early phases, is an effective tool to produce strong fields in the crust of a NS [33] [34]. Although that instability is not yet completely explored for poloidal fields, it is a plausible mechanism which does not depend on special assumptions and may account for the observed variety in the NS magnetic field strengths. Moreover, the assumption of a crustal magnetic field is in accordance with the general accepted evolutionary scenarios for isolated NSs [35], NSs in low mass binaries [36], NSs in high mass binaries [37], millisecond pulsars [38] and could account also [39] for the evolution of the Anomalous X-ray Pulsars (AXPs: [40] [41]).

A first observational suggestion about the effects of the accretion on a (crustal) magnetic field was given in 1986 by Taam & van den Heuvel [42]: they noticed a rough dependence of the surface magnetic field B_S on the amount of mass accreted onto the neutron star (see Figure 4.4).

Three years later, Shibazaki *et al.* [43] presented an empirical formula accounting for the effects of the accreted mass:

$$\mu = \frac{\mu_0}{1 + \frac{\Delta M_{acc}}{m_B}} \tag{4.3}$$

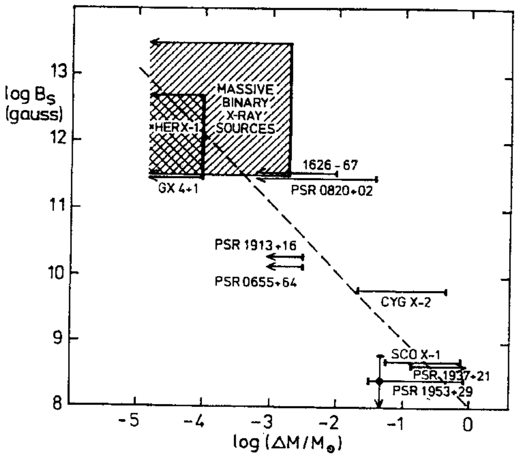

Figure 4.4: The original plot by Taam & van dev Heuvel, where a relation between the surface magnetic field B_S and the amount of accreted mass appears. [42]. The objects included are either radiopulsar and X-ray pulsars.

where μ_0 represents the initial (before accretion starting) magnetic moment, ΔM_{acc} is the amount of accreted mass and m_B a parameter to be fitted with the observations. These authors claimed that $m_B \sim 10^{-4}\mathrm{M}_\odot$ could reproduce the Taam & van den Heuvel's correlation. Zhang, Wu & Yang [44] [45] gave physical foundation to the equation (4.3) assuming that the compressed accreted matter has ferromagnetic permeability. However, using a larger database Wijers [46] showed in 1997 that no model in which the μ-decay is function only of ΔM_{acc} is consistent with the available data both on X-ray binaries and recycled pulsars.

In 1990 Romani [47] first introduced the accretion rate $\dot{M}_{acc}$ as a second parameter in driving the magnetic moment decay. He pointed out that the accretion produces two major effects: (i) heating of the crust (depending on $\dot{M}_{acc}$), which determines a lowering of the conductivity (and in turn a hastening of the ohmic decay) and (ii) advection of the magnetic field lines, trapped by the underlying crust and screened by the diamagnetic accreted material. As a result, the final value of μ depends both on ΔM_{acc} and on $\dot{M}_{acc}$. Moreover, the dragging of the field lines stops when $\mu \lesssim 10^{27}$ Gcm^3, resulting in an asymptotic values for the magnetic moment.

The existence of a bottom field was suggested also by Burderi, King & Wynn [48] on the basis of a semi-empirical model by Arons & Lea [49]. They proposed that the currents developed in the diamagnetic blobs of accreted matter can neutralize the currents sustaining the surface magnetic field of the neutron star. The process ends when accretion halts, typically when the accretion disk (whose internal radius depends on a positive power of the decaying magnetic moment: see section [2.3.4]) skims the neutron star surface. This leads to a natural lower limit for the residual field:

$$\mu_{bottom} = 1.04 \times 10^{26} \ \phi^{-7/4} \ R_6^{9/4} \ M^{1/4} \ \dot{M}_{acc,EDD}^{1/2} \tag{4.4}$$

where ϕ is of order unity, R_6 is the neutron star radius in units of 10^6 cm, M is the neutron star mass in solar masses and $\dot{M}_{acc,EDD}$ is the accretion rate in units of Eddington masses. Such relation $\mu \propto \dot{M}_{acc}^{1/2}$ was claimed [50] to have an observational support on the basis of the energy spectra of the Low Mass X-ray Binaries and of the properties of the kilohertz QPOs [51] seen in the power spectra of most of these sources.

The first fully consistent theoretical calculations of the accretion-induced-decay of the crustal magnetic field of a neutron star were performed by a team composed by Urpin, Geppert & Konenkov in the years 1994-1997 [52] [53] [54] [55]. The basic physical mechanism is the **ohmic decay and the diffusion of a magnetic field** sustained by currents circulating the non superconducting crust of the star.

The relevant equations are:

$$\frac{\partial \vec{B}}{\partial t} = - \ c \ \vec{\nabla} \wedge \vec{E} \quad eq. \ Faraday - Neumann - Lenz \tag{4.5}$$

$$\frac{\partial \vec{E}}{\partial t} = c \ \vec{\nabla} \wedge \vec{B} \ - \ 4\pi \vec{J} \qquad eq. \ Ampère \tag{4.6}$$

$$\vec{J} = \sigma \left(\vec{E} + \frac{\vec{v}}{c} \wedge \vec{B} \right) \qquad eq. \ Ohm \ for \ moving \ fluids \tag{4.7}$$

Neglecting $\partial \vec{E}/\partial t$, from the second and the third equations one gets:

$$\vec{E} = \frac{c}{4\pi\sigma} \vec{\nabla} \wedge \vec{B} - \frac{\vec{v}}{c} \wedge \vec{B} \tag{4.8}$$

and thus the *induction equation*:

$$\frac{\partial \vec{B}}{\partial t} = -\frac{c^2}{4\pi} \nabla \wedge \left(\frac{1}{\sigma} \nabla \wedge \vec{B} \right) + \nabla \wedge (\vec{v} \wedge \vec{B}) \tag{4.9}$$

where $\vec{E}$, $\vec{B}$ and $\vec{J}$ are the electric field, the magnetic induction and the current density, whereas $\vec{v}$ is the velocity of the moving fluid ($=$ 0 if no accretion occurs, $|\vec{v}| = \dot{M}_{acc}/4\pi r^2 \rho$ for a radial approximation of the accreted fluid inflow). They assumed *the core of the neutron star to be superconductive*, *thus the magnetic field cannot penetrate into it* (in the following of this *Thesis* we will refer to this boundary condition for the magnetic field at the crust-core interface as **BC I**) and solved the induction equation considering the poloidal component of a dipole field. The microphysics included in the calculation as well as the numerical recipes for performing it are fully described in sections [5.2.2] and [5.2.3]. Here we report the main consequences.

The accretion affects the spontaneous ohmic decay (described in section [4.2.2] and depicted in Figure 4.2) in the two following ways:

1. the HEATING of the crust, implying a reduction of σ, greatly SPEEDS UP THE DECAY;

2. the TRANSPORT OF THE MATERIAL into deeper layers, where σ is higher, SLOWS DOWN THE DECAY.

The detailed balance among the two effects depends on other physical parameters, such as the initial depth penetrated by the currents, the impurity content, the accretion rate, the duration of the accretion phase and the equation of state of the nuclear matter. In particular, since (see the induction equation (4.9)) the typical decay timescale $\tau_\mu \sim \Delta B/\Delta t$ depends on the lengthscale of the magnetic field $l_\mu \sim \Delta B/\Delta r$,

$$\left|\frac{\Delta B}{\Delta t}\right| \simeq \left|\frac{\Delta B}{\Delta r}\right|^2 \tag{4.10}$$

the softer the equation of state (implying a thinner crust and so a smaller l_μ), the quicker the decaying of μ.

In the frame of this *Thesis*, we are mainly interested in the evolution of the magnetic moment of a neutron star in a binary system with a low mass stars. Urpin, Geppert & Konenkov [36] dealt with this subject first in 1998, coupling the magnetic history of the star to its spin evolution. Calling for an accretion induced ohmic decay of μ, they found that **neutron stars with more or less standard magnetic moments and spin periods can evolve to low-field rapidly rotating objects**. A typical evolution is displayed in Figure 4.5, where the surface magnetic field, the rotational period and the surface temperature are plotted versus time, splitting the evolution in the first four fundamental stages of the recycling scenario (described in section [2.3]), namely: *ejector (I), propeller (II), wind accretion (III)* and *Roche-lobe overflow (IV)*.

The properties of the nuclear matter at the interface between the crust and the core of a neutron star (typical density $\simeq 2 \times 10^{14}$ gcm^3) are still an open issue for the theorists. Going through that layer, the matter should become superfluid and superconductive, but it is quite difficult to assess how these phase transitions are affected (and/or react) in presence of an ultrastrong magnetic

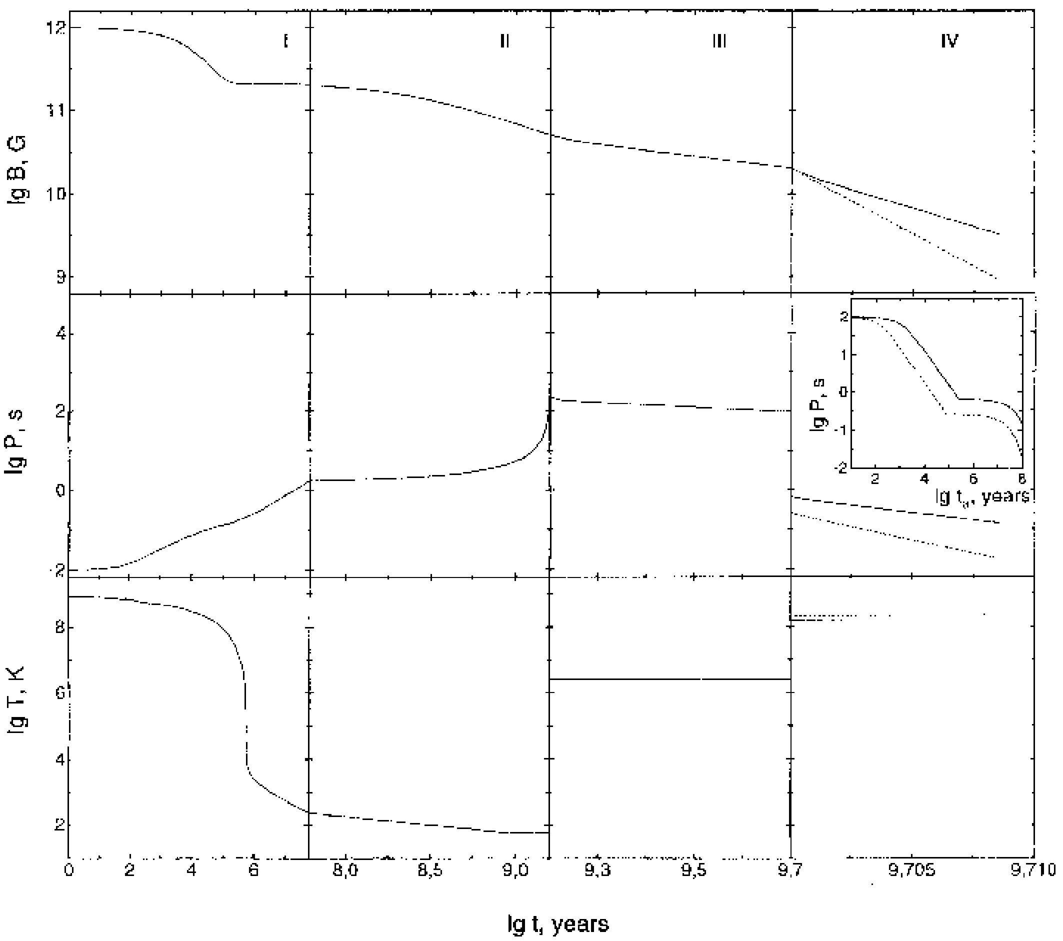

Figure 4.5: Magnetic, rotational and thermal evolution of a $1.4\ \mathrm{M}_\odot$ neutron star with surface magnetic moment of 10^{12} Gauss at birth. The adopted equation of state is the PS-EoS (a stiff one). The initial depth of the currents is $10^{13}\ gcm^{-3}$ and the impurity parameter $Q = 0.01$. The rate of accretion from stellar wind (phase III) is $2/3 \times 10^{-8}\dot{\mathrm{M}}_{\mathrm{EDD}}$, and the lifetime of the companion star on the main sequence is 5×10^9 yr. During the phase IV, the accretion rate is $2/3 \times 10^{-3}\dot{\mathrm{M}}_{\mathrm{EDD}}$ (*solid line*) or $2/3 \times 10^{-2}\dot{\mathrm{M}}_{\mathrm{EDD}}$ (*dotted line*). The phase IV lasts 10^8 yr. The inserted panel enlarges the spin evolution during the very short phase at the boundary between phase III and phase IV, that is when the Roche-lobe overflow sets in. From [36].

field. In view of these uncertainties, Konar & Bhattacharya [15] choose a different boundary condition at the crust-core interface for solving the equation (4.9). They noticed that the deposition of accreted matter on top of the crust can imply the assimilation of original current-carrying crustal layers into the superconducting core of the neutron star. In particular they assumed [15] the *newly formed superconducting material to retain the competing magnetic flux* in the form of Abrikosov fluxoids [6] rather than to expel it through the Meissner effect (in the following of this *Thesis* this boundary condition will be labeled as **BC II**). As a consequence, further decay of the magnetic flux is stopped. Within this model the effects of the accretion on the evolution of μ are three-fold:

1. the HEATING of the crust, implying a reduction of σ, greatly SPEEDS UP THE DECAY;
2. the TRANSPORT OF THE MATERIAL into deeper layers, where σ is higher, SLOWS DOWN THE DECAY;
3. the ASSIMILATION OF MATERIAL into the core, where the conductivity is huge, FREEZES THE DECAY.

As displayed in Figure 4.6, also **this hypothesis allows for a reduction of the surface magnetic field of more than 4 orders of magnitude** in 10^8 yr, easily accounting for the low μ of the millisecond pulsar population. Likewise for the boundary condition adopted by Urpin, Geppert & Konenkov [55], it emerges that the decay of μ depends not only on the total accreted mass, but also on the accretion rate itself. However, in this case **the higher the accretion rate**, the stronger the pushing of crustal material into the core and thus **the sooner the freezing of the decay**. In a subsequent paper [56], it was claimed that such a positive correlation between the accretion rate and the final value of μ is supported by some observational evidence [50] [51].

Other refinements of the accretion-induced decay scenario include the study of the effects of a non spherical symmetric accretion [57], the evolution of multipoles at the neutron star surface [57], the postaccretion increase of μ due to the rediffusion of the buried field towards the surface [58], and the relativistic corrections to the decaying history [59]. All together, they produce only slight changes to the results by Urpin, Geppert & Konenkov or by Konar & Bhattacharya; so we leave them to more extended reviews (see for example [60] [61]).

Both the calculations of Urpin, Geppert & Konenkov [36] and those of Konar & Bhattacharya [56] showed that the distribution of the final values μ and P attained by neutron stars recycled in low-mass binaries may be very wide, according to all the parameters involved. This conclusion **suggests the necessity of a statistical approach for studying the effectiveness of this scenario in producing ultra fast rotating objects**: in this *Thesis* we have built a Monte-Carlo code, simulating large populations of objects; their evolutionary parameters either have been randomly chosen in the observed intervals or (when

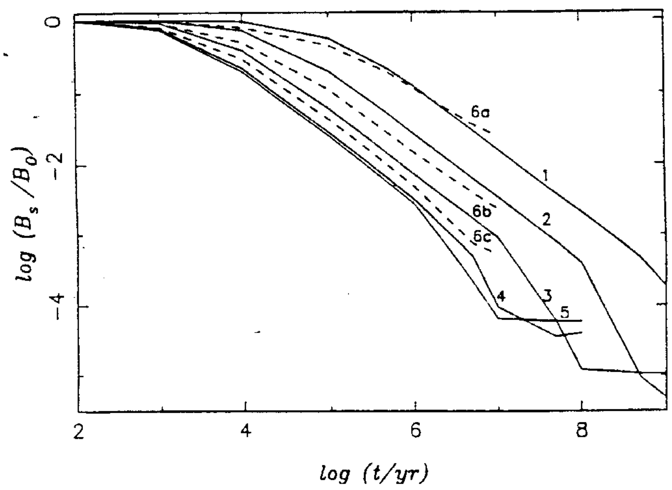

Figure 4.6: Evolution of the surface magnetic field of a $1.4\ \mathrm{M}_\odot$ neutron star undergoing accretion at six different levels. From *1* to *6* we have $\dot{M}_{acc} = 2/3 \times 10^{-5}; 2/3 \times 10^{-4}; 2/3 \times 10^{-3}; 2/3 \times 10^{-2}; 1.3 \times 10^{-2}; 2/3 \times 10^{-1}\ \dot{\mathrm{M}}_{\mathrm{EDD}}$. The three *dashed* curves for the case *6* corresponds to different hypothesis about the surface temperature of the star. The flattening of the curves for the higher accretion rates is clearly visible [15].

the direct observation is impossible) were dealt as free parameters, whose values label different models. As an example, one can look at Figure 4.7: varying the duration of the main sequence lifetime of the companion star, the surface magnetic field of a neutron star undergoes different degrees of decay before the Roche-lobe overflow begins. As a result, at the beginning of the phase IV the fields of a population of objects span the range $2 \times 10^9 \longrightarrow 5 \times 10^{10}$ Gauss.

4.3.2 *Spin driven decay*

Both the simple idea of the flux conservation during the gravitational collapse and the action of a dynamo in the convective proto-neutron star [62] lead to the existence of a magnetic field penetrating the whole neutron star. The crust occupies only a tiny fraction of the volume of the star, and thus the changings of μ are guided by the evolution of the magnetic field in the core. Due to the huge conductivity of the core matter, no ohmic decay occurs during Hubble time and so other models have been invoked to account for the population of low field neutron stars.

The rotating core of a neutron star should be composed mainly of superfluid neutrons with a much smaller fraction of superconductive protons [6]. The angular momentum of the core is believed to be carried by [63]

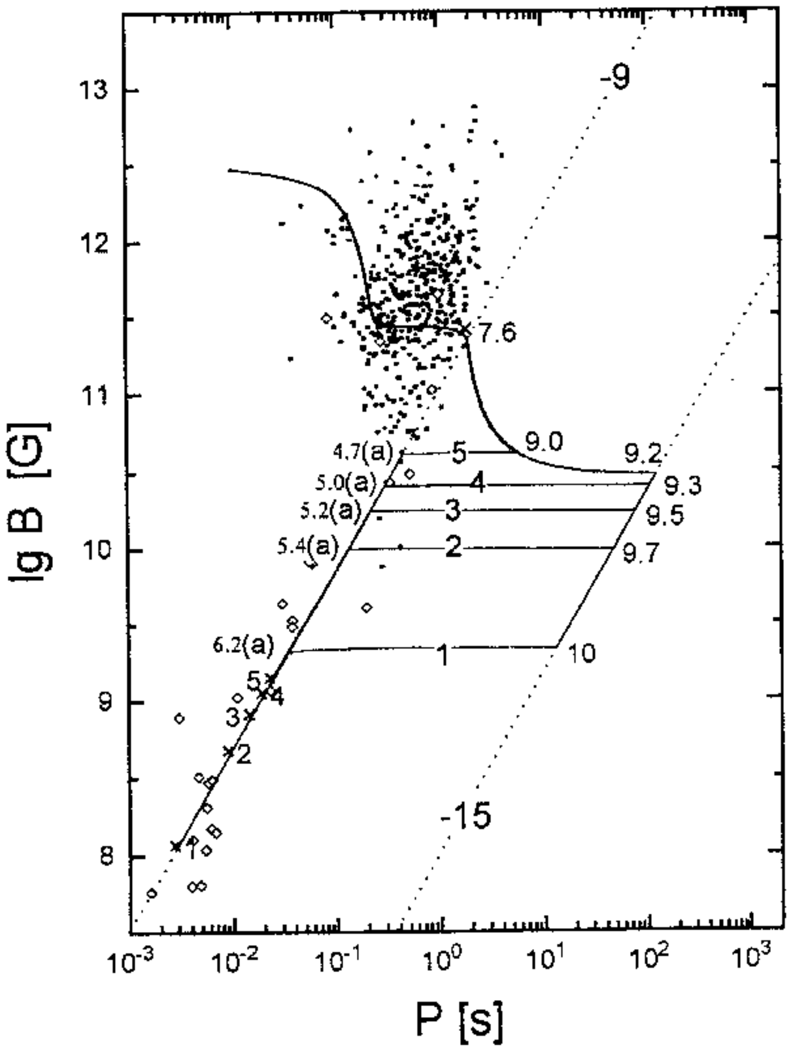

Figure 4.7: The evolutionary tracks of neutron stars in the plane $B_S - P$ for different durations of the evolution (labeled by the numbers on the right of the curves, in $log_{10}(yr)$) during the phases I+II+III+IV. The initial surface magnetic field is 3×10^{12} *Gauss*, the impurity content $Q = 0.03$, the other parameters as in Figure 4.5 [55].

$$N_{vortex} \simeq \frac{2 \times 10^{16}}{P_{\rm sec}} \tag{4.11}$$

neutron vortex lines, parallel to the spin axis of the core; in order for the core to spin down, the total number of these entities has to decrease through an outward radially motion. The magnetic flux should be confined in $N_{fluxoid}$ quantized proton flux tubes, where

$$N_{fluxoid} \simeq 10^{32} B_{C,13} \tag{4.12}$$

with $B_{C,13}$ being the average field strength in the core, expressed in units of 10^{13} Gauss. A decreasing of $N_{fluxoid}$ determines a reduction of the magnetic field in the core. Furthermore, the vortices and the fluxoids may act as pinning sites for one another [64].

In 1990, Srinivasan *et al.* [28] suggested that the interpinning between these quantized entities causes the fluxoids to be carried and deposited in the crust as the neutron star spins down: in fact, the vortices decrease in number by migrating outwards and they may drag the flux tubes along. The magnetic flux penetrated into the crust will then decay due to ohmic dissipation and the surface magnetic field of the neutron star keeps decreasing until it relaxes at the value of the residual field in the core. As a first approximation, Srinivasan *et al.* assumed the same radial velocity for both the fluxoids and the vortices. This means that $\Delta N_{fluxoid}/N_{fluxoid} = \Delta N_{vortex}/N_{vortex}$, which, in turn implies

$$\frac{\delta B_C}{B_C} = \frac{\delta P}{P} = \frac{\delta \Omega}{\Omega} \tag{4.13}$$

where Ω is the angular velocity of the neutron star. Assuming an instantaneous decay in the crust, one would have also

$$\frac{\delta B_C}{B_C} = \frac{\delta \mu}{\mu} \tag{4.14}$$

Introducing the (4.13) and the (4.14) into the magnetodipole spin down formula

$$\frac{d}{dt}\left(\frac{1}{2} I \Omega^2\right) = - \frac{2}{3c^3} \mu^2 \Omega^4 \tag{4.15}$$

one can integrate to

$$\mu = \mu_0 \left(1 + \frac{t}{\tau_{sif}}\right)^{-1/4} \tag{4.16}$$

where the typical μ-decay timescale is given by

$$\tau_{sif} = \frac{3c^3 I}{8\mu_0^2 \Omega_0^2} = 8 \times 10^6 \; \frac{P_0^2 \; I_{45}}{\mu_{0,30}^2} \; \mathrm{yr} \tag{4.17}$$

with P_0 (in seconds), Ω_0 and μ_0 being the spin period, the angular velocity and the magnetic moment at the beginning of the spin down process, whereas I_{45} represents the moment of inertia of the star in units of 10^{45} gcm^2. The equation (4.16) accounts for the power-law decay of the isolated pulsars having low magnetic moments at their birth ($\mu_{0,30} < 0.1$, see the lower tracks of Figure 4.3). Since the ohmic decay timescale $\tau_{crust-core}$ at the bottom of the crust is not negligible, the magnetic evolution must be described by a more general array of equations:

$$\left\{ \begin{array}{l} \left\{ \begin{array}{lll} \frac{\dot{B}_C}{B_C} = -\frac{\dot{P}}{P} & \text{if} & \dot{P} > 0 \\ \\ \dot{B}_C = 0 & \text{if} & \dot{P} \leq 0 \end{array} \right. \\ \\ \dot{B}_S = -\frac{1}{\tau_{crust-core}} \left(B_S - B_C \right) \end{array} \right. \tag{4.18}$$

As a consequence, there will be an exponential decay phase (on timescales $\sim \tau_{crust-core}$) until the surface field matches the field in the core: this feature appears clearly in Figure 4.3 for the case of the higher initial fields [31]. Dealing with the evolution of isolated objects, we have already noticed that this *Spin down Induced Flux expulsion* model (SIF model) cannot explain the very low magnetic moments of the millisecond pulsar population.

In the case of neutron stars in binary system, the scenario changes due to presence (besides magnetodipole emission) of a further long and much more effective phase of spin down: the so-called *propeller* phase (stage II in the recycling scenario) during which the interaction between the magnetosphere of the neutron star and the wind from the companion can extract angular momentum from the compact object transferring it to the wind matter. Miri & Bhattacharya [65] and Miri [31] explored the cases of wide and close binary systems: in summary, the magnetic moment $\mu_{post-acc}$ at the end of the Roche lobe overflow process (that is when the accretion switches off) and the final magnetic moment μ_{final} can be predicted according to:

$$\left| \begin{array}{lll} \mu_{final} & = & \left(\frac{P_0}{P_{max}} \right) \mu_0 \\ \\ \mu_{post-acc} & = & \left(\mu_0 - \mu_{final} \right) \mathrm{e}^{-t_{ms}/\tau_{crust-core}} + \mu_{final} \end{array} \right. \tag{4.19}$$

where P_{max} is the longest spin period attained during the evolution of the system

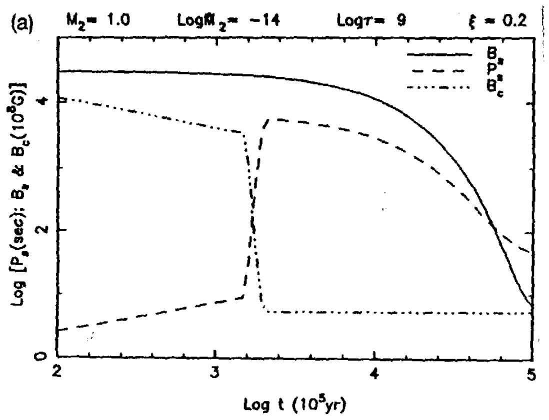

Figure 4.8: Evolution of the spin period P_S (*dashed line*) and of the core B_C (*triple dotted-dashed line*) and surface B_S magnetic field (*solid line*) of a neutron star embedded in a low mass binary with a companion star of $1\ \mathrm{M}_{\odot}$, losing matter in a wind at a rate of $2/3 \times 10^{-6}\dot{\mathrm{M}}_{\mathrm{EDD}}$. A ohmic decay timescale in the crust $\tau_{crust-core} = 10^9$ *yr* is assumed. The efficiency in the extraction of angular momentum from the star due to magnetosphere-wind interaction is set equal to 20% [65].

(usually the one at the end of the propeller stage) and t_{ms} is the main-sequence lifetime of the companion. For the case of low-mass binary systems, it should be $t_{ms}/\tau_{crust-core} \gtrsim 10$ and so, from (4.19) one obtains $\mu_{final} \simeq \mu_{post-acc}$; hence no further μ-decay occurs during the millisecond pulsar era. Assuming that the propeller effect can spin the star down to $P \lesssim 10^3$ sec, one gets a typical final magnetic moment

$$\mu_{final} \simeq \frac{0.1 \div 1 \text{ sec}}{1000 \text{ sec}}\, \mu_0 \simeq 10^{-4} \div 10^{-3}\, \mu_0 \simeq 10^8 \div 10^9 \text{ Gauss} \qquad (4.20)$$

compatible with the values observed for the millisecond pulsars population. The evolution of P, B_C and B_S for such a situation is reported in Figure 4.8.

For the case of high mass binary systems, $t_{ms}/\tau_{crust-core} < 1$ and so, from (4.19) one gets $\mu_{final} < \mu_{post-acc}$, that is the SIF model predicts *a still decaying magnetic moment for the case of pulsars recycled in binaries with high mass companions.* Within this SIF model, Miri [31] claimed the possibility of reproducing the observed distribution of points both in the diagram of the surface magnetic fields of the recycled neutron stars versus their orbital periods (for low-mass systems) and the diagram of spin periods versus orbital periods (for the high-mass systems), provided a crustal ohmic timescale $\tau_{crust-core} \sim 10^7$ yr.

Following an earlier suggestion of Ding, Chen & Chau [66], in 1999 Miri [67] improved his calculation, accounting for a detailed balance of the forces acting on the fluxoids in the interior of a neutron star: pinning and buoyancy forces show up to be the most relevant. In this dynamical description, the radially drift velocities of vortices and fluxoids are no more equal, but the overall results of the Force Balance Equilibrium model (FBE model) seem to be in close agreement with the results of the simpler SIF model.

Recently, Konar & Bhattacharya [68] re-examined the SIF scenario in the case of accreting neutron stars, incorporating the crustal microphysics and the material movements due to the accretion. They concluded that the model can reproduce the values of μ observed in the low-mass systems only for large values of the unknown impurity parameter $Q \gtrsim 0.05$ (in contrast with the *accretion driven decay* models, requiring $Q \lesssim 0.01$). Were the wind accretion phase short or absent, Q should even excess unity.

A more serious objection to this model was risen by Konenkov & Geppert [69]: they pointed out that the motion of the proton flux tubes in the core leads to a distortion of the field structure near the crust-core interface and this in turn creates a back-reaction of the crust on the fluxoids expulsion: accounting for this effect, it results that (i) the SIF can be adequate for describing the μ-evolution only for weak initial magnetic moments ($\mu_0 \lesssim 10^{29}$ Gcm^3) and (ii) the predicted correlation $\mu_{final} \propto P_{max}^{-1}$ (see equation (4.19)) is no more justified.

An early version of our population synthesis code (fully described in Chapter 5) was applied to the SIF model in 1998. It emerged that the population of synthesized objects clusters between 0.01 and 1.0 seconds, the millisecond population is spare and the region below $P = 1.56$ ms devoid of neutron stars [70]. Due to the many theoretical uncertainties of the SIF scenario and in view of such preliminary results, in this *Thesis* we focused on the *accretion induced decay* of the magnetic field, leaving to future investigations the detailed statistical examination of the *spin induced decay* scenarios.

Finally, we have to mention another class of models in which the magnetic evolution is strictly related with the spin history of the star: in 1991 Ruderman [71] [72] proposed that the coupling among P and μ could take place via crustal plate tectonics. The rotational torques acting on the neutron star cause the crustal plates to migrate, thus dragging the magnetic poles anchored in them. As a consequence the effective magnetic dipole moment can strongly vary, either in intensity (decreasing or growing) and in direction, suggesting a tendency to produce an overabundance of both orthogonal (spin axis $\perp$ magnetic axis) and nearly aligned rotators (spin axis $\|$ magnetic axis). Current observation of disk population millisecond pulsars seem compatible with this feature [73]. Moreover the crust-cracking events could account for the glitches seen in young pulsars [74]. A more extended description of the variety of the *spin driven decay* models can be found for example in [75].

Bibliography

[1] **Ostriker, J.P. & Gunn, J.E. 1969**, *ApJ*, **157**, 1395

[2] **Ruderman, M. & Sutherland, P. 1975**, *ApJ*, **196**, 51

[3] **Lyne, A.G., Manchester, R.N. & Taylor, J.H. 1985**, *MNRAS*, **213**, 613

[4] **Lamb, H. 1883**, *Phil,Trans.Roy.Soc.London*, **174**, 519

[5] **Canuto, V. 1969**, *ApJ*, **159**, 651

[6] **Baym, G., Pethick, C. & Pines, D. 1969**, *Nature*, **224**, 674

[7] **Chanmugam, G. & Gabriel, M. 1971**, *A&A*, **16**, 149

[8] **Lyne, A.G., Anderson, B. & Salter, M.J. 1982**, *MNRAS*, **201**, 503

[9] **Bailes, M. 1989**, *ApJ*, **342**, 917

[10] **Narayan, R. & Ostriker, J.P. 1990**, *ApJ*, **352**, 222

[11] **Bhattacharya, D., Wijers, R.A.M.J., Hartman, J.W. & Verbunt,** *A&A*, **254**, 198

[12] **Wakatsuki, S., Hikita, A., Sato, N. & Itoh, N. 1992**, *ApJ*, **392**, 628

[13] **Lorimer, D.R. 1994**, *Ph.D.Thesis*, University of Manchester, U.K.

[14] **Hartman, J.W., Verbunt, F., Bhattacharya, D., Wijers, R.A.M.J. 1997**, *A&A*, **322**, 477

[15] **Konar, S., & Bhattacharya, D., 1997**, *MNRAS*, **284**, 311

[16] **Bhattacharya, D. & Srinivasan, G. 1986**, *Curr.Sci.*, **55**, 327

[17] **Kulkarni, S.R. 1986**, *ApJ*, **306**, L85

[18] **van den Heuvel, E.P.J., van Paradijs, J.A. & Taam, R.E. 1986**, *Nature*, **322**, 153

[19] **Verbunt, F., Wijers, R.A. & Burm, H. 1990**, *A&A*, **234**, 195

[20] **Toscano, M.** *et al.* **1999**, *MNRAS*, **307**, 924

[21] **Yakovlev, D., & Urpin, V. 1980**, *SvA*, **24**, 303

[22] **Sang, Y. & Chanmugam, G. 1987**, *ApJ*, **323**, L61

[23] **Sang, Y. & Chanmugam, G. 1990**, *ApJ*, **363**, 597

[24] **Sang, Y. & Chanmugam, G. & Tsuruta, S. 1990**, in *Neutron stars and their birth events*, ad. W.Kundt (Dordrecht: Kluwer), 127

[25] **Urpin, V.A. & Muslimov, A.G. 1992**, *MNRAS*, **256**, 261

[26] **Urpin, V.A., & Konenkov, D. 1998**, *MNRAS*, **292**, 167

[27] **Pethick, C. & Sahrling, M. 1995**, *ApJ*, **453**, L29

[28] **Srinivasan, G., Bhattacharya, D., Muslimov, A.G. & Tsygan, A.I. 1990**, *Curr.Sci.*, **59**, 31

[29] **Itoh, N. 1989**, *Nuovo Cimento*, **12C**, 625

[30] **Itoh, N. 1990**, in *Physical Porcesses in Hot Cosmic Plasmas*, eds. W.Brinkmann *et al.* (Dordrecht:Kluwer), 197

[31] **Miri, M.J. 1996**, *MNRAS*, **283**, 1214

[32] **Camilo, F.** *et al.* **2000**, in *Pulsar Astronomy - 2000 and beyond*, Proc. of IAU Colloquium 177, ASP Conf.Series, in press

[33] **Urpin, V.A., Levshakov, S.A., & Yakovlev, D.G. 1986**, *MNRAS* **219**, 703

[34] **Wiebicke, H.J. & Geppert, U. 1996**, *A&A*, **309**, 203

[35] **Urpin, V.A., & Konenkov, D. 1997**, *MNRAS*, **284**, 741

[36] **Urpin, V.A., & Geppert, U. & Konenkov 1998**, *MNRAS*, **295**, 907

[37] **Urpin, V.A., Konenkov, D., & Geppert, U. 1998**, *MNRAS*, **299**, 73

[38] **Geppert, U., & Konenkov, D., 1998**, Proc. Symp. *Neutron Stars and Pulsars*, Tokyo, Ed. N. Shibazaki, N. Kawai, S. Shibata, T. Kifune, Universal Academy Press, Inc.,

[39] **Colpi, M., Page, D. & Geppert, U. 2000**, *ApJ*, in press

[40] **Mereghetti, S. & Stella, L. 1995**, *ApJ*, **442**, L17

[41] **van Paradijs, J. 1995**, *A&A*, **299**, L41

[42] **Taam, R.E. & van den Heuvel, E.P.J. 1986**, *ApJ*, **305**, 235

[43] **Shibazaki, N., Murakami, T., Shaham, J. & Nomoto, K. 1989**, *Nature*, **342**, 656

[44] **Zhang, C.M., Wu, X.J. & Yang, G.C. 1994**, *A&A*, **283**, 889

[45] **Zhang, C.M. 1998**, *A&A*, **330**, 195

[46] **Wijers, R.A.M.J. 1997**, *MNRAS*, **287**, 607

[47] **Romani, R.W. 1990**, *Nature*, **347**, 741

[48] **Burderi, L., King, A. & Wynn, G.A. 1996**, *MNRAS*, **283**, L63

[49] **Arons, J. & Lea, S.M. 1980**, *ApJ*, **235**, 1016

[50] **Psaltis, D. & Lamb, F.K. 1997**, Proc. Symp. *Neutron Stars and Pulsars*, Tokyo, Ed. N. Shibazaki, N. Kawai, S. Shibata, T. Kifune, Universal Academy Press, Inc.

[51] **White, N.E., & Zhang, W. 1997**, *ApJL*, **490**, L87

[52] **Geppert, U., & Urpin, V. 1994**, *MNRAS*, **271**, 490

[53] **Urpin, V.A., & Geppert, U. 1996**, *MNRAS*, **275**, 1117

[54] **Urpin, V.A., & Geppert, U. 1996**, *MNRAS*, **278**, 471

[55] **Urpin, V.A., & Geppert, U. & Konenkov 1998**, *A&A*, **331**, 244

[56] **Konar, S., & Bhattacharya, D. 1999**, *MNRAS*, **303**, 588

[57] **Sahrling, M. 1998**, astro-ph/9804047

[58] **Young, E.J. & Chanmugam, G.**, *ApJ*, **442**, L53

[59] **Sengupta, S. 1998**, *ApJ*, **501**, 792

[60] **Bhattacharya, D. 1995**, *JA&A*, **16**, 217

[61] **Bhattacharya, D. 1996**, in *Pulsar timing....*, ed. Z. Arzoumanian *et al.*, Royal Netherland Ac. of A.Sc.

[62] **Thompson, Ch. & Duncan, R. 1993**, *ApJ*, **408**, 194

[63] **Ruderman, M. 1972**, *ARA&A*, **10**, 427

[64] **Muslimov, A.G. & Tsygan, A.I. 1985**, *Ap&SS*, **115**, 43

[65] **Miri, M.J. & Bhattacharya, D. 1994**, *MNRAS*, **269**, 455

[66] **Ding, K.Y., Chen, K.S. & Chau, H.F. 1993**, *ApJ*, **408**, 167

[67] **Miri, M.J. 1999**, astro-ph/9910490

[68] **Konar, S., & Bhattacharya, D. 1999**, *MNRAS*, **308**, 795

[69] **Konenkov, D. & Geppert, U.**, astro-ph/9910492

[70] **Possenti, A., Colpi, M., D'Amico, N., Burderi, L. 1998**, *ApJL*, **497**, L97

[71] **Ruderman, M. 1991**, *ApJ*, **382**, 576

[72] **Ruderman, M. 1991**, *ApJ*, **382**, 587

[73] **Chen, K., Ruderman, M. & Zhu, T. 1998**, *ApJ*, **493**, 397

[74] **Ruderman, M., Zhu, T. & Chen, K. 1998**, *ApJ*, **492**, 267

[75] **Ruderman, M. 1995**, *JA&A*, **16**, 207

Chapter 5

The population synthesis code

In the aim of addressing the questions described in the Introduction of this *Thesis*, we developed a suitable original code. This Chapter 5 contains a detailed description of the *physical model* implemented in this code, which follows the rotational (section [5.1]) and the magnetic (section [5.2]) evolution of an accreting NS in a low mass binary. In section [5.3] the typical parameters for the population syntheses are dealt with, and section [5.4] reports on runtime and on the definitions used in discussing the results.

5.1 A semi-analytic model for the spin evolution of a Neutron Star

A semi–analytical model was developed [1] for studying the evolution of the rotational period of a magnetic neutron star undergoing accretion of matter via an accretion disk. The model accounts for the general features of the standard recycling scenario (as described in section [2.3]) and permits also the inclusion of general relativistic effects, comprising: (i) the stellar deformation (circumferential radius) as a function of angular velocity, (ii) the variation of the moment of inertia in response to the mass load and to the increasing rotation, (iii) the location of the marginally stable orbit for the computation of the angular momentum transfer rate in low-field NSs; (iv) the decrease of the mass shedding period for the compact object, due to the increase of its baryonic mass by accretion.

Section [5.1.1] contains a description of the adopted semi–analytical model, whereas in section [5.1.2] its predictions are compared with those obtained in the framework of fully relativistic calculations.

5.1.1 *The model*

We first derive a simple equation describing the evolution of the gravitational mass M_G as a function of the baryon load. We then introduce the set of equations for the evolution of the rotational frequency Ω, including rotational effects on the NS radius during recycling. The angular momentum transfer rate is computed including the corrections due to a strong gravitational field. The equations are solved numerically.

The code follows the evolution of an NS of initial gravitational mass $M_{G,0} = 1.4 M_\odot$ which is accreting at a constant rate $\dot{m}_B$. The initial values of the NS baryonic mass $M_{B,0}$ and of its radius R_0 are known once we specify the EoS (see section [3.1] and *e.g.* [2]). In our model, the gravitational and the baryonic masses M_G and M_B of the NS are related, at any given time, by $M_G = M_B(1 - \alpha/R)$, where R is the NS circumferential radius (*i.e.* the proper circumferential length at the NS equator divided by 2π) and α is a constant evaluated using the initial set of parameters. Accordingly,

$$M_G = M_B \left[1 + \left(\frac{M_{G,0}}{M_{B,0}} - 1 \right) \left(\frac{R_0}{R} \right) \right] \tag{5.1}$$

The decrease in radius due to the mass load is described using the simple relation $R \propto M_G^{-1/3}$ (for equilibrium of degenerate nonrelativistic neutrons): with this scaling we estimate the non-rotating NS circumferential radius R at any stage of the accretion. The evolution equation for M_G thus reads:

$$\dot{M}_G = \psi \, \dot{m}_B = \tag{5.2}$$

$$= \left[1 + \left(\frac{M_{G,0}}{M_{B,0}} - 1 \right) \left(\frac{M_G}{M_{G,0}} \right)^{1/3} \right] \left[1 - \frac{M_B}{3M_G} \left(\frac{M_{G,0}}{M_{B,0}} - 1 \right) \left(\frac{M_G}{M_{G,0}} \right)^{1/3} \right]^{-1} \dot{m}_B$$

The mass increase is accompanied by the increase in the rotational frequency Ω, and at any time (i.e., at any current value of M_G) we need to determine whether Ω is below or above the mass shedding limit Ω_{max}, that is the limiting angular frequency at which the gravitational pull is balanced by the centrifugal forces. Ω_{max} is estimated using the classical expression

$$\Omega_{max} = \Omega_K = \left(\frac{GM_G}{R^3_{\Omega,max}} \right)^{1/2} \tag{5.3}$$

where $R_{\Omega,max}$ denotes the circumferential radius of the rotating NS which in turn depends upon Ω_{max}. $R_{\Omega,max}$ is estimated fitting the results of [2]:

$$R_{\Omega,max} = 1.5 \; R_0 \tag{5.4}$$

where R_0 is the radius of the static configuration at the current value M_G. If $\Omega < \Omega_{max}$, spin up can proceed and the circumferential radius R_Ω of the rotating NS further increases. R_Ω is computed using the relation

$$\log_{10}(R_\Omega/R_0) = \frac{1 - (1 - \Omega/\Omega_{max})^{1/3}}{6.75} \tag{5.5}$$

derived fitting the results of [2].

In the numerical scheme, Ω_{max} is firstly determined from (5.3) using equation (5.4) for $R_{\Omega,max}$. Then (5.5) is used to calculate R_Ω.

UNMAGNETIZED CASE

During the accretion process the specific angular momentum l_{in} of the accreting matter is entirely transferred to the NS. From the angular momentum conservation $d(I_\Omega \Omega)/dt = \dot{m}_B l_{in}$ we obtain

$$\dot{\Omega} = \frac{\dot{m}_B}{I_\Omega} \left(l_{in} - \psi \Omega \frac{\partial I_\Omega}{\partial M_G} \right) \left(1 + \frac{\Omega}{I_\Omega} \frac{\partial I_\Omega}{\partial R_\Omega} \frac{\partial R_\Omega}{\partial \Omega} \right)^{-1} \tag{5.6}$$

where I_Ω is the moment of inertia of the neutron star. Taking into account the inflation of the radius caused by the rapid rotation, we extrapolate a result of Ravenhall & Pethick [3] obtained for static stars:

$$I_\Omega = 0.21 M_G R_\Omega^2 \left(1 - \frac{2GM_G}{R_\Omega c^2} \right)^{-1} \tag{5.7}$$

The value I_Ω is significantly altered at high rotational rates. Hence, its derivatives with respect to Ω and M_G cannot be neglected in the equation for $\dot{\Omega}$.

The inner rim of the disk at r_{in} is at few NS gravitational radii, where relativistic gravity is important. Therefore the specific angular momentum l_{in} carried by matter differs from the classical newtonian value $\sqrt{GM_G r_{in}}$. Assuming an accretion disk co-rotating with the NS, and the Kerr metric for the approximate description of gravity around a NS (see [4] for a more detailed analysis of the metric), we obtain from [5]:

$$l_{in} = c \frac{r_h^{1/2} (r_{in}^2 - 2 a r_h^{1/2} r_{in}^{1/2} + a^2)}{r_{in}^{3/4} (r_{in}^{3/2} - 3 r_h r_{in}^{1/2} + 2 a r_h^{1/2})^{1/2}} \tag{5.8}$$

where $r_h = GM_G/c^2$ and $a = I_\Omega \Omega / M_G c$.

For an unmagnetized neutron star the inner rim r_{in} of the accretion disk either skims the NS surface or, for very compact NS, is truncated at the radius of the last stable orbit r_{ms}. Therefore the radius r_{in} is defined as:

$$r_{in} = \begin{cases} r_{ms} & \text{if } r_{ms} > R_\Omega \\ R_\Omega & \text{if } r_{ms} \leq R_\Omega \end{cases} \tag{5.9}$$

In the Kerr metric r_{ms} is given by:

$$r_{ms} = r_h (3 + Z_2 - [(3 - Z_1)(3 + Z_1 + 2Z_2)]^{1/2}) \tag{5.10}$$

with

$$Z_1 = 1 + [1 - (a/r_h)^2]^{1/3} [(1 + a/r_h)^{1/3} + (1 - a/r_h)^{1/3}] \tag{5.11}$$

$$Z_2 = [3(a/r_h)^2 + Z_1^2]^{1/2}. \tag{5.12}$$

Solving for the differential equations (5.2) and (5.6), we determine the NS rotational evolution under the hypothesis of stationary accretion. The related computational effort is greatly reduced with respect to a fully relativistic numerical approach.

MAGNETIZED CASE

For the case of a magnetized NS, there is another characteristic length, i.e., the magnetospheric radius r_{mag}, which has to be compared with r_{ms} and R_Ω when calculating the value of r_{in}. As we have already explained in section [2.3.2], the magnetospheric radius is computed as the product of the Alfven radius (see *e.g.* [6]) times a factor $\phi \sim 1$, estimated as in [7]. For high enough magnetic moment μ, r_{mag} exceeds both R_Ω and r_{ms} and the magnetic coupling between the disk and the star determines the extent of angular momentum transfer. The angular momentum balance relation in this case reads as $d(I_\Omega \Omega)/dt = g\dot{m}_B l_{in}$, where the torque function $g = g(\Omega)$ accounts for the details of the interaction between the NS magnetosphere and the accretion disk. When $g = 0$ the NS is on the so–called "spinup line", where it can load mass without modifying its angular momentum $I_\Omega \Omega$. In the integration scheme, equation (5.6) is modified accordingly, to include the magnetic coupling.

5.1.2 *Comparison with fully relativistic calculations*

In Table 5.1 we compare equation (5.3) with the results of Cook, Shapiro & Teukolsky [2] derived using a relativistic code for 13 different EoSs ($M_G = 1.4 M_\odot$). The agreement is better than 5%.

The maximum angular speed occurs when the NS equatorial speed reaches the classical Keplerian limit computed taking M_G as gravitational mass and as radius $R_{\Omega,max}$: the rapid rotation inflates and deforms the NS surface. While the non-spherically-symmetric deformations (oblateness effects) are important in determining the radius of the spinning NS, they are almost irrelevant in changing the gravitational field felt by a test particle at the NS equator with respect to the corresponding spherical configuration. This is probably due to the fact that most of the mass is concentrated well inside the external radius, where the deformation effects due to rotation are almost negligible. This is predicted by the so called Roche Model (see *e.g.* [9]), that, in the hypothesis outlined above, conclude that the maximum expansion of a uniformly rotating star along its equator is a factor of 3/2, irrespective of the EoS adopted.

In Figure 5.1 we report the values of R_Ω vs Ω from [2], for 5 EoSs ($M_B = 1.4 M_\odot$) and the relation given by equation (5.5). The matching is pretty good, especially for the fast spinning regime. At slower Ω, our relation overestimates the NS circumferential radius by no more than $\simeq 5\%$.

Table 5.1: Minimum rotational periods

EoS	$P_{\rm lim}$ (ms) (this model)	$P_{\rm lim}$ (ms) (Cook,Shapiro,Teukolsky [8])	Difference (%)
A	0.631	0.604	4.5
C	0.907	0.894	1.4
D	0.751	0.730	2.8
E	0.677	0.656	3.1
F	0.679	0.715	-5.1
L	1.21	1.25	-2.9
M	1.48	1.49	-0.9
N*	1.03	1.08	-4.7
KC	0.910	0.888	2.5
AU	0.708	0.701	1.0
UU	0.792	0.784	1.0
UT	0.764	0.754	1.4
FPS	0.767	0.747	2.8

Table 5.1: Minimum rotational periods for the EoSs indicated in column 1. In column 2 we give the periods obtained from the analytical model derived in this work. In column 3 we collect the numerical values from Cook, Shapiro & Teukolsky [8]. The fourth column indicates the percentage differences.

As far as the relationship between the accreted baryonic mass M_{ac} and the NS angular velocity is concerned, our results are in agreement with those obtained with the relativistic code of [8] within 8%, even in the high spin regime (see *e.g.* Figure 5.2).

5.2 The crustal magnetic field evolution

For this investigation, we assumed a crustal origin of the neutron star magnetic field, *i.e.* it is created at the beginning of the NS's existence in its crustal layers. This assumption is in accordance with the general accepted evolutionary scenarios for isolated NSs [10], for NSs in low mass binaries [11], for NSs in high mass binaries [12], and millisecond pulsars [13].

5.2.1 *The induction equation*

Since, at the beginning of the Roche Lobe Overflow (RLO) phase, the anisotropies of the conductivity σ can be safely neglected, the evolution of the magnetic field

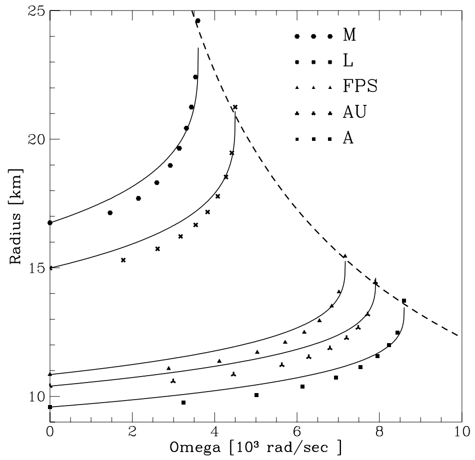

Figure 5.1: NS circumferential radii (in units of km) versus angular frequency Ω (in units of 10^3 rad/sec). The points are from Cook, Shapiro & Teukolsky [2] for 5 representative EoSs ($M_B = 1.4\ M_\odot$). The *solid lines* are relation (5.5). The *dashed line* is the keplerian relation (5.3).

(MF) is governed by the induction equation

$$\frac{\partial \vec{B}}{\partial t} = -\frac{c^2}{4\pi}\nabla \times \left(\frac{1}{\sigma}\nabla \times \vec{B}\right) + \nabla \times (\vec{v} \times \vec{B}) \tag{5.13}$$

where $\vec{v}$ is the flux velocity of the accreted matter through the crust. When considering only the evolution of an axisymmetric dipolar poloidal field the induction equation can be simplified by introducing the vector potential $\vec{A} = (0,\ 0,\ A_\varphi)$ and choosing $A_\varphi = s(r,t)\sin\theta/r$. With the spherical radius r and the polar angle θ, both the radial and meridional field components can be expressed in terms of the quantity $s(r,t) = (A_\varphi r)/\sin\theta$

$$B_r = \frac{2s}{r}\cos\theta\,, \quad B_\theta = -\frac{\sin\theta}{r}\frac{\partial s}{\partial r} \tag{5.14}$$

which gives the maximum field strength at the NS surface ($r = R$) by its polar value for B_r, that is $B_s(t) = 2s(R,t)/R$. Although in the outer layers of the crust the inflow of matter channeled by the magnetic field is certainly not radial, the mass flow will become nearly spherically symmetric in the higher density regions, where the currents are concentrated. In the approximation of a purely radial mass flow, $\vec{v} = -v_r\vec{e_r}$, the induction equation can be transformed to

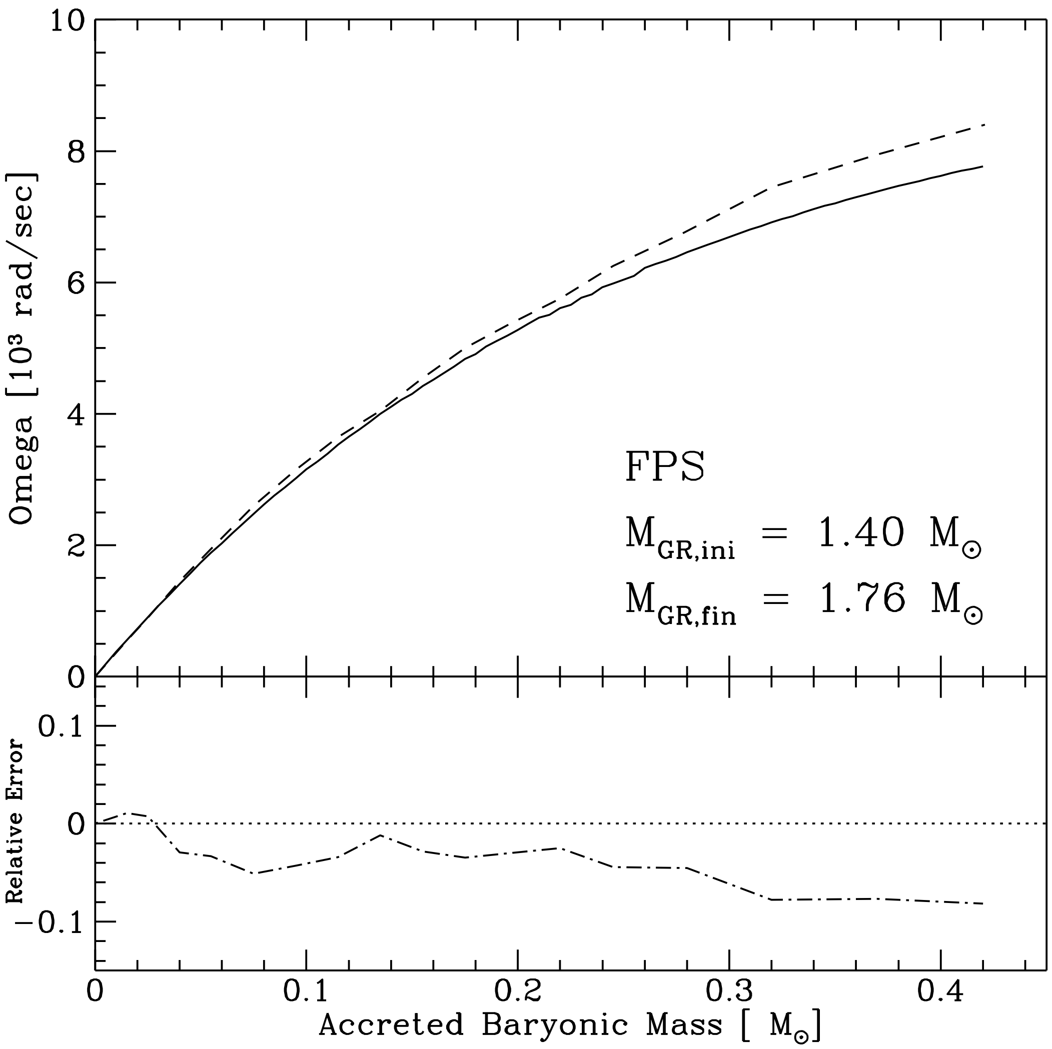

Figure 5.2: Rotational evolution of an unmagnetized NS (initial gravitational mass $M_{G,ini} = 1.40\ M_{\odot}$) undergoing steady accretion of matter. The Ω vs M_{ac} relation calculated for FPS-EoS with the semi–analytic model described in the text (*solid line*) is compared to that from [8] (*dashed line*). The relative errors in computing Ω with our approximate model are displayed in the lower panel. Accretion is halted at $M_{ac} = 0.416\ M_{\odot}$, when mass shedding sets in (the final gravitational mass of the NS is $M_{G,fin} = 1.76\ M_{\odot}$).

$$\frac{\partial s}{\partial t} = \frac{c^2}{4\pi\sigma}\left(\frac{\partial^2 s}{\partial r^2} - \frac{2s}{r^2}\right) - v_r\frac{\partial s}{\partial r} \tag{5.15}$$

where the flow velocity is given by the equation of continuity as

$$v_r(r) = \frac{\dot{M}}{4\pi r^2 \rho(r)} \tag{5.16}$$

with $\dot{M} = \dot{m}\ \dot{\mathrm{M}}_{\mathrm{E}}$ and $\rho(r)$ is the radial profile of the density (see section [5.2.2]).

5.2.2 *Structural properties of the NS crust*

In order to solve for the equation (5.15) we need the values of the conductivity σ inside the star. They in turn depend on the structural properties of the NS crust; namely, the density profile, the temperature and the chemical composition.

DENSITY PROFILE

As explained in the following section [5.3.1], we focused on two different equations of state (EoS): the FP and the PS. The former belongs to the family of the soft-EoSs and we got the related density profile from [14], whereas the latter is a stiff EoS, whose density profile is taken from [15]. The EoS valid in the core determines the thickness of the crust (the softer the EoS the thinner the crust) and hence the scale of the crustal field. Moreover, the induction equation (5.13) provides a transparent relation between the lengthscale of the magnetic field and the timescale of its decay. Thus, apart from the accretion-driven decay mechanisms, the EoS itself governs strongly the field evolution: the softer the EoS, the faster the crustal field decays. This correlation is partly counterbalanced by relativistic effects which become stronger the softer the EoS is [16].

We assume that the density profile will not be changed by the accretion of matter onto the NS. This is certainly a good approximation as long as no more than $\sim 0.1\ \mathrm{M}_\odot$ has been accreted. The chemical composition and density stratification can instead vary with increasing mass load ($0.1\mathrm{M}_\odot \rightarrow 0.5\mathrm{M}_\odot$) but these changes are considered unimportant, given the other approximations introduced.

TEMPERATURE

Various authors ([17], [18], [19]) calculated the crustal temperature as a function of the accretion rate. We used the following fitting formula, which gives the dependence of the crustal temperature T on the accretion rate in agreement with the numerical results of the above authors (see also [20]):

$$\log T = 7.887 + 0.528 \left[1 - e^{-0.899(q+11)}\right], \tag{5.17}$$

where $q = \log(\dot{M}/\mathrm{M}_\odot\ \mathrm{yr}^{-1})$. For $\log(\dot{M}/\mathrm{M}_\odot\ \mathrm{yr}^{-1}) > -9.5$, the equation (5.17) yields probably a somewhat too small crustal temperature.

CHEMICAL COMPOSITION

During an extended RLO phase the whole mass of the crust can be replaced by accreted matter. Therefore, instead of assuming that the crust is composed of cold catalyzed matter we apply the chemical composition established by the pycnonuclear reactions in the course of the accretion [21].

CONDUCTIVITY

At the beginning of the RLO, the currents maintaining the magnetic field are already located close to the crust–core boundary ($\rho_{crust-core} = 2 \times 10^{14}$ gcm^{-3}). Since even in the case of Eddington accretion the crust will not be heated up above $\simeq 5 \times 10^8$ K, the crustal matter at densities larger than 10^{10} gcm^{-3} is crystallized. Therefore, the relevant contributions to the electric conductivity in the crust are due to *electron–phonon* and *electron–impurity* scattering. We use the numerical data for the phonon conductivity σ_{ph} obtained by Itoh *et al.* [22], and a simple analytical expression for the impurity conductivity σ_{imp} derived by Yakovlev & Urpin [23]

$$\sigma_{imp} = 8.53 \times 10^{21} \frac{x^3}{\Lambda_{imp}(1+x^2)} \frac{Z}{Q_{imp}} \ \mathrm{sec}^{-1} \tag{5.18}$$

where ρ is the density of the crystallized crustal matter and

$$\Lambda_{imp} \simeq 2 \tag{5.19}$$

$$x = \left(\frac{Z\,\rho}{A\ 10^6\ \mathrm{gcm}^3} \right)^{1/3} \tag{5.20}$$

$$Q_{imp} = \frac{1}{n} \sum_{n'} n' \,(\, Z - Z'\,)^2 \tag{5.21}$$

Here n, A and Z represent the number density, the isotopic number and the charge of the dominant background ion specie, whereas n' and Z' are the number density and the charge of an interloper specie. The summation is over all species. The value of Q_{imp} is difficult to assess: in the literature it is assumed to span the interval $10^{-4} \longrightarrow 0.5$. We used a conservative $Q_{imp} = 0.01$. The total conductivity is given by

$$\frac{1}{\sigma_{tot}} = \frac{1}{\sigma_{ph}} + \frac{1}{\sigma_{imp}} \tag{5.22}$$

Electron–phonon interactions dominates the transport at high temperatures and relatively low densities, whereas the impurity concentration determines the conductivity at lower temperatures and larger densities. In particular, the accretion induced heating of the crust diminishes the electron–phonon conductivity considerably, since it is $\propto T^{-1}$ above the Debye temperature T_D and $\propto T^{-2}$ for temperatures lower than

$$T_D \;=\; 2.4 \times 10^6 \left(\frac{2A}{Z}\right)^{1/2} x^{3/2} \;\; ^{\mathrm{o}}\mathrm{K} \tag{5.23}$$

The lowest accretion rate we will consider for the RLO phase is $\log(\dot{M}/\mathrm{M}_{\odot}\ \mathrm{yr}^{-1}) = -11$, which corresponds to a crustal temperature of about 8×10^7K. For such and higher temperatures, σ_{ph} is the dominating contribution to the conductivity in the whole crust. The electric conductivities for the weakest and the strongest RLO accretion rates considered in producing the synthesized NS populations are shown in Figure 5.3.

5.2.3 *Boundary Conditions*

While at the surface of the NS the standard boundary condition for a dipolar field applies, i.e.

$$r\,\frac{\partial s}{\partial r} + s\,\bigg|_{r=R_\Omega} \;=\; 0 \tag{5.24}$$

the inner boundary condition is more complicated and still a subject of scientific debates. In order to consider the possible different evolution of the NS magnetic field at the crust–core boundary, we will apply two qualitatively different inner boundary conditions.

Expulsion of the field from the core: BC I

During the accretion process onto a NS its field both diffuses and is advected towards inner layers. It is generally accepted that the core of a NS older than 10^9 yr is in a superfluid/superconductive (SF/SC) state, a state which will not be changed even by the intense heating during the RLO phase. Thus, in case of $\vec{v} = 0$, at the crust–core boundary the correct boundary condition is $s = 0$, since the Meissner–Ochsenfeld effect prevents the magnetic field from diffusion into the core. Our first boundary condition (BC I) assumes that, during the process of

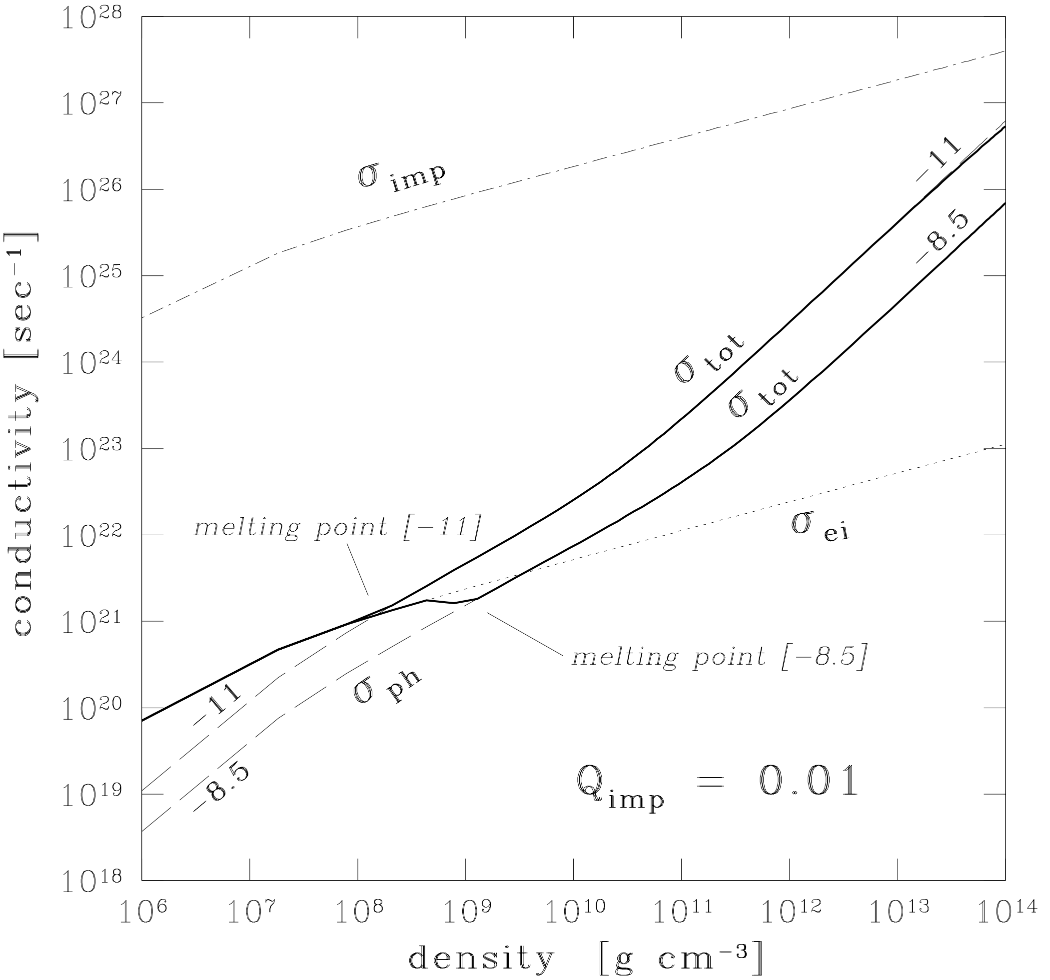

Figure 5.3: The electric conductivity in the crust as a function of the density for $\log(\dot{M}/\mathrm{M}_\odot\ \mathrm{yr}^{-1}) = -8.5$ and -11. The *heavy solid lines* correspond to the total conductivity σ_{tot}. Since the impurity conductivity (σ_{imp}, *dot-dashed line*) is not dependent on the temperature, it is the same for both accretion rates. The conductivity in the liquid region (σ_{ei}, *dotted line*) is determined by electron–ion collisions and also practically not dependent on T, contrary to the phonon conductivity (σ_{ph}, *dashed lines*), which dominates σ_{tot} at highest densities. The shift of the melting point towards higher densities for higher accretion rates is seen.

assimilation, $\vec{B}$ will be expelled immediately by the crustal material undergoing the SF/SC phase transition. Thus we define:

$$\text{BC I}: \qquad s = 0 \qquad \text{at} \qquad r = r_{crust-core} \tag{5.25}$$

ADVECTION OF THE FIELD INTO THE CORE: BC II

In case of $\vec{v} \neq 0$, the field, frozen in on timescales of matter flow, can cross the crust–core boundary and becomes assimilated in the core, together with the former crustal material. Thus, we consider a second boundary condition (BC II), which allows an advection of the magnetic field into the core. There, it will be not further decayed due to superconductivity, but further advected as long as accretion lasts. This assumption results in:

$$\text{BC II}: \qquad s = 0 \qquad \text{at} \qquad r = 0 \tag{5.26}$$

which may cause the occurrence of a residual field remaining constant with time, (*freezing* of the field) whereas BC I allows for an exponential magnetic field decay down to zero. The situation assuming BC II has been described by Konar & Bhattacharya [24] and we apply also their trick to simulate an effectively infinite conductivity in the assimilated core region.

5.2.4 *Typical evolution of the magnetic moment*

Figure 5.4 displays (for durations τ_{RLO} of the RLO phase spanning the interval $5 \times 10^6 \longrightarrow 5 \times 10^8$ yr) the decay of the surface magnetic field under the influence of different accretion rates both for the soft and the stiff adopted EoSs and for the two boundary conditions (BCI & BCII) considered here.

The BC I allows for an exponential decay down to zero if the accretion period is extended enough. It is clearly seen that the larger the accretion rate the hotter the crust (see eq. (5.17)) and, hence, the more rapid the crustal field decays. The more rapid decay in case of the soft EoS in comparison with the stiff one is a result of the smaller spatial scale of the magnetic field.

For both EoS we see that the assumption of BC II results in a much stronger surface field. Only for nearly Eddington accretion rates and soft EoS (lower right panel: curve labeled by -8.5), the very rapid field decay is practically unaffected by the choice of the boundary condition. In that case, perhaps, effects of submersion play an important role because for such large accretion rates the characteristic time for the mass flow in the lower density layers of the crust is smaller than the ohmic (re–)diffusion time in that region.

For the soft EoS a trend in establishing a residual field is at most suggested for $\log(\dot{M}/\mathrm{M}_\odot\ \mathrm{yr}^{-1}) = -10$ and -9.5. The existence of residual fields seems to

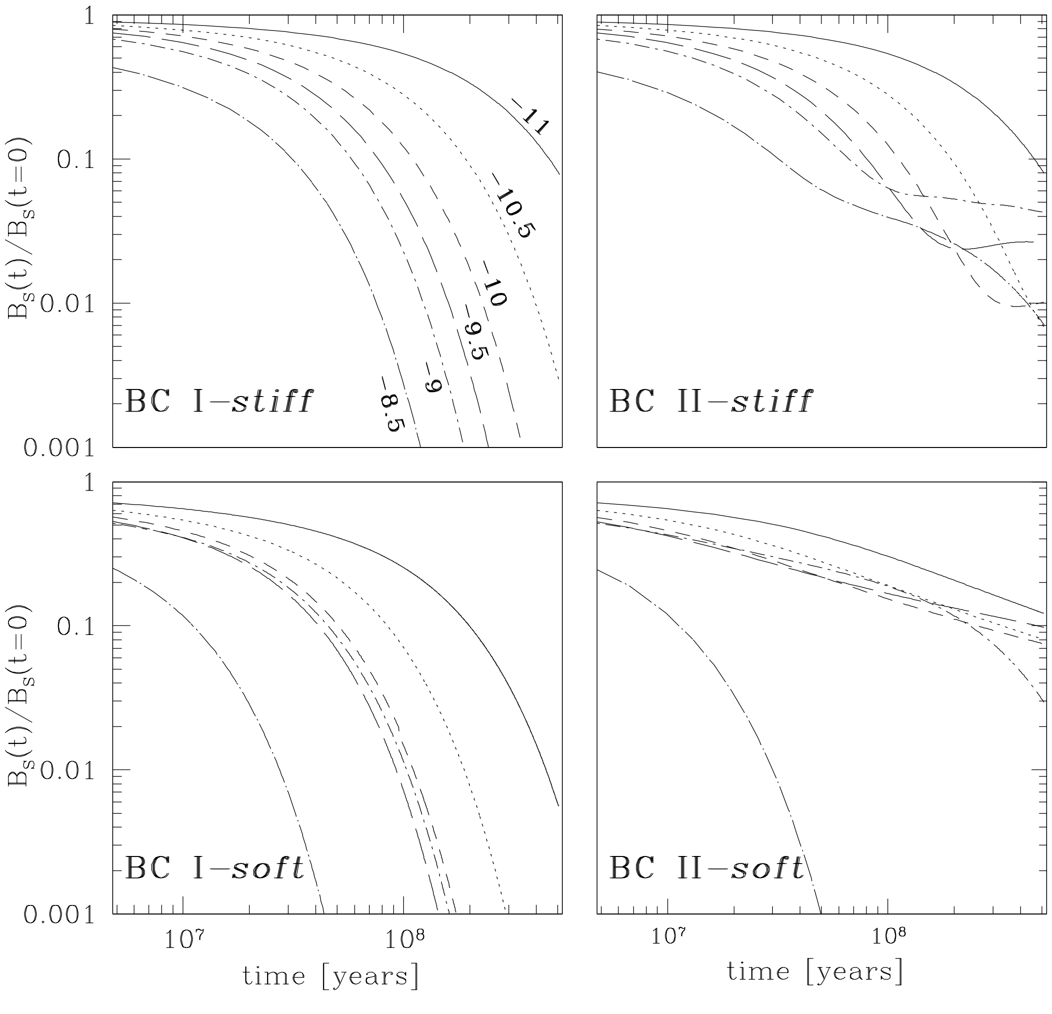

Figure 5.4: The dependence of the surface magnetic field, $B_s(t)$, on the time, normalized on the surface magnetic field strength at the beginning of the RLO phase ($t = 0$). The different accretion rates are labeled according to $\log(\dot{M}/\mathrm{M}_\odot\ \mathrm{yr}^{-1})$. The four explored cases are located here as in all the following figures: stiff-EoS on the upper panels, soft-EoS on the lower ones; boundary condition BC I on the left panels and BC II on the right.

be much more evident for stiff EoS. For the lowest accretion rates the velocity of mass flow at the crust–core boundary is certainly too small to create residual fields during $\tau_{RLO} \leq 5 \times 10^8$yr and for the near Eddington accretion the effect of submersion acts. However, for $\log(\dot{M}/\mathrm{M}_\odot\ \mathrm{yr}^{-1}) = -9, -9.5$ and -10, the development of a residual *frozen* field is clearly seen and its strength is positively correlated to the accretion rate, as Konar & Bhattacharya already pointed out [25].

5.3 Values adopted for the runs

This section reports on the initial values and/or distributions of the physical quantities used in producing and evolving a NS population. A complete summary of these parameters can be found in Table 5.2.

Table 5.2: Population syntheses parameters

Physical quantity	Distribution	Values	Units
NS period at t_0^{RLO} (*)	Flat	$1 \rightarrow 100$	sec
NS μ at t_0^{RLO} (*)	Gaussian	$\mathrm{Log}< \mu_0 > =$ 28.50 ; σ=0.32	G cm^3
$\dot{m}$ in RLO phase ($\sharp$)	Gaussian	$\mathrm{Log}< \dot{m} > =$ − 1.00 ; σ=0.50	$\dot{\mathrm{M}}_{\mathrm{E}}$
Minimum accreted mass	One-value	0.01	$\mathrm{M}_\odot$
RLO accretion phase time (†)	Flat in Log	$10^6 \rightarrow \tau_{RLO}^{max}$(‡)	year
MSP phase time	Flat in Log	$10^8 \rightarrow 3 \times 10^9$	year

Table 5.2: (*) t_0^{RLO} = initial time of the Roche Lobe Overflow phase
($\sharp$) baryonic accretion rate during the Roche Lobe Overflow phase
(†) a maximum accreted mass of $0.5 M_\odot$ is permitted during the RLO phase
(‡) maximum duration of the Roche Lobe Overflow phase; typical explored values: 5×10^7 yr - 10^8 yr - 5×10^8 yr

5.3.1 *EoS*

The NSs evolved in our population synthesis model have an initial gravitational mass of 1.4 $\mathrm{M}_\odot$, fully compatible with the narrow range of masses measured by Thorsett & Chakrabarty [26] for the double neutron stars relativistic systems. The compact objects in this kind of binaries must have accreted only a tiny amount of matter ($\lesssim 10^{-2}\mathrm{M}_\odot$) and their current mass is nearly equal to the initial one (*i.e.* prior to the mass transfer). Note, however, that theoretical arguments could be suggestive of a bimodal distribution of the masses of the NSs at their birth [27].

We investigated two EoSs: the FP-EoS [28] and the PS-EoS [15], similar to the A-EoS and the L-EoS (see [29] for the labeling of the EoSs). The *FP is a soft equation of state* (radius $R = 1.06 \times 10^6$cm for a 1.4 $M_\odot$–static neutron star and central density $\rho_c = 1.27 \times 10^{15}$ g cm^{-3}), whilst the *PS is one of the stiffer* EoS ($R = 1.64 \times 10^6$cm and $\rho_c = 3.6 \times 10^{14}$ g cm^{-3} for the same canonical mass). In the most favourable circumstances and accreting 0.5 $M_\odot$ (an acceptable amount for the baryonic mass transferred in a low mass binary), a NS can spin up to a period of

$$\begin{aligned} P_{sh} &= 0.73 \text{ msec} \qquad\qquad \text{for FP} - \text{EoS} \ \ (\textit{mild soft}) \\ P_{sh} &= 1.40 \text{ msec} \qquad\qquad \text{for PS} - \text{EoS} \ \ (\textit{very stiff}) \end{aligned}$$

These values have been computed according to the spin evolution model described in section [5.1.1] and [1].

5.3.2 *Recycling*

We start with a population of NSs at the onset of the Roche Lobe Overflow (RLO) phase. The adopted parameters are collected in Table 5.2. Urpin, Geppert & Konenkov [11] calculated the tracks in the $\mu - P$ plane for a sample of pulsars, assuming different hypotheses for the binary evolution times, for the magnetic field decay and for the angular momentum transfer between the intervening plasma and the magnetosphere.

Starting with pulsar parameters (μ_{ini} and P_{ini}) in accordance with the most updated observational analyses ([30], [31], [32]), they showed that, at the end of the wind phase (see for reference sections [2.3.3] and [4.3.1]), the typical NS magnetic field is about $1.5 - 3$ orders of magnitude lower than at the onset of the pulsar phase (almost fully depending on the duration of wind accretion), whilst the period P spreads between ~ 0.1 sec and ~ 1000 sec. During the RLO accretion the spinup line is reached after a time $\tau_{sp} \simeq 10^5 \div 10^6$ yr which is shorter than the duration of the RLO accretion phase. Thus, the rotational evolution of a NS is almost independent of P at the onset of the RLO phase. Therefore, we adopted a simple flat distribution in period (see Table 5.2) as input parameter for the calculations, verifying that the statistical outcome of the subsequent phases are insensitive to the exact range of P or/and to its detailed initial distribution.

The logarithm of the accretion rate $\dot{m}$ (in Eddington mass $\dot{M}_E$) during the RLO stationary phase is randomly selected from a gaussian distribution, with peak value (0.1 $\dot{M}_E$) and spread σ (half dex) compatible with the observed values. In fact, the typical X-ray luminosities of the stationary low mass X-ray binaries (LMXBs) cluster in the interval $10^{36} \rightarrow 10^{38}$ erg/sec [33], implying accretion rate in the range $\sim 10^{-10} \rightarrow\sim 10^{-8} M_\odot$/yr (for masses ~ 1.4 $M_\odot$). Uncertainties in distance of the sources and/or in the radiative efficiency of the accretion process could affect these estimates. We note that the typical selected mean accretion rates span the interval of values calculated by Ergma *et al.* [34] within scenarios with conservative mass transfer. Low luminosity LMXBs might exist, yet undetected, so we explore lower mean rates on the synthesized population of recycled NSs.

We calculated [1] the minimum mass for spinning a *magnetized* ~ 1.40 $M_\odot$ NS up to $P < 10$ msec: one obtains ~ 0.01 $M_\odot$, whilst this value doubles for unmagnetized neutron stars. A complete report about this calculation is included in the section [6.5]. Therefore that value, ~ 0.01 $M_\odot$, was adopted as lower limit to the total mass accreted, in our synthesized populations. As regard to the upper limit, the maximum value of the mass transferred (i) must grant for the radial stability of the accreting NS and (ii) has to be compatible with the maximum duration of the RLO phase τ_{RLO}^{max}. For both EoSs, the first criterion is safely satisfied by assuming an upper limit of 0.5 $M_\odot$ (as extrapolated from Cook, Shapiro & Teukolsky [8]). The second request introduces a free parameter. Therefore we investigated the consequences of different choices on τ_{RLO}^{max}, picking it up around the commonly cited reference value of $\sim 10^8$ yr. Nevertheless, τ_{RLO}^{max} could be shortened if evaporation of the companion sets in [35], and we explore accordingly also values as short as $\sim 10^7$ yr.

We considered a flat probability distribution for the logarithm of time of duration of the terminal phase of recycling, when the NS could emit as a radiopulsar. The minimum adopted value largely accounts for the time necessary to clean up the NS surroundings before the magnetic dipole emission could set in again. The maximum time is limited by the age of the disk of the galaxy, therefore we put an upper limit on the total duration of the entire recycling process.

The behaviour of the torque function g and the value at which it zeroes (dubbed as critical fastness parameter $\Omega_{s,crit}$) are still uncertain. Therefore we adopted two different forms for g, following the suggestions of Ghosh & Lamb [36] and of Wang [37]. However, both their calculations considered only the positive branch of the g-function, which governs the transfer of angular momentum from the disk to the NS. For a slowly rotating NS, their estimates for the torque efficiency are respectively $g(\Omega = 0) = 1.17$ for Wang, and $g(\Omega = 0) = 1.40$ for Ghosh & Lamb. The predicted values of $\Omega_{s,crit}$ cover a larger range due to the different approximations used in the calculation. However we noticed that our results do not change sensitively if $\Omega_{s,crit}$ varies in the interval $0.85 \div 1.00$ (in units of the Keplerian angular velocity at the inner rim of the accretion disk) compatible with the most updated estimates (but see [38] for a different point of view).

The shapes of the g-function near $\Omega_{s,crit}$ have to be assumed cautiously. No fully consistent calculation of the torque function is available yet for the description of the *propeller* phase. In order to include this effect (especially at the end of the RLO phase), we extrapolated the known g functions to their negative branch, introducing a central symmetry with respect to their zero-point. This preserves continuity and derivability with the minimum number of additional physical hy-

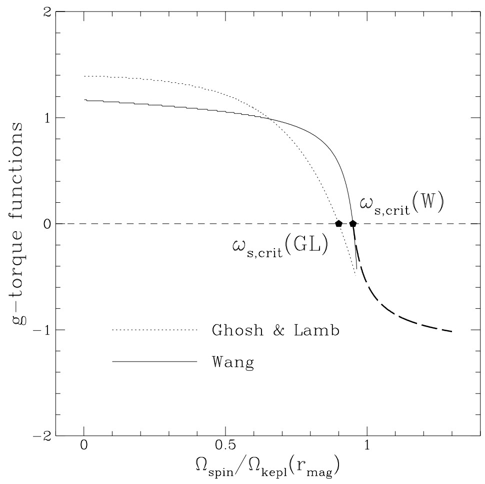

Figure 5.5: The shape of the g-function proposed by Wang [37] (*solid line*) and one of those predicted by Ghosh & Lamb [36] (*dotted line*). Dots indicate the position of the critical fastness parameter $\Omega_{s,crit}$, above which no reliable calculation of the g-functions exists insofar. In order to mimic the propeller effect, the drawn extrapolation of the Wang-function (*dashed line*) was used.

potheses: this extrapolation and the g-functions proposed by Ghosh & Lamb and by Wang are displayed in Figure 5.5. Different semi-qualitative approximations (*e.g.* Menou, Esin & Narayan [39] adopted a linear relation between g and Ω) do not affect our statistical findings once $\Omega_{s,crit}$ is close to 1.00.

5.3.3 *Magnetic moment*

The typical value of the magnetic moment μ for the observed *normal* pulsar population lies in the range of $10^{29.5} \div 10^{31.5}$ Gcm^3 ([30], [31], [32]).

During the subsequent evolutionary stages in a low mass binary, μ decays either by ohmic diffusion during the cooling of the NS (ejector and/or propeller phase) or by accretion driven decay mechanisms during the comparatively extended wind accretion phase, which can last up to 10^{10} years. In these phases the depth of the crust initially penetrated by the magnetic field determines its strength. When the standard NS enters the RLO phase it has an age $\gtrsim 10^9$ yrs, and the field have had enough time to diffuse down to the crust–core boundary, where the steep increase of the electric conductivity prevents further inward diffusion, wherever the field was initially contained. Thus, at the onset of RLO, the field is located at the core-crust boundary, and its absolute strength is the parameter to be varied in the population synthesis. Examining the various paths in the $\mu - P$ plane calculated by various authors ([13], [11]), it appears that, at the end of the wind phase, the bulk of the evolved NSs groups on the μ-axis at values around $10^{28} \div 10^{29.5}$ Gcm^3. Such a clustering of the NSs, in a relatively narrow interval in μ, allows us to bar the uncertainties in the magnetic evolution of the objects during the first three stages of the recycling scenario. Hence, the values μ_0 for the magnetic moment at the onset of the RLO era (t_0^{RLO}) are selected from a gaussian distribution (see Table 5.2) with a mean chosen in that interval.

5.3.4 *Persistent and non-stationary accretion*

With the aim of exploring the effect of a decreasing $\dot{m}$ on the population of fastly spinning objects, we compared two possibilities:

- persistent accretion for a time τ_{RLO};
- persistent accretion for a shorter time followed by a transient phase mimicking the quenching of the mass transfer.

We modeled the switching off of the accretion as a power law decay for $\dot{m}$

$$\dot{m}(t) = \begin{cases} \dot{m}(0) & \text{if} \quad 0 \leq t \leq (1-\mathcal{F}_{que})\tau_{RLO} \\ \dot{m}(0)\left[1 - \left(\frac{t - (1-\mathcal{F}_{que})\,\tau_{RLO}}{\mathcal{F}_{que}\,\tau_{RLO}}\right)^{1/\Gamma_{que}}\right] & \text{if} \quad (1-\mathcal{F}_{que})\tau_{RLO} < t \leq \tau_{RLO} \end{cases} \tag{5.27}$$

investigating the effect of varying the two parameters: (i) the ratio $\mathcal{F}_{que}$ between the duration of the quenching phase with respect to the total RLO phase and (ii) the index Γ_{que} of the power law. Adopted values for $\mathcal{F}_{que}$ range from $0.0 \rightarrow 0.5$ and for Γ_{que} from $1 \rightarrow 10$ (the last value is representative of an almost sudden switch off). Figure 5.6 displays some examples of our parametrization of this phenomenon.

Probably the quenching of the accretion is not a smooth process, but develops through alternate phases of higher and lower mass transfer rate, transforming the NS in a transient source of X-rays. Due to the short timescales of outburst and recurrence (with respect to the duration of the whole quenching process), our crude model could describe satisfactorily also this more realistic situation. On the contrary, our model can not account for those cases in which the accretion rate initially decreases and later increases substantially; for example in tight systems [34] or for MSPs recycled in Intermediate Mass Binaries as recently suggested by Podsiadlowski & Rappaport [40].

We account for the angular momentum losses by propeller, both for persistent and for non-stationary accretion during phase IV of the recycling. An extended spin down phase is quite unlikely in the former case, because a steady accretion rate and a reduced magnetic moment imply a very small magnetosphere. On the

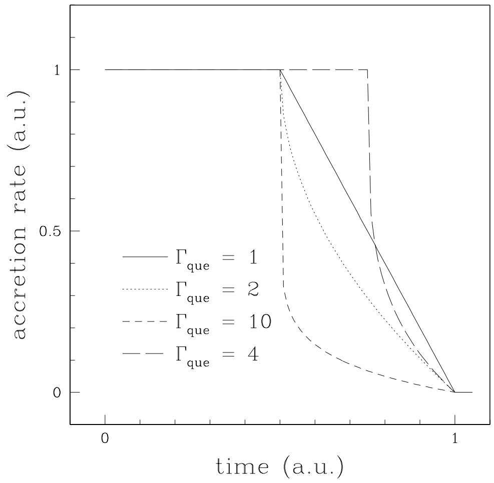

Figure 5.6: Different dependences of the switching off of the accretion on the time. The plot reports four representative cases, whose parameters are: (i) $\mathcal{F}_{que} = 0.5$ and $\Gamma_{que} = 1$; (ii) $\mathcal{F}_{que} = 0.5$ and $\Gamma_{que} = 2$; (iii) $\mathcal{F}_{que} = 0.5$ and $\Gamma_{que} = 10$; (iv) $\mathcal{F}_{que} = 0.25$ and $\Gamma_{que} = 4$.

contrary, if, at the end of the RLO phase, $\dot{m}$ decreases, the magnetospheric arm can increase, allowing for an efficient loss of angular momentum from the NS.

5.4 Runtime & definitions for the statistical analysis

To execute the evolution we built a Monte Carlo code, usually producing 3,000 particles. A typical distribution of the initial NS population in the $\mu - P$ diagram is depicted in Figure 5.7. The statistical analysis is performed only on those NSs reaching the so-called "millisecond strip" at the end of the fifth stage (*radio*) of the recycling scenario, the ones having period $P \leq 10.0$ ms and any value of the magnetic moment.

In accordance with the values of P_{min} (the shorter rotational period observed in PSRB1937+21; $P_{min} = 1.558$ msec) and μ_{min} (the weakest magnetic moment observed in PSRJ2317+1439; $\mu_{min} = 7.3 \times 10^{25}$ G cm^3), we divided our particles in four groups. As a guideline to classify them, we used their putative radioemission observability. In particular:

I those filling the first quadrant in the millisecond strip ($P \geq P_{min}$ and $\mu \geq \mu_{min}$) behave as the known MSPs;

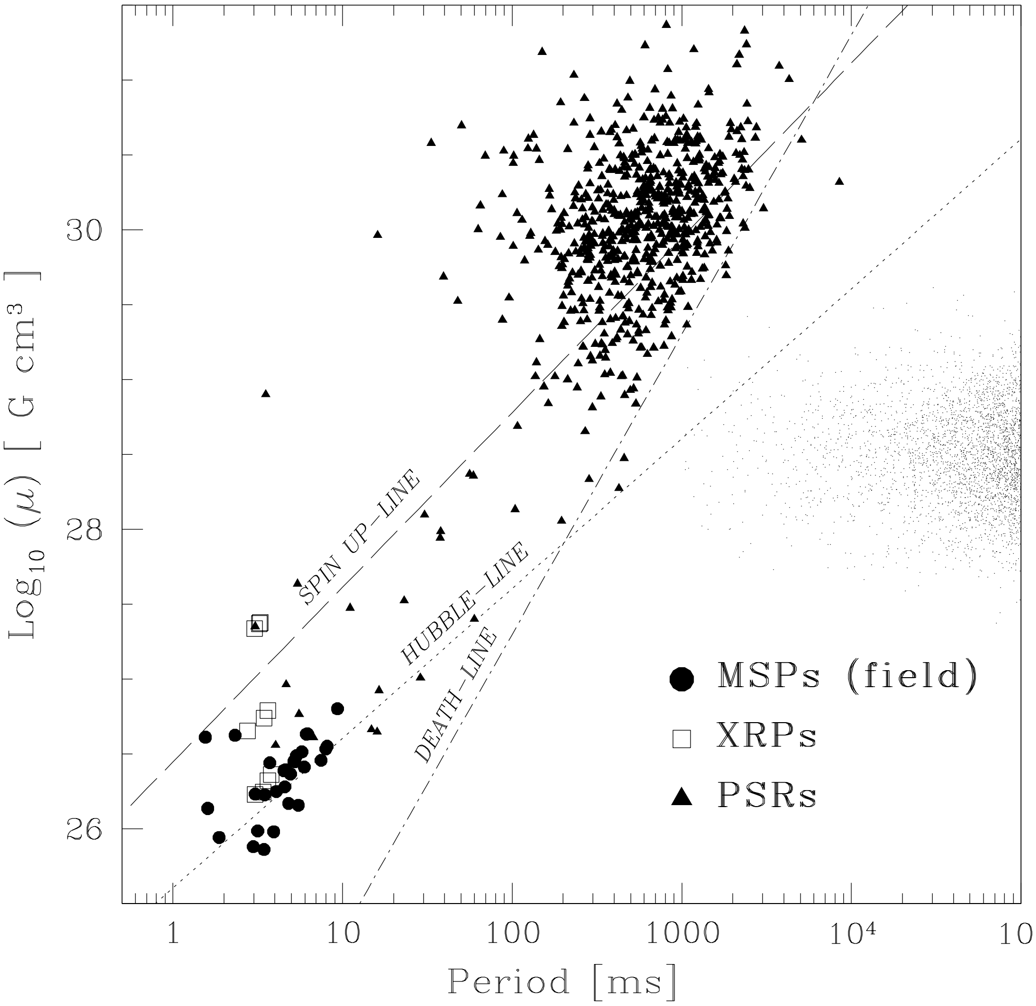

Figure 5.7: A typical initial distribution in the $\mu - P$ plane of the 3000 particles (*small dots*) we evolved in each run. The plot displays also the known pulsars (*triangles*), the millisecond pulsars discovered in the galactic field (*large dots*) and the kHz-QPO X-ray pulsars (*empty squares*).

II also the objects belonging to the second quadrant ($P < P_{min}$ and $\mu \geq \mu_{min}$) should shines as pulsars (see *e.g.* [41]);

III the effective observability of the objects in the third quadrant ($P < P_{min}$ and $\mu < \mu_{min}$) as radio sources represents instead a challenge for the modern pulsar surveys. Most of them will be above the Chen and Ruderman [42] "death-line", and might have a bolometric luminosity comparable to that of the known MSPs;

IV objects in the fourth quadrant ($P \geq P_{min}$ and $\mu < \mu_{min}$) are probably radio quiet neutron stars (RQNSs), because they tend to be closer to the theoretical "death-line", and they are in a period range which was already searched with good sensitivity by the radio surveys.

Thereafter we shortly refer as *sub*-MSPs to all the objects having $P < P_{min}$ and μ above the "death-line". In the discussion of the results, we will deal also with the observability of the synthesized neutron star populations in the X-ray band.

Bibliography

[1] **Burderi, L., Possenti, A., Colpi, M., Di Salvo, T., D'Amico, N. 1999**, *ApJ*, **519**, 285

[2] **Cook, G.B., Shapiro, S.L., Teukolsky, S.A. 1994b**, *ApJ*, **424**, 823 (CSTb)

[3] **Ravenhall, D.G., Pethick, C.J. 1994**, *ApJ*, **424**, 846

[4] **Shibata, M., Sasaki, M. 1998**, submitted, gr-qc/9807046

[5] **Bardeen, J.M., Press, W. H., Teukolsky, S. A. 1972**, *ApJ*, **178**, 347

[6] **Lipunov, V.M. 1992**, *Astrophysics of neutron stars*, Springer, Berlin

[7] **Burderi, L., Di Salvo, T., Robba, N.R., Del Sordo, S., Santangelo, A., Segreto, A., 1998**, *ApJ*, **498**, 831

[8] **Cook, G.B., Shapiro, S.L., Teukolsky, S.A. 1994a**, *ApJ*, **423**, L117 (CSTa)

[9] **Shapiro S.L., Teukolsky, S.A. 1983**, *Black Holes, White Dwarfs and Neutron Stars* (J.Wiley & Sons: New York), 178

[10] **Urpin, V.A., & Konenkov, D. 1997**, *MNRAS*, **284**, 741

[11] **Urpin, V.A., Geppert U., & Konenkov, D. 1998**, *MNRAS*, **295**, 907

[12] **Urpin, V.A., Konenkov, D., & Geppert, U. 1998**, *MNRAS*, **299**, 73

[13] **Geppert, U., & Konenkov, D., 1998**, Proc. Symp. *Neutron Stars and Pulsars*, Tokyo, Ed. N. Shibazaki, N. Kawai, S. Shibata, T. Kifune, Universal Academy Press, Inc.

[14] **van Riper, K.A. 1988**. *ApJ*, **329**, 339

[15] **Pandharipande, V., & Smith, R. 1975**, *Nucl.Phys. A*, **237**, 507

[16] **Sengupta, S. 1998**, *ApJ*, **501**, 792

[17] **Fujimoto, M., Hanava, T., Icko Iben, Jr., Richardson, M. 1984**, *ApJ*, **278**, 813

[18] **Miralda-Escude, J., Haensel, P., & Paczynski, B. 1990**, *ApJ*, **362**, 572

[19] **Zdunik, J., Haensel, P., Paczynski, B., Miralda-Escude, J. 1992**, *ApJ*, **384**, 129

[20] **Urpin, V.A., & Geppert, U. 1996**, *MNRAS*, **278**, 471

[21] **Haensel, P., & Zdunik, J.L. 1990**, *A&A*, **227**, 431

[22] **Itoh, N., Hayashi, H., & Kohyama, Y. 1993**, *ApJ*, **418**, 405

[23] **Yakovlev, D., & Urpin, V. 1980**, *SvA*, **24**, 303

[24] **Konar, S., & Bhattacharya, D., 1997**, *MNRAS*, **284**, 311

[25] **Konar, S., & Bhattacharya, D., 1999**, *MNRAS*, **303**, 588

[26] **Thorsett, S.E., Chakrabarty, D. 1999**, *ApJ*, **512**, 288

[27] **Woosley, S.E., & Timmes, F.X. 1996**, *Nucl.Phys. A*, **606**, 137

[28] **Friedman, B. & Pandharipande, V. 1981**, *Nucl.Phys. A*, **361**, 502

[29] **Arnett, W.D., & Bowers, R.L. 1977**, *ApJS*, **33**, 415

[30] **Bhattacharya, D., Wijers, R., Hartman, J., Verbunt, F. 1992**, *A&A*, **254**, 198

[31] **Lorimer, D.R. 1994**, Ph.D. Thesis, University of Manchester, U.K.

[32] **Hartman, J.W., Verbunt, F., Bhattacharya, D., Wijers, R.A.M.J. 1997**, *A&A*, **322**, 477

[33] **van Paradijs, J. 1995**, in *X-Ray Binaries*, eds. Lewin, van Paradijs, van den Heuvel, Cambridge University Press

[34] **Ergma, E., Sarna, M.J. & Antipova, J. 1998**, *MNRAS*, **300**, 352

[35] **Muslimov, A.G. & Sarna, M.J. 1993**, *MNRAS*, **262**, 164

[36] **Ghosh, P., & Lamb, F.K. 1991**, in Proc. NATO/ASI Ser **344**, *Neutron Stars: Theory and Observations*, ed. J.Ventura & D.Pines (Dordrecht: Kluwer), 363

[37] **Wang, Y. 1996**, *ApJ*, **465**, L111

[38] **Li, X.D., & Wang, Z.R. 1999**, *ApJ*, **513**, 845

[39] **Menou, K., Esin, A.A., & Narayan, R., Garcia, M.R., Lasota, J-P. & McClintock, J.E. 1999**, *ApJ*, **520**, 276

[40] **Podsiadlowski, Ph. & Rappaport, S. 1999**, astro-ph/9906045

[41] **Burderi, L., & D'Amico, N. 1997**, *ApJ*, **490**, 343

[42] **Chen, K. & Ruderman, M. 1993**, *ApJ*, **402**, 264

Chapter 6

The results

This Chapter 6 presents the bulk of the original results produced in this *Thesis*. In particular, the questions asked in the Chapter 1-Introduction are addressed, one by one, in the next six sections. Section [6.7] reports on other mechanisms which could affect the efficiency of the recycling of neutron stars to ultra short periods.

6.1 Are submillisecond pulsars a natural outcome of evolution in LMBs?

In this paragraph, we discuss the results of our population synthesis calculations without including the propeller effect. We will refer thereafter to them as *standard* models. In Figure 6.1 we report the observed sample of millisecond pulsars (MSPs) and the calculated populations for the two EoSs and the two adopted boundary conditions at the crust-core interface. The input parameters are those of Table 5.2 with $\tau_{RLO}^{max} = 5 \times 10^8$ yr. It appears that objects with periods $P < P_{min}$ are present in a significant number. In effect, although the detailed distributions of particles in the millisecond strip are influenced both by the EoS and by the magnetic field decay (see also Figures 6.2 & 6.3), **a tail of potential *sub*-MSPs always emerges.**

In the synthetic sample for the *soft*-EoS, the "barrier" at $P_{sh} \simeq 0.7$ ms is clearly visible in Figure 6.1, indicating that the field decay in longliving persistent LMBs proceeds fast enough to allow a significant fraction of objects to attain P_{sh}. The results are more clearly illustrated in Figure 6.3 (solid line): the **soft-EoS gives rise to period-distributions that increase rather steeply toward values smaller than 2 ms**, irrespective to the adopted BCs. Instead, the boundary condition affects the distribution on μ: BC II produces a smaller number of objects with low field, as the field initially decays but, when the currents are advected toward the crust-core boundary, their decay is halted and the field reaches a bottom value. In particular, as already found by Possenti, Colpi, D'Amico & Burderi [2] (where a BC of type II was considered), the fourth quadrant in Figure

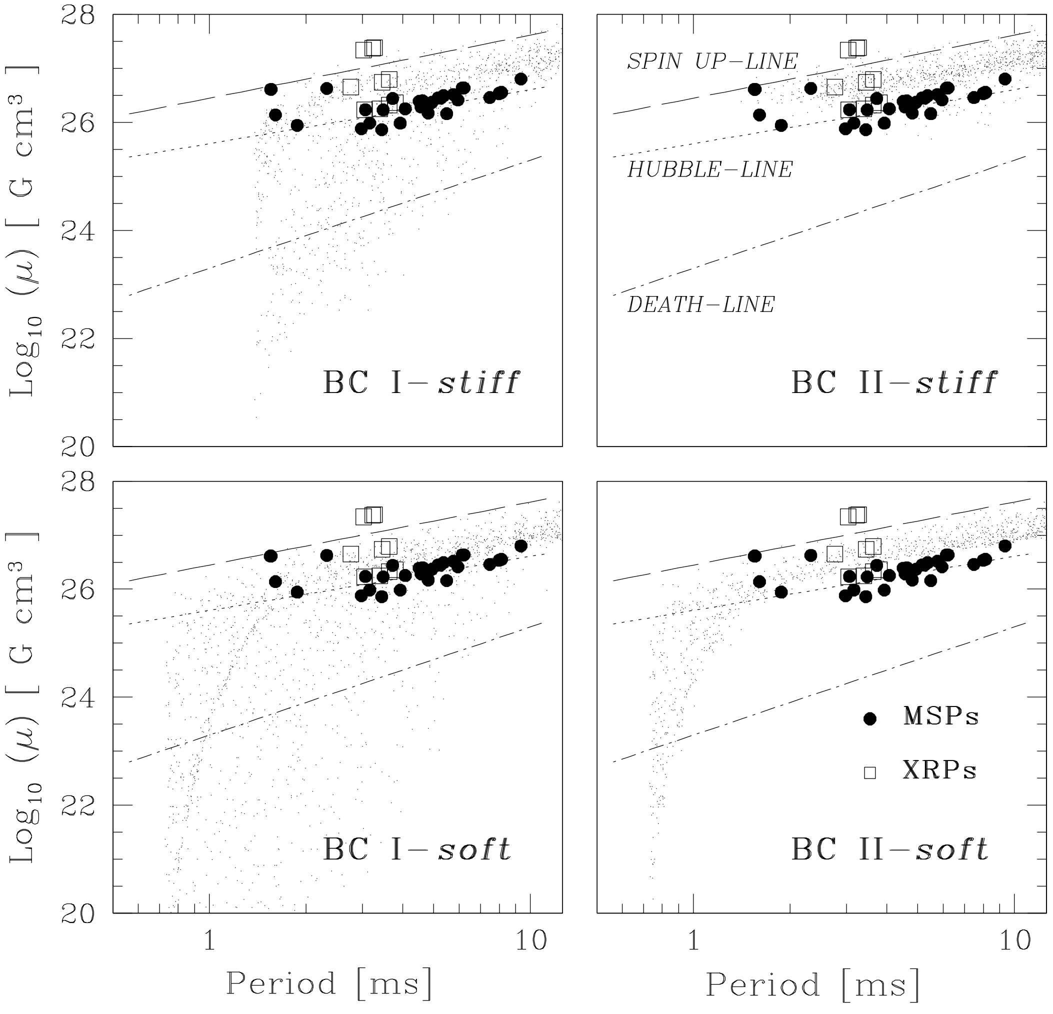

Figure 6.1: Statistical properties of the synthesized populations in the $\mu - P$ plane, for $< \dot{m} >= 0.1$ and $\tau_{RLO}^{max} = 5 \times 10^8$ yr. *Full dots* represent the sample of detected MSPs (online catalogue), while *open squares* represent the NSs in LMBs for which the period and the magnetic field have been inferred either from the kHzQPOs seen in their X-ray power spectrum, or from coherent pulsations during burst, as reported in White & Zhang [1].

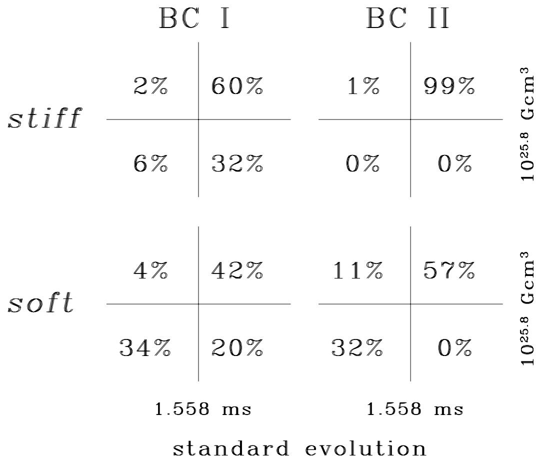

Figure 6.2: Distributions of the synthesized NSs, derived normalizing the sample to the total number of stars with $P < 10$ ms. We have divided the $\mu - P$ plane in four regions. As a guideline the upper left number in each cross gives the percentage of objects having $P < P_{min}$ and $\mu > \mu_{min}$ (the typical variance is about 1%). On the left side, we have indicated the EoS used. The crosses in the first column refer to the boundary condition BC I, whereas those in the second column to BC II.

6.2 is underpopulated (for a comprehensive examination of the statistical results inspect also Table 6.1).
The very *stiff*-EoS allows only periods P longer than 1.4 ms, and the minimum observed period P_{min} is already close to the "barrier" of mass shedding. Moreover, the field decay takes place on time scales longer than for a soft EoS and, on average, the sample of objects has a higher mean field. As a consequence, only few objects appear on the left of P_{min} (Figure 6.1). NSs with $\mu < \mu_{min}$ are rare objects for a BC of type II, and the ratios of *sub*-MSPs to MSPs are reduced with respect to the soft EoS. In particular, for the boundary condition BC II we have 0.003 for the stiff EoS and 0.573 for the soft one.

Major differences appear also examining Figure 6.3 (solid line): The **period distribution for the stiff-EoS is much flatter than that for the soft-EoS**, and for BC II it shows a broad maximum at $P \sim 3$ ms. It was recently claimed that X-ray sources in LMBs (possible progenitors of the MSPs, see Chapter 2 for details) show rotational periods clustering in the interval $2 \rightarrow 4$ ms ([1] [3]). This effect could be explained introducing a fine tuned relation between μ and $\dot{m}$ ($\mu \propto \dot{m}^{1/2}$ [1]). Alternatively, gravitational waves emission has been invoked:

either due to the growing of r-mode instability in the accreting NS [4] or due to a thermally induced quadrupole moment in the NS crust [5]. Here we note that such a clustering can be a natural statistical outcome of the recycling process.

6.2 Is unsteady or transient accretion in LMBs a threat to the existence of *sub*-MSPs?

The suggestion that NSs in low mass binaries may become transiently accreting sources after having experienced a phase of persistent accretion prompted us to consider the effect of decreasing the mean accretion rate $\dot{m}$ to mimic either the quenching of the accretion phase or the phases of quiescence in transient sources. If the magnetic field is high enough for the magnetosphere to affect the flow, the propelled matter may transfer outward the angular momentum of the NS. Therefore, we have considered the possibility that the NSs spend a fraction of the RLO phase in transit to final quiescence. The quenching of the accretion rate was modeled with a simple power law in time with index Γ_{que} lasting a fraction $\mathcal{F}_{que}$ of the duration of the RLO phase. Figures 6.3, 6.4, 6.5 & 6.6 and Table 6.1 show a summary of the results.

In Figure 6.3 the dashed areas give the distributions of the NSs at the end of evolution, including a strong propeller phase ($\mathcal{F}_{que} = 0.50; \Gamma_{que} = 8$) during the quenching of the RLO. The emerging distributions are depleted of the fastest rotating NSs. However, it is remarkable that **for the soft EoS the distributions preserve a maximum just about P_{min}**.
In Figure 6.4 we display the distribution of P for our synthesized populations at the end of the RLO phase (including strong propeller: dashed lines) and at the end of the magnetic dipole emission phase (dashed areas). It appears that dipole losses produce a clear shift of the entire population toward longer periods. However, it affects preferentially the distribution of NSs at periods longer than $\sim$4 ms. In our simulation we have noticed that dipole losses reduce considerably the number of NSs in the millisecond strip (especially for $\mu > \mu_{min}$). In particular Figure 6.5 shows that dipole losses are much more effective than a mild propeller ($\mathcal{F}_{que} = 0.25; \Gamma_{que} = 1$) in drifting the overall population at $P > 10$ ms, whereas it only slightly influences the very rapidly spinning objects.
Figure 6.5 allows also for the comparison of the different number of objects synthesized in the millisecond strip with different models. These numbers mainly depend on the timescale for μ to decay down to $\sim 10^{27.5}$ Gcm^3, the value requested for a particle to enter the millisecond strip: the shorter the decay timescale is, the more filled is the millisecond strip. With BC I, the soft EoS gives a number of objects that is about 50% greater than the stiff EoS. For BC II such a distinction is smoothed out except for a very short RLO phase ($\tau_{RLO}^{max} \simeq 5 \times 10^7$ yr), for which the freezing of μ is not operating yet.

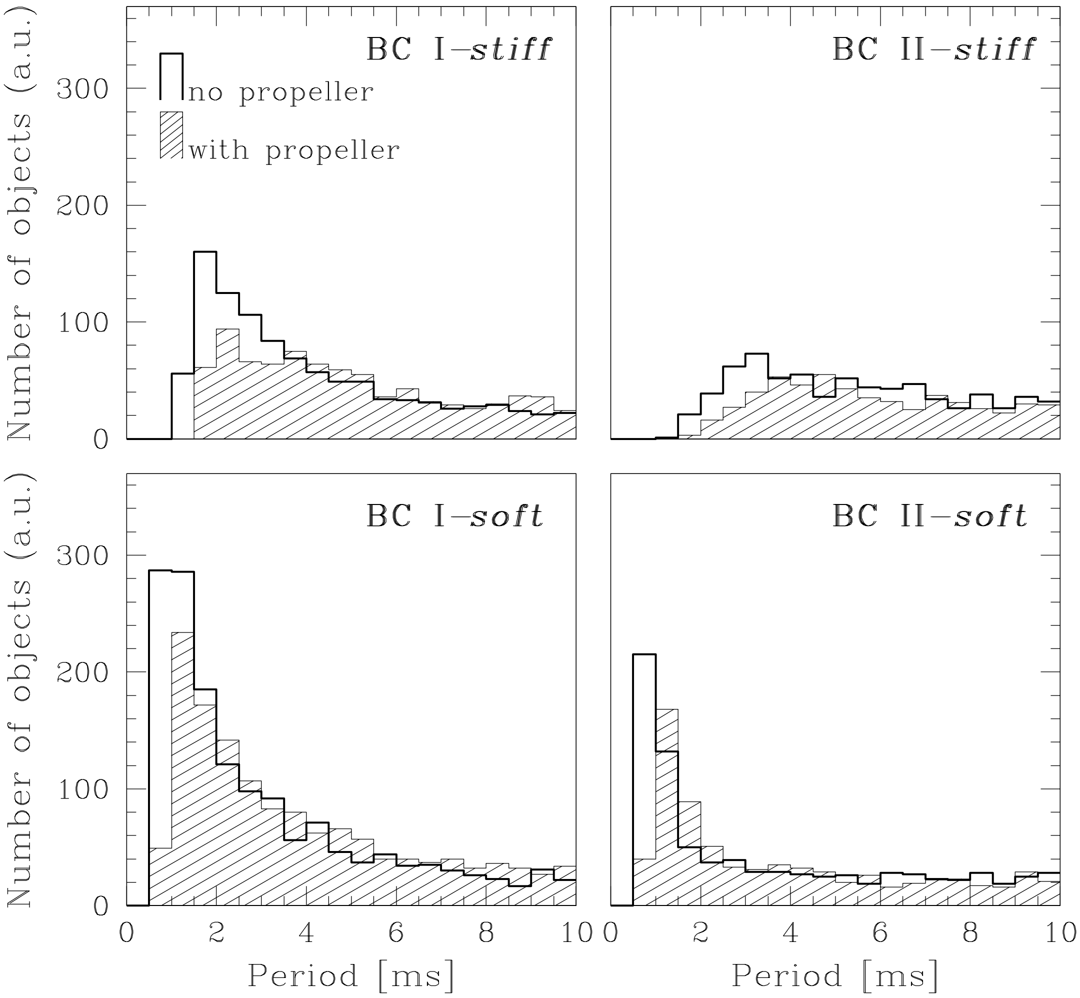

Figure 6.3: Calculated distribution of millisecond NSs as a function of the spin period P. The selected interval is $P_{sh} < P < 10$ ms and μ is let vary over the whole range. *Solid line* denotes the distribution in absence of propeller, whilst *dashed area* give the one with a strong propeller effect included ($\mathcal{F}_{que} = 0.50$ and $\Gamma_{que} = 8$). The absolute number of objects is in arbitrary units.

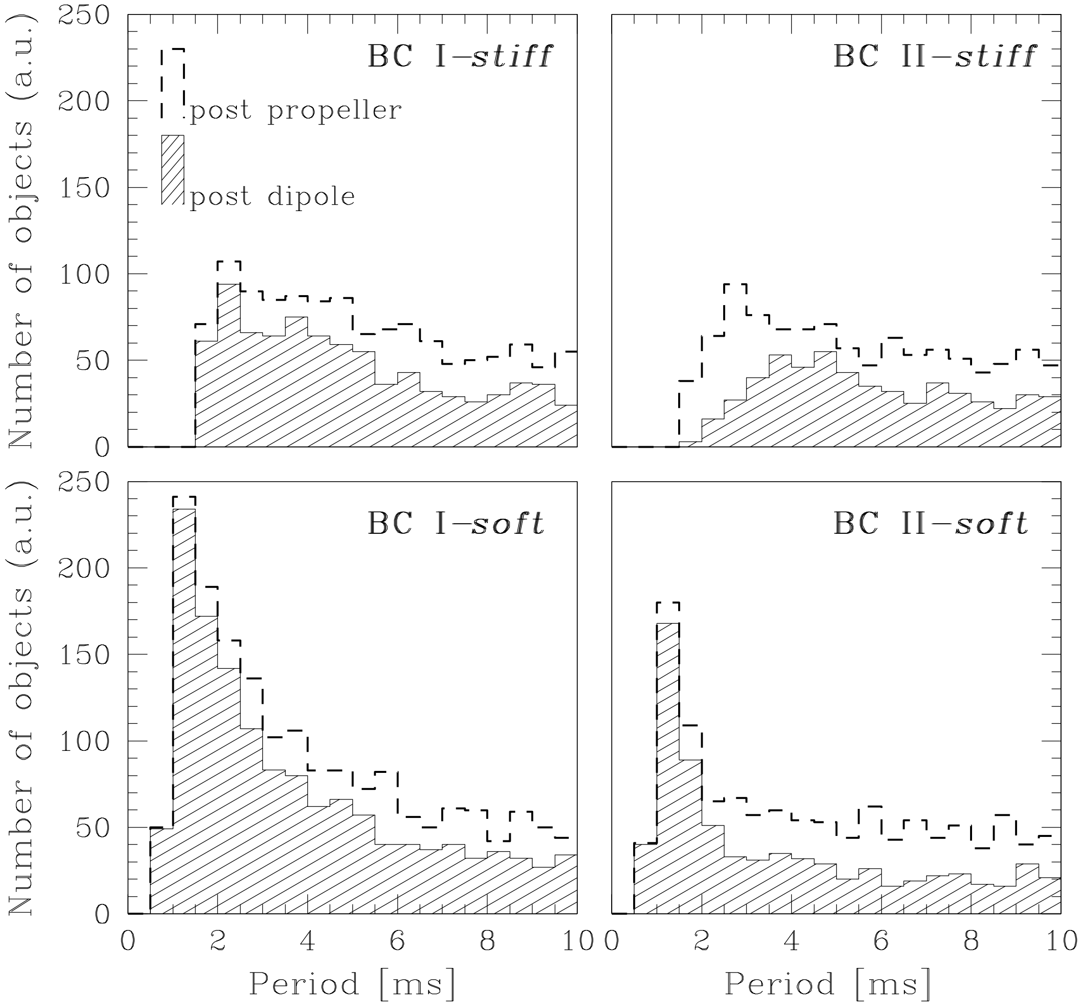

Figure 6.4: The four panels depict the NSs distributions at the end of the propeller phase (dashed lines), and at the end of the magnetic dipole phase (dashed area). μ is kept constant during the radio phase. The propeller is mimicked as for the case of Figure 6.3.

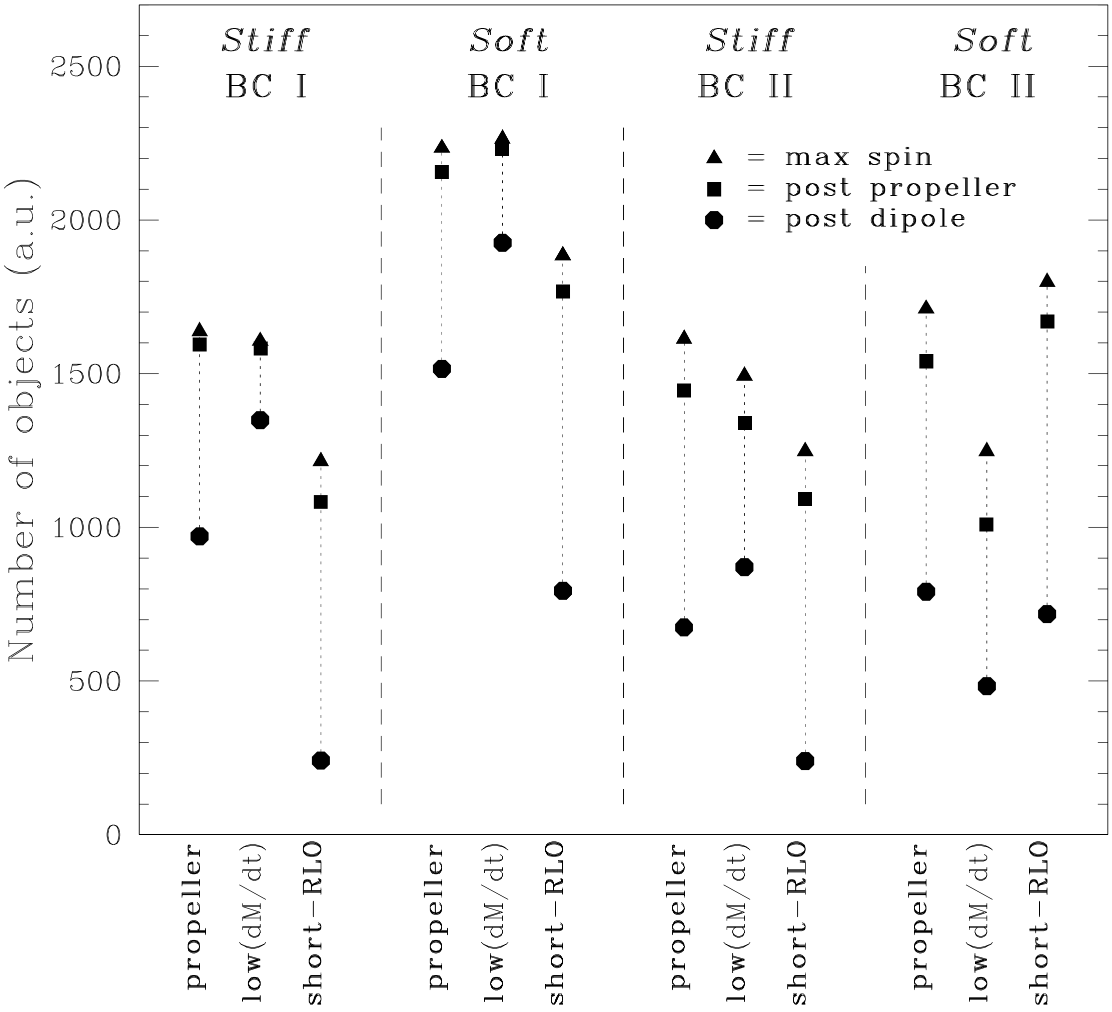

Figure 6.5: Number of synthesized objects with $P < 10$ ms at different stages of their evolution and for different models as indicated in the labels. "Propeller" model refers to $\tau_{RLO}^{max} = 5\times\ 10^8$ yr, $< \dot{m} >= 0.1$ in Eddington units, $\mathcal{F}_{que} = 0.25$, $\Gamma_{que} = 1$. For the "Low(dM/dt)" model we used $< \dot{m} >= 0.01$; while for the "short-RLO" model we adopted $\tau_{RLO}^{max} = 5\times\ 10^7$ yr. *Triangles* give the number of NSs at the end of the spinup phase during the RLO; *squares* give the number of NSs at the end of the propeller phase; *big dots* give the number of NSs at the end of the radio phase. The numbers calculated for each models are connected by a thin dotted line. These numbers are in arbitrary units, but with the same normalization for all the cases.

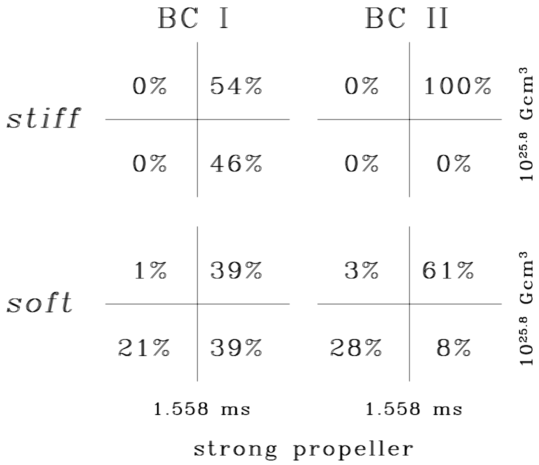

Figure 6.6: Distributions of the synthesized NSs, when a strong propeller ($\mathcal{F}_{que} = 0.50; \Gamma_{que} = 8$) is applied. Labels as in Figure 6.2.

Comparing Figure 6.6 with Figure 6.2, we note that **a strong propeller can threaten the formation of NSs with $P < P_{min}$ and $\mu > \mu_{min}$** especially in the case of the stiff-EoS (see also Table 6.1). For objects with $\mu < \mu_{min}$, the spin-down torque is weaker: accordingly, the III quadrant is less depleted than the second one and a non negligible number of low magnetic field fastly spinning NSs can survive at periods $\simeq 1$ ms, for the soft EoS.

6.3 Are the MSPs a tool for discriminating EoS and μ-decay?

In this paragraph we summarize the results of our statistical analysis considering in particular those objects having $P < P_{min}$. Table 6.1 collects the main results derived for the different scenarios (indicated in column ten). *Standard* evolution is the one discussed in section [5.3.2]. The other cases comprise a *propeller* phase at the end of the RLO (section [5.3.4]): here we adopted a propeller of intermediate effectiveness ($\mathcal{F}_{que} = 0.25$ and $\Gamma_{que} = 1$). To account for the uncertainties in the distribution of the accretion rates and/or in the maximum duration of the RLO stage, we run synthesis calculations either in the case of a *low* $\dot{m}$ ($\dot{m} = 0.01$ $\dot{\rm M}_{\rm E}$) or in the case of a *short* RLO phase ($\tau^{max}_{RLO} = 5 \times 10^7$ yr). Finally we combined the last two hypotheses.

The results are grouped by columns according to the adopted boundary condition (BC) for the magnetic field at the crust-core interface and by rows as regard to the EoS. In particular, columns 2 (for BC I) and 6 (for BC II) give the number of MSPs produced during the runs, normalized to the number of MSPs (set equal to 1000) synthesized in the case labeled by (iii) in the eleventh column. These figures give an estimate of the efficiency of the recycling process in producing objects in the first quadrant. The third (for BC I) and the seventh columns (BC II) give the fraction of NSs in quadrant II relative to I. The fourth and the eighth columns (respectively for BC I and BC II) report the fraction (II+III)/I while in brackets we give f_{sub}, i.e., the fraction of NSs with $P < P_{min}$ and μ lying above the death line relative to the sample of NSs filling quadrant I.

The estimate of f_{sub} can give indication on the fraction of *sub*-MSPs relative to the observed MSPs: if selection criteria similar to those found in the interval $P_{min} < P < 10.0$ ms apply as well at periods below P_{min}, f_{sub} provides an estimate of the number of pulsars that might be observable below P_{min}. We find that f_{sub} varies between 0%$\rightarrow\sim$57%; the lower figure applies only to the case of an EoS of extreme stiffness. These objects should be observable with experiments like the survey in progress at the Northern Cross radio telescope near Medicina [6], which has similar sensitivity in the MSPs and in the *sub*-MSPs range.

Inspection of Table 6.1 suggests that the EoS for the nuclear matter has a major role in determining the ratio f_{sub}: the formation of a *sub*-MSP is quite a rare event, for the very stiff EoS. On the contrary, in the case of a moderately soft EoS, the *sub*-MSP population is significant, irrespective to the details of the evolutionary scenario. Thus, the detection of a significant number of *sub*-MSPs would be strongly suggestive of a not too stiff EoS. A clear distinction in the models can be seen comparing case (iv) with (ix). If a moderate propeller takes place and the typical RLO timescale is shorter than usually assumed, for a soft-EoS f_{sub} $\simeq$30% (irrespective the BC), whilst no *sub*-MSPs could appear if the nuclear matter behaves as predicted by the stiff-EoS.

The details of the evolution can blur the outcome of the statistical analysis preventing a clear distinction between the equation of states when based on the simple ratio f_{sub} (e.g. cases (i), (ii) and (iii) versus (x) for the BC I). The boundary condition for the magnetic field at the crust-core interface weakly affects the figures of Table 6.1 (except for case (viii)) when considering only the objects filling the I and the II quadrant (compare the columns 2 and 3 with the columns 6 and 7). Due to their effects on the decay of the surface magnetic field, **the differences between the two BCs are revealed mainly in the synthesized populations having $\mu < \mu_{min}$.**

Table 6.1: Population Syntheses Results

	BC I				BC II					
EoS	*Number* **I**	*Percentage Ratio* II/I	(II+III)/I	(III+IV)/I	*Number* **I**	*Percentage Ratio* II/I	(II+III)/I	(III+IV)/I	*Kind of Evolution*	*Idx*
Stiff	**689**	4.0	14.2 (11.5)	63.5	**823**	0.3	0.3 (0.3)	0.0	standard	i
	671	1.5	8.6 (6.9)	65.3	**774**	0.1	0.3 (0.3)	0.0	propeller	ii
	738	0.0	8.4 (2.3)	110.3	**1000**	0.1	0.3 (0.3)	0.0	low $\dot{m}$+propeller	iii
	277	0.0	0.0	0.0	**275**	0.0	0.0	0.0	short$_{RLO}$+propeller	iv
	125	0.0	0.0	0.0	**116**	0.0	0.0	0.0	short$_{RLO}$+low $\dot{m}$+propeller	v
Soft	**742**	10.1	91.9 (46.0)	129.0	**547**	19.4	74.3 (57.3)	54.9	standard	vi
	730	8.0	83.9 (40.5)	131.1	**523**	16.3	73.8 (55.9)	57.5	propeller	vii
	720	0.6	85.1 (21.1)	207.4	**390**	12.1	42.5 (34.2)	30.4	low $\dot{m}$+propeller	viii
	677	17.7	34.2 (34.2)	17.2	**640**	18.2	28.8 (28.8)	10.6	short$_{RLO}$+propeller	ix
	410	3.4	7.6 (7.6)	5.9	**231**	7.0	11.9 (11.9)	5.5	short$_{RLO}$+low $\dot{m}$+propeller	x

Table 6.1: Legend:
I = Number of synthesized objects in the first quadrant ($P > P_{min}$ and $\mu > \mu_{min}$). These numbers are normalized to the case (iii) for Boundary Condition BC II, set equal to 1000. newline **II/I** = Percentage ratio of the objects filling the II quadrant over those filling the I quadrant.
(II+III)/I = Percentage ratio of the objects filling the II and the III quadrant over those filling the I quadrant. In parenthesis the percentage ratio of the objects having $P < P_{min}$ and μ above the death line over those filling the first quadrant.
(III+IV)/I = Percentage ratio of the objects filling the III and the IV quadrant over those filling the I quadrant.
Idx = Index for the specific synthesized population. The different kinds of evolution are labeled as in the text.

6.4 Do weakly magnetized rapidly spinning NSs exist?

Except for the most unfavorable case (very stiff-EoS & BC II), **all our synthesis runs produce a significant amount of objects with $\mu < \mu_{min}$** (see III & IV quadrants in Figures 6.2 & 6.2). Their period distribution is very sensitive to the adopted internal boundary condition for the magnetic field diffusion at the crust–core interface. BC II clearly favours fastly rotating objects ($P \lesssim 1.5$ ms), the IV quadrant in Figures 6.2 & 6.6 being (scarcely) populated only in the case of a very strong propeller. For BC I the distributions are broader and the stiffer the EoS is, the more depleted is the III quadrant. In principle, such a distinction could allow a discrimination among the two BCs. On the observational point of view, very low magnetized NSs in the IV quadrant (upon which we focus in this paragraph) might be elusive sources. Irrespective to the selection effects or survey sensitivity thresholds, these objects might be rather close to the theoretical "death line" to be observable as radio, and it is not clear if we can observe them in the X-ray band.

6.4.1 *Comparison with the determination of μ in kHzQPO X-ray sources*

Recently a neutron star rotating in the millisecond interval (SAX J1808.4-3658 with $P = 2.49$ ms) has been detected in X-rays [7]. It is in a binary system with a low mass companion [8] which transfers mass to the compact object. As the rotational period is known, one can constrain the surface magnetic field of the accreting NS [9].

(a) An **upper limit** on μ relies on the requirement that accretion is not centrifugally inhibited at the minimum accretion rate at which coherent pulsations are detected.

(b) The standard disk-magnetosphere model [10] interprets coherent X-ray pulsations as due to a complete or a partial funneling of the disk plasma along the NS magnetic field lines. Many improvements had to be added to this model (Ghosh & Lamb [11] for a review) to account for the variety of observations (see also Bildstein [12]); but in this framework, a rotating NS can appear as an accretion powered pulsar only if the magnetic moment is strong enough to terminate the Keplerian disk above the stellar surface ([9], [13]). This requirement translates in a **lower boundary** on the possible value of μ.

For the case of SAX J1808.4-3658, Psaltis & Chakrabarty [9] found $3 \times 10^{25} \lesssim \mu \lesssim 10^{27}$ Gcm^3, with a preferred value about a few times 10^{26} Gcm^3.

So, this object seems to be placed near the separation of the quadrants I and IV. Alternative models, not related or poorly related to μ, could explain coherent X-ray modulation at the NS spin frequency (e.g. azimuthal variation in optical depth for absorption or scattering) from which no further constraints on μ arise.

Already from the half of the nineties, the spin periods for a handful of NSs in low mass X-ray binaries have been inferred either from coherent pulsations during Type-I bursts or, indirectly, from the so-called kHz-QPOs (van der Klijs [3] for a review). In the latter case, the paradigm is the so-called beat frequency model, in which the frequency difference $\Delta\nu_{qpo}$ among the two peaks appearing in the X-ray power spectrum of the source is representative of the spin frequency of the NS or of an overtone [14]. From the inferred spin, and assuming that these NSs rotate at about their equilibrium period (that is, near their competing spinup line), one can estimate (through condition (a)) the value of μ. In Figure 6.1, we display (*open squares*) the positions of the NSs of this group in the $\mu - P$ plane, adopting the values of White & Zhang ([1] and reference therein for a discussion about the errors in the determination of P and μ). It appears that no X-ray source shows $\mu < \mu_{min}$.

Prompted by the evidence that the value for $\Delta\nu_{qpo}$ is not constant ([15], [16]), other models for explaining the kHz-QPOs have been proposed. For instance, Stella & Vietri [17] interpret the upper QPO frequency ν_2 as due to matter inhomogeneities orbiting the NS at the inner disk boundary (just as in the standard beat frequency model), whilst the lower QPO frequency ν_1 is produced by the periastron precession at the inner edge of the accretion disk. Apart from negligible corrections (due to the effect of the NS rotation on the exterior metric), the observed difference $\Delta\nu_{qpo} = \nu_2 - \nu_1$ is unrelated to the spin frequency of the NS. Being P not constrained by the observation, condition (b) for a lower limit on μ does not apply anymore.

Hence, we argue that also the magnetic moment estimates become questionable in this framework. Li & Wang [18], constructed refined slim disk models in LMBs, incorporating the effects of both magnetic field and general relativity: for the kHz-QPO sources they found values of the surface magnetic field smaller than the previous authors. If this is the case, the values of μ in kHz-QPO sources ($\lesssim 10^{25}$ Gcm^3) are systematically weaker than those of MSPs sample and these X-ray emitting objects would populate our IV quadrant.

As a general comments on the observability of low magnetic field NSs in the X-ray band, we note that if the capability of coherently emitting X-rays pulses requires high enough values of μ, missing rotating NSs with P close to a millisecond would not be surprising: as shown in section [6.5], only a rapid and substantial decay of μ allows a NS to reach $P < P_{min}$. Therefore, low magnetic field fastly spinning NSs could be just those not showing coherent X-ray pulsations. Instead, the signature of very rapidly spinning objects might hopefully emerge from low amplitude features in their power spectrum, related to incoherent modulation of the X-ray brightness.

6.5 Which is the minimum mass of a NS approaching P_{sh}?

Using the semi-analytical model described in section [5.1.1], we compute the relation between the period P and the accreted baryonic mass M_{ac} for the case of an unmagnetized NS (as in [19]) considering three selected EoSs (labeled as in Arnett & Bowers [20]). The EoS-A (Reid soft core; [21]) is a soft equation of state, slightly softer (maximum static mass of 1.66 $M_{\odot}$ and a circumferential radius of 9.58 km for a canonical 1.40 $M_{\odot}$ NS) than the EoS-FP used in the population synthesis calculation. The EoS-L (Mean Field: [22]) belongs to the group of the stiff equations of state, not very different from the PS-EoS used in sections [6.1] to [6.4]: maximum static mass of 2.70 $M_{\odot}$ and a circumferential radius of 14.99 km for a canonical 1.40 $M_{\odot}$ NS. Here, also the case of an intermediate EoS was explored, namely the FPS (based on UV14+TNI: [23]). It has a maximum static mass of 1.80 $M_{\odot}$ with a circumferential radius of 10.85 km.

As illustrated in Figure 6.7 the spin period P shows a steep dependence on the mass loading just above $\sim$ 3 ms and small values of M_{ac} $(0.04 - 0.06 M_{\odot})$ are sufficient to produce a millisecond NS. By contrast, substantial mass load is requested for spinning the NS below the observed minimum period P^{obs}_{min} = 1.558 ms (PSR B1937+21). When approaching the limiting period P_{lim} for mass shedding, the relation P vs M_{ac} flattens.

As already noted by Cook, Shapiro & Teukolsky [19], all EoSs allow a NS to be spun up to P^{obs}_{min}, but a stiffer EoS requires a higher value of M_{ac}: 0.25 $M_{\odot}$ for EoS L (stiff) as compared to 0.1 $M_{\odot}$ for EoS A (soft). We have verified that such figures are only slightly affected by assuming a lower initial gravitational mass for the NS (*e.g.* 1.30 $M_{\odot}$ - 1.35 $M_{\odot}$).

In the case of a magnetized NS, the rate at which angular momentum is transferred to the NS is controlled by the interaction of the magnetosphere with the inner boundary of the accretion disk. Thus, the mass load M_{ac} which is necessary to attain a period P depends upon the magnitude of the B-field, on its evolution and on the torque function g(Ω). We describe different evolutionary pathways, during recycling, introducing two characteristic times: the spinup time τ_{up} and the timescale τ_{μ} of decay of the star's magnetic moment μ

$$\tau_{up} = \frac{P}{\dot{P}} \quad ; \quad \tau_{\mu} = \frac{\mu}{\dot{\mu}} \tag{6.1}$$

As a guideline we consider:

(i) a two-steps evolution in which a phase of significant μ-decay (with $\tau_{\mu} \ll \tau_{up}$) precedes the phase of spinup at constant μ (with $\tau_{\mu} \gg \tau_{up}$);

(ii) evolutionary pathways with $\tau_{\mu} = (6/7)\ \tau_{up}$.

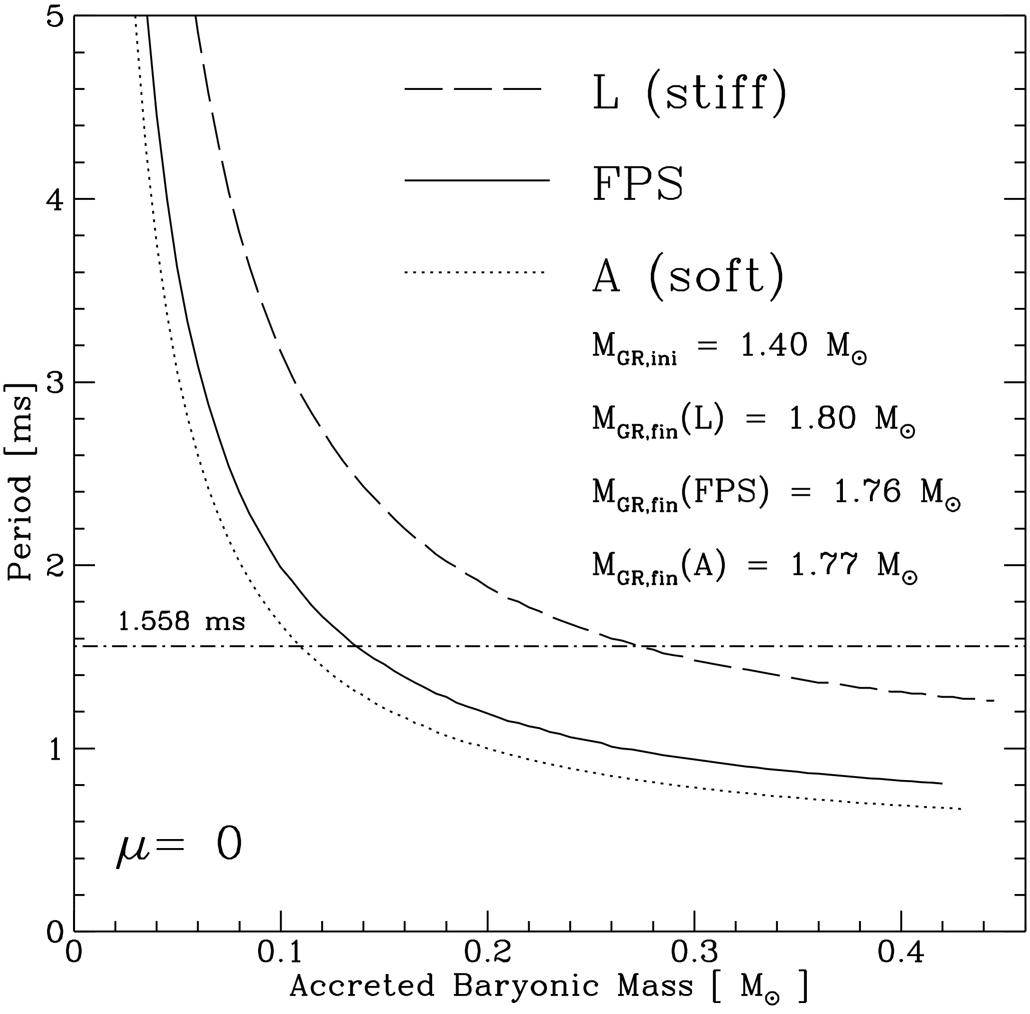

Figure 6.7: P vs M_{ac} relations for the case of a unmagnetized NS considering three selected equations of state: L (stiff: *dashed line*), A (soft: *dotted line*), FPS (intermediate: *solid line*). The initial gravitational mass of the NS is always $1.40\ M_\odot$. The period P is measured in millisecond, the accreted baryonic mass M_{ac} is in solar mass. The dashed–dotted line represents the minimum rotational period observed so far. Accretion is halted when the centrifugal limit is reached.

The latter condition describes the idealized situation of a NS sliding parallel to the spinup line (corresponding to a fixed accretion rate) without braking along it. In other words, the decay of μ is tuned just to allow for the NS to approach but never reach the equilibrium period, where the efficiency of the spinup process drops steeply [24] [11]. In fact, at the equilibrium period, the star would accrete matter without increasing its rotational rate. It is easy to demonstrate that the mass necessary to attain a final period P in case (i) exceeds that of case (ii) by a factor 4/3. For $\tau_\mu \gg \tau_{up}$ even larger amounts of mass are needed. Thus, **case (ii) provides a *lower limit* on the mass load onto the NS during the recycling process.**

The relativistic corrections at short rotational periods and the details of the disk-magnetosphere interaction prevent a simple analytical study of the spin evolution. Hence, we explored numerically the NS evolution. Figure 6.8 collects a sample of pathways in the plane P vs M_{ac} obtained for the equation of state FPS (the intermediate EoS), combining various initial conditions (periods in the range $1-100$ sec, μ_{ini} between $10^{28}-10^{30}$ G cm^3, accretion rates in the interval $0.01-1.00\ \dot{M}_{Edd}$) and selecting decay histories according to models (i) and (ii). As illustrated in such figure, the values requested to drive a NS to a final period P depend on the magnetic field evolution. We notice, however, that only for NSs with $P>$ 5 ms at the end of binary evolution the mass load is sensitive to the history of the μ-field. For a magnetized NS the demand of accreted matter can at most halve, relative to the value inferred for a unmagnetized NS. If evolution proceeds to drive P below 5 ms, the request of M_{ac} depends weakly on the evolution of μ since the magnetospheric radius shrinks, becoming comparable to the radius of the last marginally stable orbit or to the physical radius of the star. Therefore, the P vs M_{ac} relation relaxes to the line that characterizes a unmagnetized NS.

We calculated the absolute *minimum amount of mass* needed to attain a rotational period P. Assuming a very slow μ-decay, or introducing other effects in the recycling process, the requested mass would increase, making even questionable the possibility of spinning the NS up to P. Indeed, loading mass without significantly accelerating the star could push the compact object beyond the maximum equilibrium mass, forcing it to collapse to black hole. The *thin solid line* in Figure 6.8 just represents the effect of a slow μ-decay: the evolution along the spinup line is "braked" and the requested mass load increases.

6.6 Which is the typical mass of a NS recycled in a LMXB?

Our statistical analysis can provide also information on the NS mass distribution as a function of P at the end of evolution. We examined the M_G vs P histograms related to the outcomes of our synthesis calculations, in which the NS populations

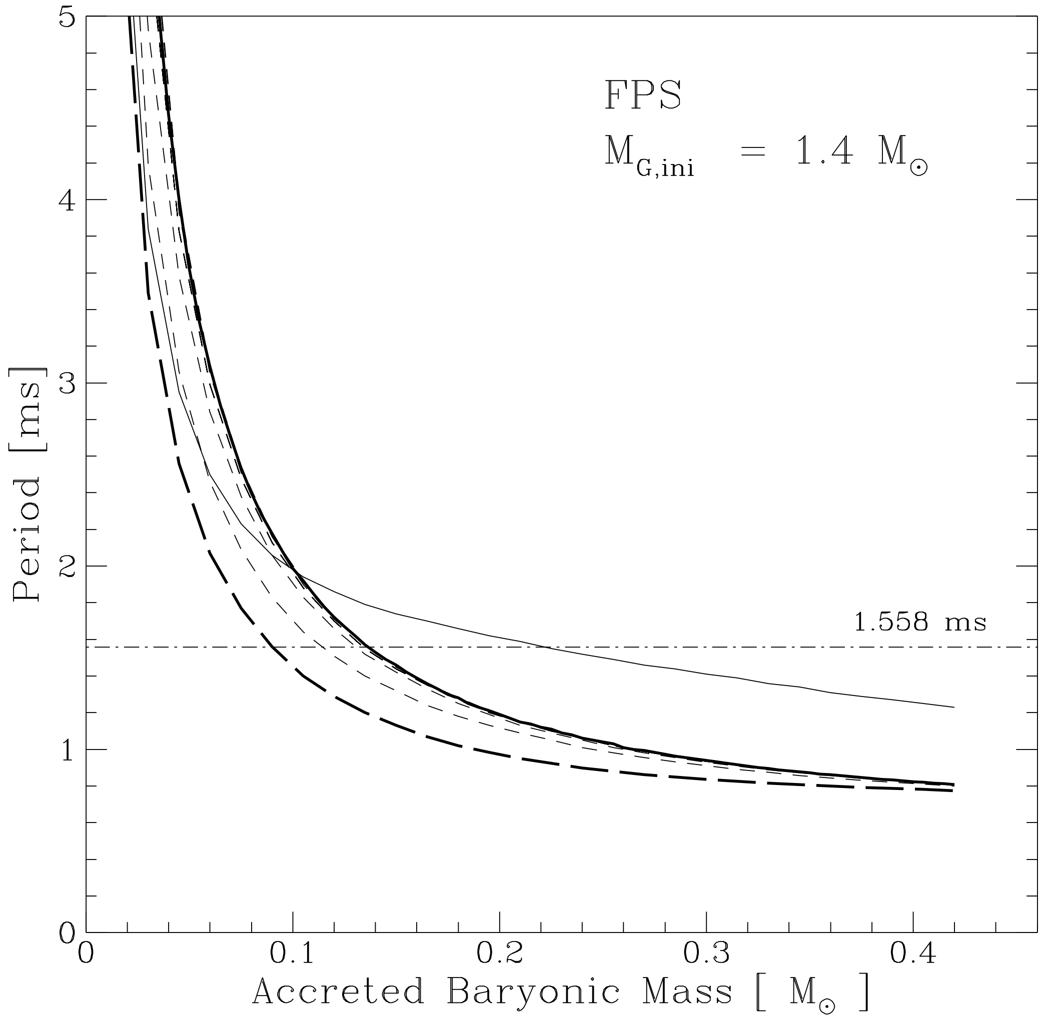

Figure 6.8: P vs M_{ac} relations for a magnetized NS using FPS-EoS and an initial gravitational mass of $1.40\ M_\odot$. The different pathways (a sample is represented by the *dashed lines*) define a strip, which narrows towards shorter periods (see text for details). The strip is upper bounded by the evolutionary path for an unmagnetized NS (*bold solid line*). The *bold long dashed line* refers to the evolution along the spinup line and is calculated assuming a step shaped g-torque function (an extreme situation which maximizes the efficiency of the spinup process). The *thin solid line* refers to a very slow μ-decay.

have been evolved according to the parameters reported in Table 5.2. In particular in Figure 6.9 we display the results for the *standard* evolution and for the one with a significant *propeller* phase at the end of the Roche Lobe Overflow stage.

We find that the mass function steepens toward high values when P falls below P_{min}: the distribution approaches values close to $M \sim 1.7 \div 1.8 M_{\odot}$. That is a straight consequence of the results of the previous section [6.5]: a large mass deposition is required to spin a NS to ultra short periods.

One could suspect that the small amount of mass $M_G \lesssim 0.1\mathrm{M}_{\odot}$ needed for reaching the millisecond periods ($1.558 < P < 10$ ms) were an effect of the *unphysical ad-hoc* model for the $\mu - decay$ we adopted in section [6.5]. Conversely, Figure 6.9 shows that, also assuming a detailed fully consistent model for the evolution of the magnetic field, the typical average gravitational mass $M_{G,ave}$ of the observed millisecond population should not be significantly different from that of the NSs at their birth. Only particular evolution pathways from uncommon initial parameters could provide the conditions for producing some more massive millisecond pulsars.

The action of the propeller during the evolution has the clear effect of inhibiting the mass infall: the mass distribution is only slightly affected for the soft EoS, while for the stiff EoS the difference is more pronounced.

6.6.1 *Comparison with the observation of NS masses*

Few estimates of the masses of millisecond pulsars in low mass binaries are now available and are reported in Figure 6.10. The data, taken from Thorsett & Chakrabarty [25], are all compatible with the P vs M_{ac} relation derived in section [6.5]. In particular for PSR B1855+09, the MSP with a mass estimate based on GR alone ($M_G = 1.41 \pm 0.1 M_{\odot}$), the (minimum) mass requested to reach the observed period ($P = 5.362$ ms) would be of at most $0.06 M_{\odot}$ (for the stiff EoS and an initially low value of μ).

Thorsett & Chakrabarty [25] found that data obtained collecting the mass measurements of all the known radio pulsars in binary systems are consistent with a remarkably narrow underlying gaussian mass distribution, with $M_G = 1.35 \pm 0.04 M_{\odot}$. Their sample of objects contains however five relativistic NS-NS binary systems that contaminates the statistics of MSP binaries, narrowing the value of M and in turn of M_{ac}. The progenitors of the NS-NS systems are massive X-ray binaries, a population which does not lead to the formation of fast spinning pulsars. If the proposed value of $M_{ac} < 0.1\ M_{\odot}$ is representative of the MSPs observed sample, this figure is suggestive that a fast decay of the magnetic field has occurred in these systems (not only in PSR B1855+09). This is not in contradiction with our estimates on M_{ac} because *only for those MSPs recycled to limiting periods $P < P^{obs}_{min}$ the demand of mass load would exceed that of Thorsett & Chakrabarty.*

Moreover, also LMXBs could harbour NSs with such high values of the mass

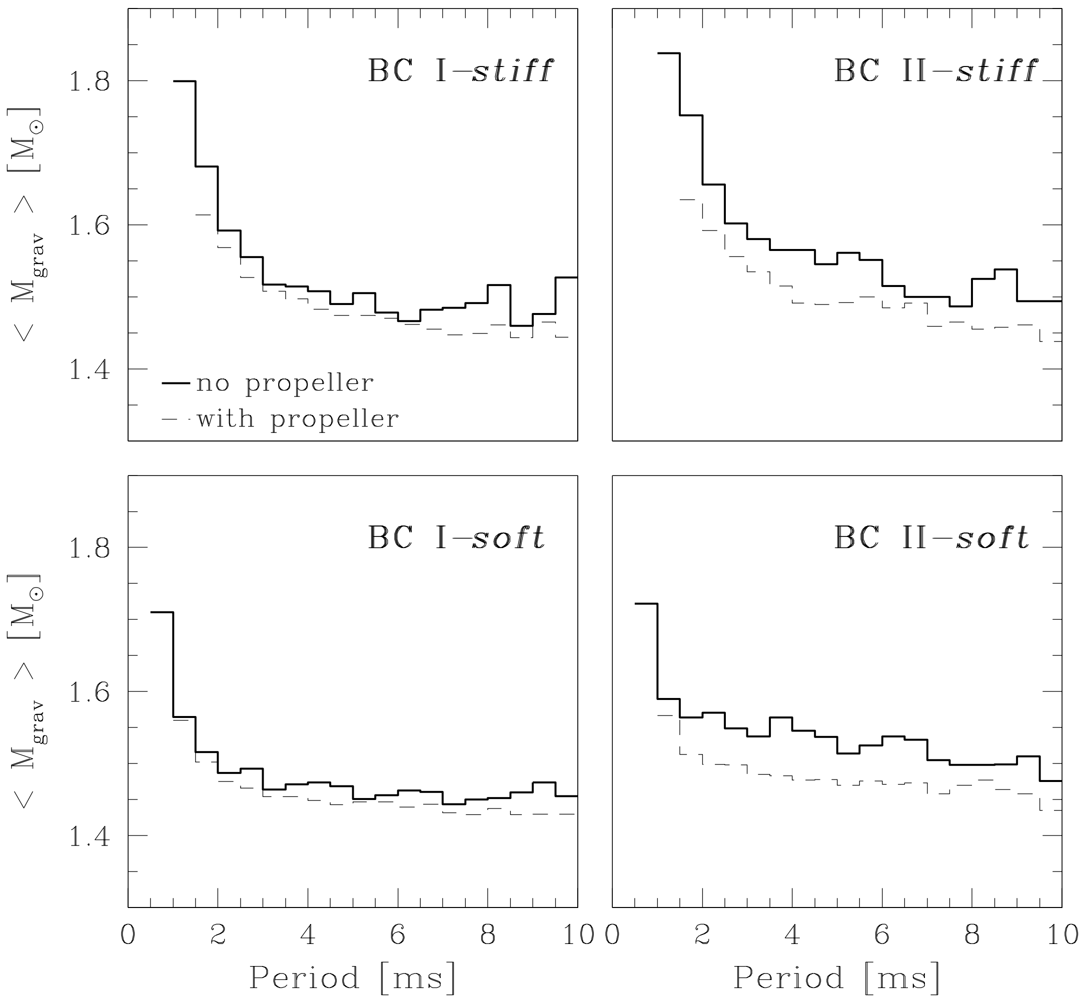

Figure 6.9: Average gravitational masses of the re-accelerated NSs as a function of their final spin period P. μ is let vary over the whole range and the synthesized NSs are binned in 0.5 ms wide intervals. The initial mass of the static NSs is set equal to $1.40\mathrm{M}_{\odot}$ for all the cases. *Thick solid line* denotes the mass-distribution in absence of propeller, whereas *thin dashed line* gives the one with a strong propeller effect included ($\mathcal{F}_{que} = 0.50$ and Γ_{que}=8).

and a first indication comes from Casares, Charles & Kuulkers [26] who inferred for Cyg X-2 a lower mass limit of 1.88 $M_\odot$.

Interestingly, a further suggestion of the existence of NSs with masses larger than $1.4 M_\odot$ arises also from a the recent model of Stella & Vietri [17] already described in section [6.4.1]. It accounts for the pair kHz-QPOs observed in many LMXB sources (see *e.g.* van der Klis [3] for a review). In particular Stella & Vietri interpret the upper QPO frequency ν_2 as due to matter inhomogeneities orbiting the NS at the inner disk boundary, while the lower QPO frequency ν_1 is produced by the periastron precession at the inner edge of the accretion disk. In this framework, the observed clustering of the differences $\Delta\nu = \nu_2 - \nu_1$ around 250 - 360 Hz is naturally explained provided the gravitational mass of the typical accreting NSs is $\sim 2\ M_\odot$.

The detection of millisecond X-ray pulsations from SAX J1808.4-3658 at different luminosity levels of the source suggests the presence of a massive NS also in this system as discussed by Burderi and King [13].

6.7 Which other effects could inhibit the formation of ultra fastly rotating neutron stars?

So far, **there is no observational evidence against the existence of NSs rotating at submillisecond periods**. In the evolutionary scheme adopted, the formation of such *submillisecond NSs* is a natural outcome if a minimum mass of $\simeq 0.25 - 0.30 M_\odot$ is accreted and if the magnetic moment decays down to values $10^{25} - 10^{26}$ Gcm^3 *before* the end of recycling.

6.7.1 *Highly non-conservative scenarios for mass transfer*

In our framework, only highly non-conservative scenarios may indeed prevent the transfer of $M_{ac} \geq 0.3\ M_\odot$ in low-mass binaries. In fact, evolutionary considerations shows that the mass transfer occurs either because of the nuclear evolution or because of orbital angular momentum losses of a $\sim 1\ M_\odot$ companion (see *e.g.* [27], [28])

- A more massive companion ($M \gtrsim 2\ M_\odot$ – if we retain the hypothesis that the NS mass at birth is $\sim 1.4\ M_\odot$) would determine a dynamically unstable mass transfer probably ending into a common envelope phase [29] [30].

- On the other hand, a low mass companion ($M \lesssim 1\ M_\odot$) would either underfill its Roche lobe, because its nuclear evolution timescale is longer than the age of the Galaxy for initial orbital periods $\gtrsim 0.5$ days, or, for shorter initial orbital periods, would fill its Roche lobe during its main sequence lifetime, resulting in a near–permanent faint LMXB, whose compact object will never appear as a radiopulsar.

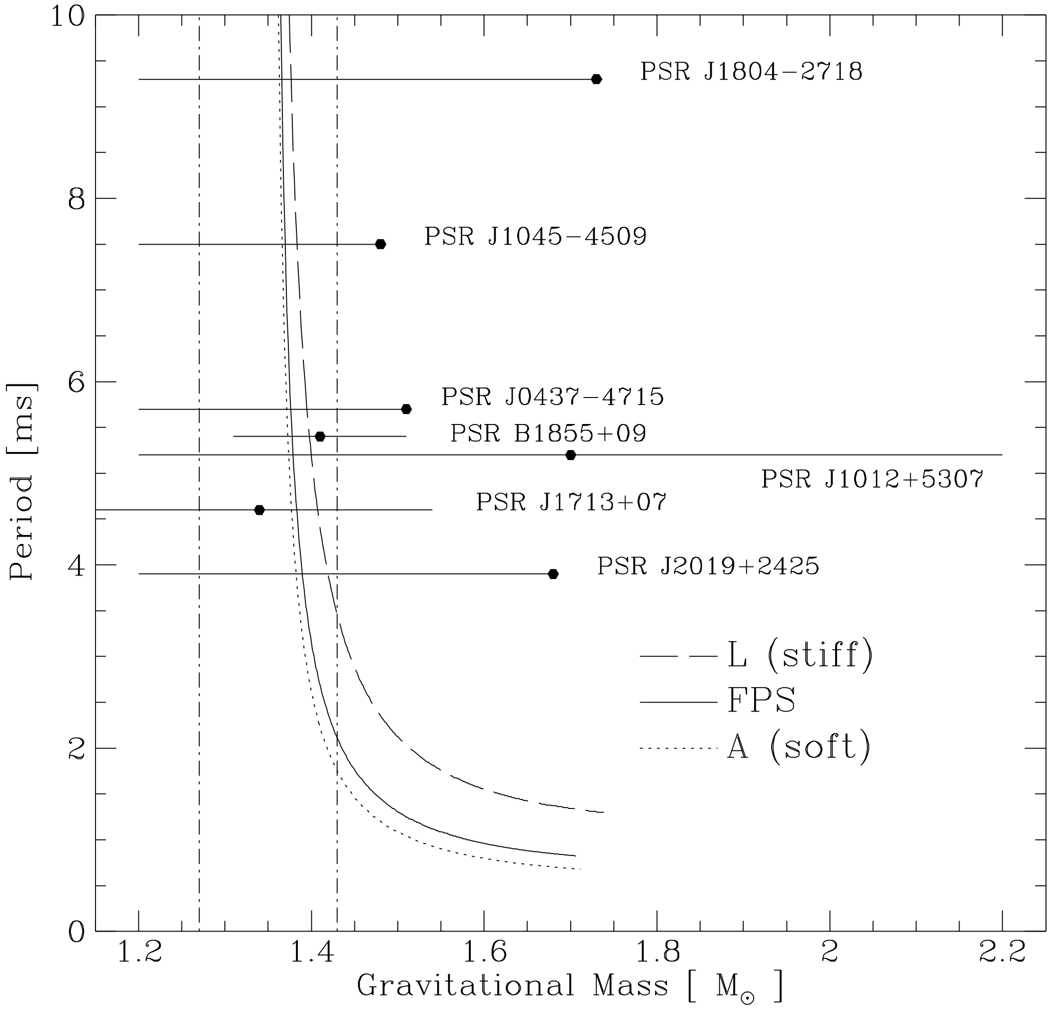

Figure 6.10: Available mass estimates for MSPs ($P < 10$ ms) compared with the evolutionary lines labeled as in Figure 6.7, but calculated for an initial gravitational mass of $M_{G,ini} = 1.35\ \mathrm{M}_\odot$. The error bars indicate central 68% confidence limits, while upper limits are one-sided 95% confidence limits. All the estimates are from Thorsett & Chakrabarty [25]. Vertical lines bind the 2σ-confidence region for the NSs masses ($M_G = 1.35 \pm 0.08$) derived by the same authors.

Therefore, in order to produce a fastly rotating NS, we are restricted to a quite narrow range of companion masses, (namely $1-2\ M_{\odot}$), and of initial orbital periods (namely $0.5-10$ days). For such binary systems, typical timescales for intense accretion are $\lesssim 10^8$ years. Once the mass–transfer ceases, the endpoint is often a circular binary containing a millisecond radio pulsar and a low–mass ($\sim 0.2-0.3 M_{\odot}$) white dwarf companion, the latter being the degenerate helium core of the sub-giant which transferred mass to the compact object [31]. This implies that the companion has lost $\gtrsim 1\ M_{\odot}$ during the evolution of the system. Even taking into account the case of an highly non-conservative mass transfer phase, it is difficult to believe that the NS in these systems has accreted less than $0.3\ M_{\odot}$.

6.7.2 *r-mode instability and emission of gravitational waves*

As discussed in section [3.4.2], non-axisymmetric instabilities in a NS should arise, if any, at rotational rates very close to the the mass shedding limit, thus not significantly affecting the spinup process modeled in Chapter 5.

A possible exception is represented by the so-called r-mode instabilities, discovered by Andersson in 1998 [32] and described in section [3.4.3]. For NSs with hot interiors, the viscosity of the nuclear matter may become inefficient in damping the growth of this kind of instabilities of the star and the related emission of gravitational waves [33] could limit the spin of a NS to a small fraction ($\sim 0.2-0.3$) of its mass shedding rotational rate. For young NSs with $T > 10^9$, this effect could spindown the star at $P > 10$ ms in a very short time (~ 1 yr), so accounting for the lack of young NSs spinning at period of few milliseconds [34].

Andersson, Kokkotas & Stergioulas [4] claimed that a similar mechanism could occur during the LMXB-phase, thus preventing the spinup of a NS below $\sim P^{obs}_{min}$. However, the difficulties in the calculations of the values of the shear and bulk viscosity for superfluid nuclear matter at $T \sim 10^7 - 10^{8.5}$ K (relevant for the accretion phase) leave a large uncertainty in the role of this instability in the recycling process.

6.7.3 *Crustal deformations and emission of gravitational waves*

In 1998 Bildsten suggested a further mechanism to inhibit the acceleration of accreting NS up to very short rotational periods [5]. Namely, he estimated the crustal deformations induced by accretion, assuming that the heating released in the process is transferred anisotropically in the crust due to the presence of a strong magnetic field. The thermal gradients turn into density gradients, developing a mass-quadrupole moment in a layer of the crust, which can excite emission of gravitational waves preventing the spin-up process to period shorter than ~ 3 ms. This model mostly addresses the period distribution of the NSs currently undergoing the X-ray emitting Roche Lobe Overflow phase and, indeed, it could explain the apparent clustering of the rotational periods of the NSs in the LMXBs ($\sim 2.5 \rightarrow\sim 4.0$ ms as inferred from the standard model for the kHz-QPOs detected in the X-ray power spectrum of these sources).

However, the existence of millisecond radio pulsars rotating at periods well below 2 ms might be a challenge for this picture, and the cited clustering of periods could naturally emerge also as a statistical outcome of the standard recycling scenario (once assumed a *stiff* Eos), as shown in section [6.1].

Bibliography

[1] **White, N.E., & Zhang, W. 1997**, *ApJL*, **490**, L87

[2] **Possenti, A., Colpi, M., D'Amico, N., Burderi, L. 1998**, *ApJL*, **497**, L97, (paper I)

[3] **van der Klijs, M. 1998**, in *The Many Faces of Neutron Stars*, eds. Alpar,Buccheri, van Paradijs, Dordrecht: Kluwer, 337

[4] **Andersson, N., Kokkotas, K.D., & Stergioulas, N. 1999**, *ApJ*, **516**, 307

[5] **Bildsten, L. 1998**, *ApJ*, **501**, L89

[6] **D'Amico, N., et al., 1998**, Proc. Symp. *Neutron Stars and Pulsars*, Tokyo, eds Shibazaki, Kawai, Shibata, Kifune, Universal Academy Press, 235

[7] **Wijnands & van der Klijs, M. 1998**, *Nature*, **394**, 344

[8] **Chakrabarty, D., & Morgan, E.H. 1998**, *Nature*, **394**, 345

[9] **Psaltis, D., & Chakrabarty, D. 1998**, *ApJ*, **521**, 332

[10] **Pringle, J.E. & Rees, M.J. 1972**, *A&A*, **21**, 1

[11] **Ghosh, P., & Lamb, F.K. 1991**, in Proc. NATO/ASI Ser **344**, *Neutron Stars: Theory and Observations*, ed. J.Ventura & D.Pines, 363

[12] **Bildsten, L. 1997**, *ApJS*, **113**, 367

[13] **Burderi, L., & King, A.R. 1998**, *ApJ*, **505**, L135

[14] **Miller, M.C., Lamb, F.K., & Psaltis, D. 1998**, *ApJ*, **508**, 791

[15] **Psaltis, D.,** *et al.* **1998**, *ApJ*, **501**, L95

[16] **Mendez, M., van der Klis, R., Wijnands, R., Ford, E.C., van Paradijs, J., Vaughan, B.A. 1998**, *ApJ*, **505**, 23

[17] **Stella, L., & Vietri, M. 1999**, *Phys. Rev. Lett.* **82**, 17

[18] **Li, X.D., & Wang, Z.R. 1999**, *ApJ*, **513**, 845

[19] **Cook, G.B., Shapiro, S.L., Teukolsky, S.A. 1994a**, *ApJ*, **423**, L117

[20] **Arnett, W.D., & Bowers, R.L. 1977**, *ApJS*, **33**, 415

[21] **Pandharipande, V. 1971**, *Nucl.Phys. A*, **174**, 671

[22] **Pandharipande, V., & Smith, R. 1975**, *Nucl.Phys. A*, **237**, 507

[23] **Lorenz, C.P., Ravenhall D.G. & Pethick, C.J. 1993**, *Phys.Rev.Lett.*, **70**, 379

[24] **Wang, Y. 1996**, *ApJ*, **465**, L111

[25] **Thorsett, S.E., Chakrabarty, D. 1999**, *ApJ*, **512**, 288

[26] **Casares, J., Charles, P., & Kuulkers, E. 1998**, *ApJL*, **493**, L39

[27] **Burderi, L., King, A. R., Wynn, G. A. 1996**, *ApJ*, **457**, 348

[28] **Webbink, R.F., Rappaport, S.A., & Savonije, G.J. 1983**, *ApJ*, **270**, 678

[29] **Kalogera, W., & Webbink, R.F. 1996**, *ApJ*, **458**, 301

[30] **Kalogera, W., & Webbink, R.F. 1998**, *ApJ*, **493**, 351

[31] **Burderi, L., King, A. R., Wynn, G. A. 1998**, *MNRAS*, in press

[32] **Andersson, N. 1998**, *ApJ*, in press, gr-qc/9706075

[33] **Stergioulas, N. 1998**, *Rotating Stars in Relativity, Living Reviews in Relativity*, gr-qc/9805012

[34] **Lindblom, L., Owen, B.J., Morsink, S.M. 1998**, to appear in *Phys.Rev.Lett.*, gr-qc/9803053

Conclusions

The calculation presented in the Chapters 2 $\rightarrow$ 6 have shown that:

(i) Detailed models for the decay of the crustal magnetic field, including also refined relativistic corrections, show the presence of a **tail in the period distribution of the synthetic NSs population at periods shorter than 1.558 ms.**

(ii) For a **mild-soft EoS**, and irrespective to the boundary condition at the crust-core interface for the magnetic field evolution, recycling in LMBs gives rise to **a NS distribution** which is **increasing towards shorter periods**, and a clear barrier is present at the minimum period for mass-shedding. For a *stiff EoS, the distribution is flatter.*

(iii) If NSs at the end of the persistent accretion in a LMB experience a phase of smooth decrease of the accretion rate (to mimic transient sources and/or quenching of accretion), the magnetospheric *propeller produces a depletion of fastly spinning NSs* but, at least for the soft EoS, it preserves a distribution that peaks at periods $\sim$ 1.5 ms.

(iv) The estimated fraction of *sub*-MSPs over the entire MSPs population varies between 0 to $\simeq 50\%$. The adopted EoS and the parameters for the recycling play an important role in determining those percentages. The *detection of such rapid rotating compact objects represents a challenge for the modern searches.*

(v) The models for the **decay of a crustal magnetic field predict** the existence of **spun up NSs with very low magnetic moment**: their period distribution is a neat signature for the physics at the crust–core interface.

(vi) The discovery of a submillisecond neutron star would imply a **lower limit for its gravitational mass of about 1.7** $M_\odot$.

(vii) Unless a physical mechanism limits the rotational period, there may exist a yet undetected population of ultra fastly spinning neutron stars with a gravitational mass significantly greater than the canonical value of **1**.4 $M_\odot$.

Moreover, as far as the observations, the discussion of the Appendixes A, B & C shows that:

(viii) Apart from a small volume in the solar neighbourhood, the **Galaxy has not been searched** with satisfactorily sensitivity **in the submillisecond period range**. The first experiments devoted at the detection of ultra-rapid pulsations are running right now.

(ix) Many factors could interplay **in making submillisecond period pulsations elusive**: large duty cycle of the pulses, strong interstellar scintillation, low luminosity and spare distribution of the sources.

Future developments

This *Thesis* addressed the study of the distribution in the $P - \mu$ diagram of neutron stars recycled in galactic field binaries. In Chapter 6, we concluded that, given typical parameters for the reacceleration process, there should be a non negligible number of objects spinning at periods less than the minimum observed so far. On the other hand, as shown in Appendix B, these ultra fast rotating sources are still elusive. So the next steps in this work will be:

- ↪ assembling the final results of all the current relevant surveys and searches, with the aim of estimating the effectiveness of the observational biases described in Appendix C;

- ↪ refining the population synthesis calculation accounting for the detailed orbital evolution of the binary during the last stages of the mass transfer. This is not a trivial task, due to many existing uncertainties, for example as regard the conservation of the mass and/or of the angular momentum during the binary evolution.

In addition it should be worthwhile deserving another *research line to the globular clusters*. The dynamics of the binaries included in these environments is far to be completely understood, but many peculiar mechanisms (capture, exchange interactions, etc...) seem very promising for the possibility of creating exotic binary systems and hence recycled objects with extreme features. In this respect, we are undertaking both a theoretical study and an observational one:

- ↪ a statistical calculation for investigating how the morphology and other physical and chemical features of a globular cluster can affect the probability it hosts peculiar binaries and perhaps rapidly rotating neutron stars;

- ↪ a deep ($S_0 \lesssim 70\mu$Jy) high frequency ($\nu = 1400$ MHz) radio survey of a large sample of globular clusters, with long integration times ($\gtrsim 2.5$ hr), unprecedently fast sampling rate ($\delta t \simeq 50 \div 80\mu$s), and very high spectral resolution ($\delta\nu = 500$ kHz). In principle it should be sensitive to unaccelerated periods $P_{65}(\mathrm{DM} = 26) = 0.25$ ms. Given the high fraction of binarity observed in the known sample of globular cluster millisecond pulsars, all the data will be processed taking into account also the possible effects due to the acceleration of the emitter during its orbit around a companion star.

Appendix A

The searches for short period pulsars

The search for pulsars rotating at very short periods requires a suitable experimental apparatus and great computational efforts. Here we shortly describe the main characteristics of this investigation (section [A.1]), and report on the results (section [A.2]) and on the limits (subsection [A.2.3]) of the completed experiments.

A.1 Survey sensitivity

A.1.1 *The basic formulae*

The relevant parameters of a pulsar search apparatus are the following:

- ν_{MHZ} = center observing radiofrequency in MHz
- $\Delta\nu_{MHZ}$ = observing bandwidth in MHz
- $\delta\nu_{MHZ}$ = width of a single radiofrequency channel in MHz
- T_{sky} = sky background temperature in K
- T_{sys} = system noise temperature in K
- G = antenna gain in K/Jy
- N_p = number of polarizations
- Δt = integration time of a single observation in seconds
- δt = sampling time in seconds
- β = parameter accounting for post-detection time constant and anti-aliasing filter; it is usually ~ 2

The radiometer equation provides us with a formula for estimating the *minimum mean flux density S_{min} of a detectable pulsar* (see *i.e* [1] or [2]):

$$S_{min} \simeq \frac{T_{sys} + T_{sky}}{G\sqrt{N_p \Delta t \Delta\nu_{MHZ}}} \cdot \sqrt{\frac{W_e}{P - W_e}} \tag{A.1}$$

The fundamental relation (A.1) implies that the effectiveness in detecting pulsars depends not only on the experimental apparatus, but also on the shape of the received signals; namely on the relation between the pulse period P and its effective width W_e (both expressed in seconds). The more $W_e \longrightarrow P$, the higher S_{min} and so the worst the sensitivity.

Observations show that the typical pulse profiles have a duty-cycle ($\sim W/P$) of $\lesssim 10\%$, where W is the intrinsic pulse width (expressed in seconds). Were the pulsar signal to propagate in vacuum, the effective width W_e would be close to the intrinsic pulse width and $W_e/(P - W_e) \lesssim 1/9$. For a suitable choice of the sampling time $\delta t \ll P$, the minimum flux S_{min} detectable by an assigned instrument would reach an asymptotic value almost independent on P.

The presence of the interstellar medium (ISM) deeply affects such an idealized scenario. It produces a broadening of the emitted signal, according to two main physical effects:

Dispersion

In travelling through the Galaxy, the radiowaves are dispersed in frequency by the ionized component of the ISM (mainly electrons). The dispersion causes a spread in the arrival times of the pulses at different radiofrequencies. In particular, lower frequencies lag the higher ones, according to [3]:

$$t_{low} - t_{high} = \frac{8\pi^3 e^2}{m_e c}\left(\frac{1}{\nu_{low}} - \frac{1}{\nu_{high}}\right) \quad DM \tag{A.2}$$

where m_e and e are the mass and the charge of the electron and DM is the so-called **Dispersion Measure**, defined as

$$DM = \int_0^d n_e dl \tag{A.3}$$

where n_e is the electron density which is encountered along the path joining the source (at distance d) and the receiver. Substituting ν_{low} and ν_{high} with the lower and upper frequencies of a channel of the detector, and introducing suitable units, from (A.2) we get the relation (A.4) accounting for the smearing of the pulse in a single channel

$$\delta t_{DM} = 8.3 \times 10^3 \ \ DM \ \frac{\delta\nu_{MHZ}}{\nu_{MHZ}^3} \tag{A.4}$$

where DM is expressed in pc/cm^3, δt_{DM} in seconds, $\delta\nu_{MHZ}$ and ν_{MHZ} in MHz.

Scattering

Local dishomogeneities of the electron density n_e in the ISM behave as center of scattering for the radiowaves emitted by a pulsar. Any detected pulse profile is the superposition of signals characterized by slightly different optical paths and therefore suffering a relative time shift. In particular the delay between a ray seen at a small angle θ and a direct ray (θ=0) from the same source is $t_\theta - t_0 \simeq d\theta^2/2c$ (d is the distance of the pulsar). Assuming a Gaussian distribution of density fluctuations in the ISM and the simple geometry of the thin screen model [4] one obtains the following scaling for the broadening of an impulsive signal:

$$\delta t_{scatt} \propto \frac{d^2}{\nu_{MHZ}^4} \tag{A.5}$$

Figure A.1 clearly displays how the scattering at different observing frequencies affects the shape of the integrated pulse. More refined models [5] introduce a Kolmogorov turbulence spectrum for describing the density irregularities in the ISM. Such models predict a scaling law similar to (A.5); in particular $\delta t_{scatt} \propto \nu_{MHZ}^{-4.4}$

The effective pulse width W_e eventually results by the contributions of the intrinsic width, of the propagation in the ISM and of the instrument time resolution:

$$W_e = \sqrt{W^2 + (\beta\delta t)^2 + (\delta t_{DM})^2 + (\delta t_{scatt})^2} \tag{A.6}$$

A.1.2 *The choice of the experimental parameters*

Due to economical, technical and computational limits, any pulsar search experiment can probe only a selected volume of the pulsar parameter space. In the following, we describe how the interplay between different experimental parameters, together with the choice of their values, lead to the search of different pulsar populations.

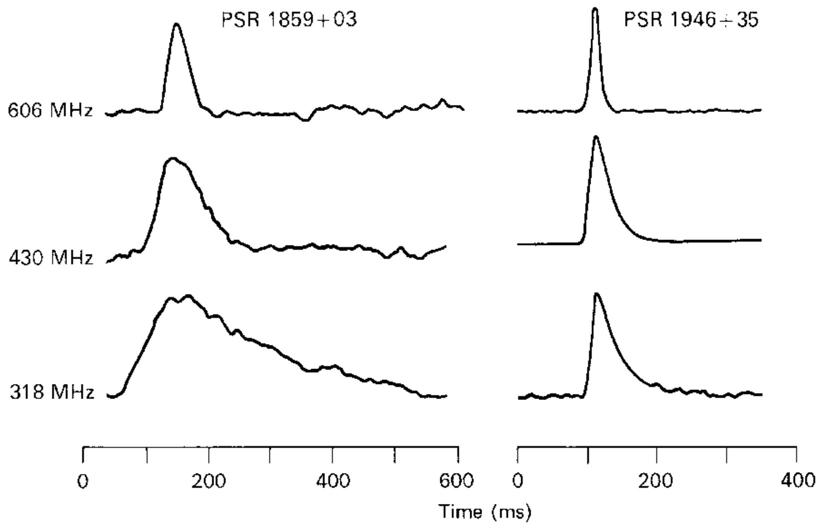

Figure A.1: The broadening of the integrated profile of two pulsars is a manifestation of the frequency dependent effects of the interstellar scattering [6].

Observing bandwidth vs Frequency resolution

Pulsars are wide-band radioemitters, whose signals have been detected in an interval of frequencies varying from $\sim$ 10 MHz up to tens of GHz. So, in order to improve the sensitivity S_{min} of a pulsar search experiment (see equation (A.1)), one would like to adopt a very large value of the total bandwidth $\Delta\nu_{MHZ}$ of the receivers. Were the signal collected only in one channel, the dispersion in the ISM would smear the pulse (see equation A.4 with $\delta\nu_{MHZ} = \Delta\nu_{MHZ}$) even for low values of DM. Therefore only a small galactic region around the Sun would be explored.

A good sensitivity for the detection of more distant pulsing sources can be recovered by splitting the signal into an adequate number of frequency channels, thus reducing $\delta\nu_{MHZ} = \Delta\nu_{MHZ}/(\text{number of channels})$. This can be achieved using hardware devices (*i.e.* filterbanks [2]) or suitable software [7], but of course, the greater the number of channels, the larger the amount of data and the longer the time for its processing.

Integration time vs Time resolution

The best options for minimizing S_{min} would be an extremely long integration time Δt and a very fast sampling rate $1/\delta t$, for selected values of the remaining parameters. The former permits the collection of a greater amount of energy from the source, the latter implies that the effective width W_e of the pulse increases of only a negligible amount. (see equation (A.6)). As for the case of the two parameters "observing bandwidth" and "frequency resolution", the current computational capabilities limit the choice of Δt and δt, whose ratio $\Delta t/\delta t$ gives the total number of samples which the algorithms for periodicity search must deal with.

OBSERVING FREQUENCY VS "COVERED AREA"

The selection of the best observing frequency must take into account various factors, namely:

i _ *pulsar spectral shape* $\longrightarrow \quad \propto \quad \nu^{-\alpha}$ with $\alpha \gtrsim 1.5 \div 2.0$;

ii _ *galactic background spectrum* $\longrightarrow \quad \propto \quad \nu^{-2.7}$;

iii _ *interstellar scattering* $\longrightarrow \quad \propto \quad \nu^{-4.4}$;

iv _ *interstellar dispersion* $\longrightarrow \quad \propto \quad \delta\nu\ \nu^{-3}$;

v _ *telescope beam* $\longrightarrow \quad \propto \quad \nu^{-1}$.

In summary [8], **high frequencies** (typical values $\sim$ 1400 MHz, $\lambda \sim$ 20 cm) are selected **for surveys in the galactic plane** or **for targeted searches of SuperNova Remnant cores**: they are much less sensitive to the interstellar scattering and need a moderate frequency resolution to remove dispersion. In particular *high frequency surveys* in the galactic plane [9] [10] are ideal *for searching young pulsars* ($\lesssim 10^6$ yr), whose typical progenitors are massive stars born in the disk. Moreover, due to their strong magnetic fields, young pulsars evolve rapidly implying a low number density and a large average distance, thus favouring high observing frequencies. The *searches for millisecond pulsars in globular clusters* at DM $\gtrsim$ 100 pc cm^{-3} are another suitable target for high frequency experiments [11] [12]. In these stellar systems the bulk of the observed pulsar population underwent a phase of reacceleration due to mass transfer in binaries; so we expect short rotational periods, whose detection requests the scattering smearing of the pulse to be kept negligible.

On the contrary, **low frequencies** ($\sim$ 400 MHz, $\lambda \sim$ 70 cm) are preferred **for all-sky surveys**: they take advantage from the wider telescope beams (thus reducing the needed number of pointings) and the steep pulsar spectra. Thus, *low frequency surveys* [2] represent the best option *for investigating the low-luminosity tail of the pulsars in the neighbourhood of the Sun*, where a population of relatively old objects prevails. Also the *globular clusters at high galactic latitude and small DM* (*i.e.* 47 Tucanae having $DM \sim 24.6$ pc cm^{-3} [12]) can be fruitfully probed using low frequencies observations. In these cases, the scattering is not significant and the dispersion effect can be overcome with a relatively cheap filterbank of moderate frequency resolution.

A.1.3 *Recipes for searching short period pulsars*

It is well known that no periodicity can be detected in a signal if its period is shorter than about twice the sampling time, that is only pulsations at period $P \gtrsim 2\delta t$ are observable. This rule is implicitly included in the second factor of the equation (A.1) ($\sqrt{W_e/(P-W_e)} \sim \sqrt{2\delta t/(P-2\delta t)} \longrightarrow \infty$ for $P \longrightarrow 2\delta t$), but this term accounts also for the effects of the propagation through the ISM. As a result, it favours the detection of sharp pulses and, conversely, determines a significant loss of sensitivity when the effective width W_e of the pulse exceeds about 50% of the pulsar period P. Moreover, most search algorithms are optimized for detection of narrow pulses: when W_e becomes comparable with P, the dedispersed signal shows a sinusoidal modulation, typical of the interferences; thus it is often rejected by automatized processing. Inspecting these problems, Burderi & D'Amico [13] argued that *highly dispersed pulses and periodicities in the period range* $2\ \delta t \rightarrow 4\ \delta t$ *are usually missed by data-processing strategies.*

From (A.4) and with little algebra, we get the maximum dispersion measure at which a pulsating source of period P (in seconds) could be detected (assuming negligible scattering):

$$\mathrm{DM}_{max}(\mathrm{pc\ cm^{-3}}) = 120 \cdot \frac{\nu_{GHZ}}{\delta\nu_{GHZ}} \cdot \nu_{GHZ}^2 \cdot \frac{\delta t_{DM}}{P} \cdot P \ \lesssim\ 30 \cdot \frac{\nu_{GHZ}}{\delta\nu_{GHZ}} \cdot \nu_{GHZ}^2 \cdot P \quad \text{(A.7)}$$

where $\delta t_{DM}/P \sim 1/4$ is the maximum fraction of the dispersion smearing in one channel still compatible with the detection of a pulsation of period P. Adopting a typical average value for the number density of electrons in the ISM ($n_e \simeq 0.03\ \ e/\mathrm{cm}^3$), we can translate (A.7) into an equation for the maximum distance

$$d_{max}(\mathrm{kpc}) \ \lesssim\ \frac{\nu_{GHZ}}{\delta\nu_{GHZ}} \cdot \nu_{GHZ}^2 \cdot P \qquad \text{(A.8)}$$

Thus, the shorter the period P, the smaller the maximum distance of a source whose dispersed signal can be reconstructed and detected. In particular for the case of the millisecond pulsars ($P \lesssim 0.01$ sec) the galactic volume searched would be extremely small, unless adopting a suitable frequency resolution $\nu_{GHZ}/\delta\nu_{GHZ}$.

In summary, the sensitivity equation (A.1) and the previous discussion imply that the detection of rapidly rotating pulsars calls for

- very short sampling time $\delta t \lesssim \frac{P}{4}$,
- very high frequency resolution $\frac{\nu_{GHZ}}{\delta\nu_{GHZ}} \propto \frac{1}{P}$ (for a fixed maximum distance)

What about the collected flux at the detector? Examining the relation (A.8), we note that a very narrow band $\delta\nu_{GHZ}$ should be preferred for probing a larger galactic volume. In principle, a value $\delta\nu_{GHZ} \longrightarrow 0$ would allow to search pulsating

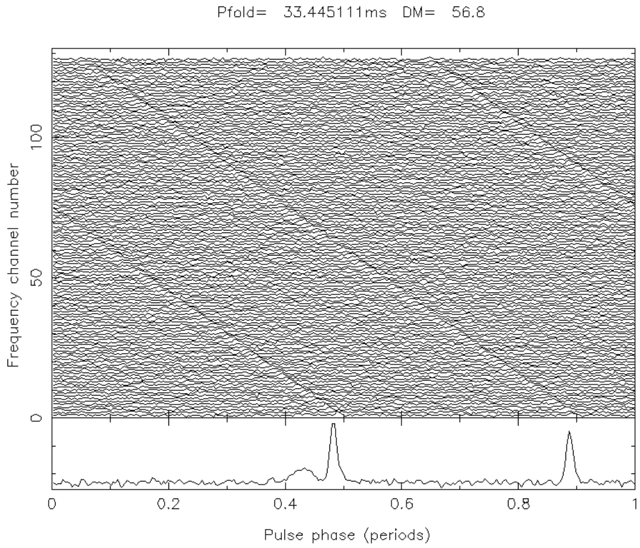

Figure A.2: Observation of the Crab pulsar made at the Northern Cross radiotelescope. The center observing frequency is $\nu_{MHZ} = 408$, the bandwidth is $\Delta\nu_{MHZ} = 4$ and the signal is split in 132 channels, each 132 kHz wide. The sampling time is 64 μs.

sources in the whole Galaxy (neglecting the problem of the scattering). On the other hand, narrowing the bandwidth reduces the sensitivity and $\delta\nu_{GHZ} \longrightarrow 0$ would lead to $S_{min} \longrightarrow \infty$ (see (A.1)), preventing the detection of whatsoever pulsating signal.

As described in section [A.1.2], the problem can be bypassed just introducing an array of N_{ch} adjacent channels (each with a passing bandwidth $\delta\nu_{GHZ}$) among which the total signal is spread. While preserving the possibility of recovering a dispersed pulse, such a strategy allows to collect a much larger energy from the pulsating signal, thus improving the sensitivity.

An example of this approach is shown in Figure A.2.

As $\delta\nu_{GHZ} = \Delta\nu_{GHZ}/N_{ch}$, one can rewrite equation (A.8) in term of the minimum number of needed channels:

$$N_{ch} \gtrsim 100 \frac{d_{max}(\mathrm{kpc})}{\nu_{GHZ}^3} \frac{\Delta\nu_{100MHZ}}{P_{-3}} \tag{A.9}$$

where P_{-3} is the period expressed in milliseconds and d_{max} is in kiloparsecs. Therefore to search pulsars rotating up to 1 millisecond in a region of 1 kpc around the Sun, one would need about a hundred frequency channels adopting a band of 100 MHz. The wider the bandwidth, the greater the number of requested channels. Of course, increase of N_{ch} deeply affects the technical and computational difficulties of an experiment, in turn determining a non-linear growth of the related economical costs.

In conclusion, the **main problem** in deciding the strategy to detect very short periodicities **involves the conflict between** the requirement of a **large bandwidth and integration time and** the need to sample with **high resolution** both the time and the frequency domain.

The adopted parameters of a search experiment have always been the result of a compromise: sometimes it was privileged the achievement of a better sensitivity at intermediate or slower periods; other experiments focused on the detection of ultra rapid pulsations, hence accepting a decrease of the sensitivity at slower pulsations.

A.2 Recent pulsar searches

In the following sections [A.2.1] and [A.2.2] we present a short summary of the parameters and the results of the most recent pulsar surveys, reporting also on the directed searches, such as those probing globular clusters, supernova remnants and other promising targets. In particular, we focus on the searches sensitive to short pulsation periods.

Table A.1: MSPs sensitive searches

Survey	ν (MHz)	$\delta\nu$ (MHz)	δ t (ms)	S_{min} (mJy)	Sky	N_{psr}	N_{new}	Ref.
JBank 2	1400	5	2	1	$\|b\| < 1^o$	62	40	[14]
					$-4^o < l < 105^o$			
GBank 3	400	0.25	2	3	$\delta \geq$ -18^o	87	20	[15]
Arecibo 2	430	0.06	0.3	3	$\|b\| < 10^o$	24	5	
					$40^o < l < 60^o$			[15]
Parkes 1	1500	5 [1]	1.2 [0.3]	1 [3]	$\|b\| < 4^o$	100	46	
					$[270^o < l < 40^o]$			[16]
Arecibo 3	430	0.08	0.5	1	$\|b\| < 8^o$	61	24	
					$40^o < l < 60^o$			[17]

Table A.1: Labels are as defined in section [A.1.1]. N_{psr} represents the total number of detected pulsars, whereas N_{new} refers to the new discoveries [8].

A.2.1 *Historical overview*

The on-line pulsar catalogue [18] provides a list of the major surveys carried out so far. In view of their targets and of their sensitivity in the short period range, they can be grouped into four classes [8]:

- ▷ *Pre-MSP discovery surveys.* They have been performed during the fifteen years interval between the discovery of the first pulsar (1967: [19]) and the discovery of the first millisecond pulsar (1982: [20]). They collected enough pulsars to allow the first population studies, but the adopted sampling times ($\delta t \simeq 10 \div 20$ ms) made them completely insensitive at short period pulsations.

- ▷ *MSP sensitive surveys.* They have been carried out after the discovery of the first MSP, with parameters allowing a moderate or very good sensitivity at periods $P \leq 100$ ms.

- ▷ *High latitude surveys.* The discovery (1991: [21]) of a millisecond pulsar in a binary system at high galactic latitude prompted several large scale experiments devoted to search fastly rotating objects in regions of the sky far from the galactic plane.

- ▷ *Directed searches.* The evolutionary scenarios for the neutron stars suggest various promising locations where a pulsar could be found. Hence, during the nineties, selected deep pointings with very long integration times Δt have been carried out. The principal targets have been the supernova remnants (likely birthplaces of the neutron stars), the OB runaway stars (possibly forming binary systems with a radioemitting neutron star [22]), the γ-ray unidentified sources (interpreted as young or middle-aged pulsars [23]) and the globular clusters (where pulsars have been detected since 1987 [24]).

A.2.2 *Experimental parameters & results*

Tables A.1, A.2 and A.3 displays the relevant features and results of the pulsar surveys belonging to the second and the third group of the classification introduced in section [A.2.1]. We report the survey name (in the first column), the sky coverage, the number N_{psr} of pulsars detected and the number N_{new} of the new discoveries. The limiting sensitivity is calculated for pulsars having long period P and low dispersion measure DM. The other parameters are defined as in section [A.1.1].

The high frequencies adopted by the *Parkes 1* and the *Jodrell Bank 2* surveys led to the detections of ten new pulsars with characteristic ages $\leq 10^5$ yrs, in particular PSR B1706-44 (a γ-ray pulsar too [25]) and PSR B1259-63 (forming

Table A.2: High latitude searches at Arecibo

ν (MHz)	$\delta\nu$ (MHz)	δ t (ms)	S_{min} (mJy)	N_{new}
403	0.25	0.25	0.5-0.9	55

$-2^o < \delta < 38^o$

Group	R.A. interval	Ref.
Princeton (Arecibo 4a)	21:30 – 01:00	[26]
Caltech	08:00 – 13:00	[27]
Penn-State (Arecibo 4e)	13:00 – 18:00	[28]

$00:00 < R.A. < 24:00$

Group	Declination interval	Ref.
Princeton	8x1^o interleaved strips	[29]
Caltech	8x1^o interleaved strips	[27]
Penn-State	8x1^o interleaved strips	[30]
Caltech-Berkeley (SHL-DHL-AC)	8x1^o interleaved strips	[31] [32]
STScI/NAIC	8x1^o interleaved strips	[33] [34]

Table A.2: Labels as described in the caption of Table A.1.

an eccentric binary system with a Be-star [35]). The narrow width $\delta\nu_{MHZ} \lesssim 0.1$ of the adopted spectral channels and the short sampling time ($\lesssim 0.5$ ms) allowed the *Arecibo* low frequency surveys (*2* and *3*) to discover two remarkable objects over a total of 29: the millisecond binary pulsars PSR B1855+09 ($P = 5.3$ ms, orbiting a $0.26 M_\odot$ companion [36]) and PSR B1957+20 (the second most rapidly rotating compact object, $P \lesssim 1.6$ ms, with a very low mass companion, $0.03 M_\odot$ [37]).

Taking advantage of the low dispersion, scattering and sky background temperature of the regions far away from the galactic plane, many different research

Table A.3: Other high latitude searches

Survey	ν (MHz)	$\delta\nu$ (MHz)	δ t (ms)	S_{min} (mJy)	Sky	N_{psr}	N_{new}	Ref.
Parkes 70	430	0.125	0.3	3	$\delta \le 0^o$	298	102	[2]
JBank 3	408	0.125	0.3	4	$\delta \ge 35^o$	-	1	[38]
GBank 4	378	0.078	0.25	8	$\delta \ge 0^o$	84	8	[39]

Table A.3: Labels as described in the caption of Table A.1.

groups performed extended surveys at high latitudes during the early nineties. The preferred frequencies spanned the interval 378 $\longrightarrow$ 430 MHz, the typical channels had a width of $\gtrsim$ 1kHz and the sampling rates clustered at about 0.3 ms. The searches carried out in *Arecibo* (see Table A.2) collected 15 new millisecond pulsars over a total of about 100 new pulsar discoveries. Other 18 millisecond pulsars were discovered by the two experiments *Parkes 70* and *Jodrell Bank 3* (Table A.3), performed using similar observational parameters in the Southern and Northern sky. Among the most interesting objects there were PSR 0437-4715 (a bright nearby millisecond pulsar [40], the first observed also in the X-rays), PSR J2051-0827 (an eclipsing millisecond pulsar [41]) and PSR J1012+5307 (a 5.3 ms pulsar in a 14.5 hours binary system [38]). In particular, the *Parkes 70* survey is representative of the complexity of a modern large scale experiment: it needed about $\lesssim$ 50000 beams for covering the sky and produced a huge amount of data (a few Terabytes) requiring a widespread network of workstations (ATNF in Sydney, Jodrell Bank in UK and Bologna in Italy) for their processing.

A summary of the directed pulsar searches is shown in Table A.4, where the experiments have been grouped according to their targets. In these cases the limiting flux density S_{min} represents a nominal value, due to the different sky temperatures in the directions of the various targets.

A.2.3 *Limits of the searches for short period PSRs*

In this section we focus on the selection effects affecting the performed searches for short period pulsars, showing that the range $P \lesssim 1$ ms has been poorly explored up to now.

Figures A.3a and A.3b depict the theoretical minimum flux densities S_{min} of the major completed experiments, computed using the equation (A.1) and the published parameters as reported in Tables A.5 and A.6.

In particular Figure A.3a refers to the searches in the galactic field and so the mean DM value ($\simeq$ 26 cm^{3}pc) of the known field millisecond pulsars has been adopted. On the contrary, the individual DM value of each globular cluster has been used in drawing Figure A.3b. An inspection of both plots shows *a general cut-off of the nominal sensitivity below $\simeq 1$ ms.*

In order to compare the different experiments, Burderi & D'Amico introduced the parameter P_{65}(DM) [13]. It represents the value of the period corresponding to a smearing of the pulsation equal to 65% of the pulse period, that is $W_e(\mathrm{DM}) = 0.65\ P_{65}(\mathrm{DM})$ (W_e(DM) being calculated according to (A.6)). Greater values of the relative smearing make the detection of the pulsation higly unlikely (see also the discussion of section [A.1.3]) and so P_{65}(DM) *is an estimate of the minimum period below which a given experiment becomes ineffective in discovering pulsars with dispersion measure larger than DM.* The eighth column of Tables A.5 and A.6 lists the values of this quantity for the relevant completed surveys, assuming the reference dispersion measures DM$_{ref}$ as for Figures A.3a and A.3b. In addition,

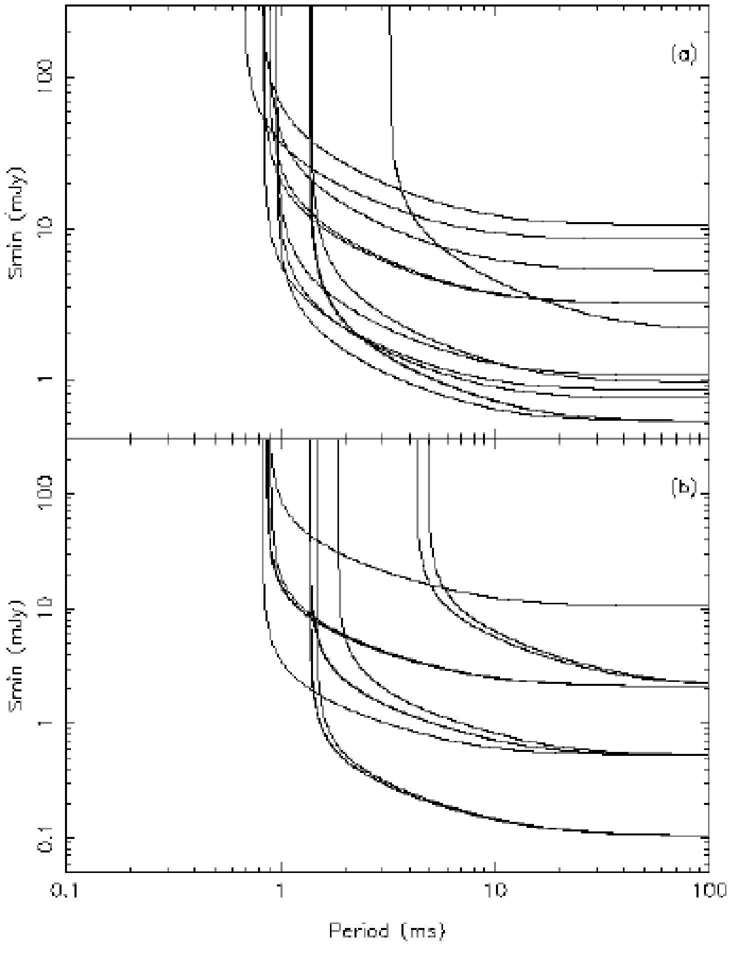

Figure A.3: The sensitivity curves for the galactic field surveys (*upper panel*) and for the globular clusters searches (*lower panel*) listed in Table A.5 and A.6. [13]

Table A.4: Directed Searches

Telescope	ν (MHz)	$\delta\nu$ (MHz)	δ t (ms)	S_{min} (mJy)	Number of targets	N_{new}	Refer.
			Supernova Remnants				
Arecibo	1400	0.3	0.5-1	0.2	18	0	[42]
	430	0.078	0.5-1	0.2			
Arecibo	1400	0.3	1	0.3	10	1	[43]
JBank	610	0.125	0.3	2	30	0	[44]
Parkes	1500	5	1.2	0.1	40	2	[45]
	610	0.25	1.2	0.5			
	430	0.125	1.2	2			
			OB stars				
VLA	1400	4	2.6	0.2	44	0	[46]
NRAO 43 m	575	0.078	1	1	40	1	[47]
	770	0.078	1	1			
Parkes	1500	0.078	1.2	0.1	50	2	[48]
			γ-ray unidentified sources				
Arecibo	430	0.25	0.2	0.2	680	1	[49]
NRAO 45 m	1390	0.078	0.25	0.5	27	0	[50]
	770	0.078	0.25	1			
	370	0.078	0.25	1			
			Globular Clusters				
Arecibo	430	0.078	0.5	0.02-0.5	5	14	[51] [52] [53] [54]
JBank	1400	1	0.3	0.3	1	1	[24]
	610	0.125	0.3	2	85	4	[44]
Parkes	430	0.125	0.3	0.3	70	10	[55]
	640	0.25	0.3	0.4	70	2	[56] [57]
	1500	1-5	0.3-1.2	0.1	70	3	[58] [59]

Table A.4: Labels as defined in section [A.1.1] and in Table A.1. In this case S_{min} is the nominal published value. Indeed, it varies from target to target accounting for different sky temperatures. Details are contained in the quoted references.

the minimum detectable mean flux density for long period sources S_0 appears in column seven. No globular cluster search (Table A.6) and only a couple among the galactic field surveys had actual sensitivity at periods $P_{65}(\mathrm{DM})$ shorter than 1.0 ms. Moreover the two experiments (*Parkes 1b* and *Molonglo*) nominally capable of exploring $P \leq 1.0$ ms were limited by an intrinsic sensitivity S_0 worse than the other ones. In summary, apart from a small volume in the solar neighbourhood (*i.e.* a distance of $\simeq 270$ pc corresponds to DM$=5$, and the $P_{65}(\mathrm{DM}=5)$ value of the *Arecibo CBHL* experiment goes down to $\simeq 0.6$ ms), so far **the Galaxy has not been searched with satisfactorily sensitivity in the ultra short period range**.

Table A.5: Values of P_{65} for the searches of the Galactic Field

Experiment name	δt (ms)	$\delta\nu$ (MHz)	ν (MHz)	Δt (s)	$\Delta\nu$ (MHz)	S_0 (mJy)	P_{65}(DM) (ms)	DM_{ref} (pc cm^{-3})	Ref.
Arecibo 4a	0.25	0.250	430	33	8	0.5	1.3	26	[26]
Arecibo 4e	0.25	0.250	430	33	8	0.5	1.3	26	[30]
Ar HL-1	0.5	0.080	430	40	10	0.5	1.6	26	[21]
Ar SHL	0.25	0.250	430	8	8	1.	1.3	26	[31]
Ar DHL	0.25	0.250	430	32	8	0.7	1.3	26	[31]
Ar AC	0.506	0.080	430	67	10	0.5	1.6	26	[31]
Ar CBHL	0.180	0.250	430	47	8	0.8	1.2	26	[60]
Arecibo 3	0.51	0.080	430	67	10	0.9	1.6	26	[17]
Arecibo 2	0.3	0.060	430	39	1	3	1.0	26	[15]
Parkes 70	0.3	0.125	430	157	32	3	1.1	26	[2]
Parkes 1	0.3	1.	1400	157	80	3	0.9	26	[16]
Parkes 1	1.2	5.	1400	157	320	1	3.7	26	[16]
JBank 3	0.3	0.125	430	320	8	4	1.1	26	[38]
JBank GP	2.0	5.	1400	157	40	2	6.2	26	[61]
Molonglo	0.25	0.125	843	120	4	8	0.8	26	[62]

Table A.5: The labels in the columns from 2 to 6 are as introduced in section [A.1.1], apart the units of δt, here expressed in ms. S_0 refers to the limiting sensitivity for long period pulsars (in mJy). $P_{65}(\mathrm{DM})$ is defined in the text and expressed in ms. Both this last two quantities are calculated adopting the reference DM value of column 9 [13].

Bibliography

[1] **Johnston, S.** *et al.* **1992**, *MNRAS*, **255**, 401

[2] **Manchester, R.N.** *et al.* **1996**, *MNRAS*, **279**, 1235

[3] **Ginzburg, V.L. 1970**, in *The propagation of the Electromagnetic Waves in Plasma*, New York, Pergamon

[4] **Cronyn, W.M. 1970**, *Science*, **168**, 1435

[5] **Lee, L.C. & Jokipii, J.R. 1975**, *ApJ*, **201**, 532

[6] **Manchester, R.N. & Taylor, J.H. 1977**, in *Pulsars*, Freeman & Co., San Francisco

[7] **Kouwenhoven, M.L.A. 2000**, in *Pulsar Astronomy - 2000 and beyond*, Proc. of IAU Colloquium 177, ASP Conf.Series, in press

Table A.6: Values of P_{65} for the searches of the Globular Clusters

Cluster name	δt (ms)	$\delta\nu$ (MHz)	ν (MHz)	Δt (s)	$\Delta\nu$ (MHz)	S_0 (mJy)	P_{65}(DM) (ms)	DM_{ref} (pc cm^{-3})	Ref.
47 Tucanae	0.3	0.250	650	2500	32	0.5	1.0	24.	[55]
M53	0.506	0.080	430	5400	10	0.1	1.6	24.	[51]
M5	0.506	0.312	1400	5400	40	0.5	1.6	29.5	[63]
M4	0.3	0.125	610	320	4	2.	1.0	62.9	[64]
M13	0.506	0.080	430	5400	10	0.1	1.6	30.	[65]
NGC 6342	0.3	0.125	610	320	4	2.	1.1	70	[66]
NGC 6440	0.3	0.25	650	2500	32	0.5	2.7	220	[57]
Terzan 5	1.2	5.	1400	2500	320	2	6.8	242	[67]
NGC 6539	1.2	5.	1400	2500	320	2	5.7	187	[52]
NGC 6624	0.3	0.125	610	320	4	2	1.1	87	[68]
M28	0.3	1.	1400	5000	32	10	1.1	120	[24]
NGC 6760	0.506	0.312	1400	4200	40	0.5	1.6	200	[69]
M15	0.506	0.080	430	5400	10	0.1	1.8	67	[54]

Table A.6: Labels and units are as in Table A.5. Here S_0 and $P_{65}(\mathrm{DM})$ are calculated using the dispersion measure DM_{ref} of each individual cluster observed, whose name is reported in the first column [13].

[8] **D'Amico, N. 1996**, *Cospar Symp. 1996*

[9] **Camilo, F.** *et al.* **2000**, in *Pulsar Astronomy - 2000 and beyond*, Proc. of IAU Colloquium 177, ASP Conf.Series, in press

[10] **D'Amico, N.** *et al.* **2000**, in *X-ray Astronomy '999*, special issue of Astrophysical Letters & Communications, in press

[11] **D'Amico, N., Possenti, A.** *et al.* **2000**, in preparation

[12] **Lyne, A.G., Camilo, F., Freire, P., Lorimer, D., Manchester, R.N. 2000**, in *Pulsar Astronomy - 2000 and beyond*, Proc. of IAU Colloquium 177, ASP Conf.Series, in press

[13] **Burderi, L., & D'Amico, N. 1997**, *ApJ*, **490**, 343

[14] **Clifton, T.R. & Lyne, A.G. 1986**, *Nature*, **320**, 43

[15] **Stokes, G.H., Segelstein, D.J., Taylor, J.H., Dewey, R.J. 1986**, *ApJ*, **311**, 694

[16] **Johnston, S., Lyne, A.G., Manchester, R.N., Kniffen, D.A., D'Amico, N., Lim, J., Ashworth, M. 1992**, *MNRAS*, **255**, 401

[17] **Nice, D.J., Fruchter, A.S., Taylor, J.H. 1995**, *ApJ*, **449**, 156

[18] **web page**, address: `http://pulsar.princeton.edu/pub/catalog`

[19] **Hewish, A., Bell, S.J., Pilkington, J.D.H., Scott, P.F., Collins, R.A. 1968**, *Nature*, **217**, 709

[20] **Backer, D.C., Kulkarni, S.R., Heiles, C., Davis, M.M., Goss, W.M. 1982**, *Nature*,**300**, 615

[21] **Wolszczan, A. 1991**, *Nature*, **350**, 688

[22] **Kaspi, V.M.** *el al.* **1994**, *ApJ*, **423**, L43

[23] **D'Amico, N. 1983**, *Space Sci Rev*, **36**, 195

[24] **Lyne, A.G., Brinkow, A., Middledtich, J., Kulkarni, S.R., Backer, D.C., Clifton, T.R. 1987**, *Nature*, **328**, 399

[25] **Thompson, D.J.** *et al.* **1992**, *Nature*, **359**, 615

[26] **Camilo, F., Nice, D., Taylor, J.H. 1996**, *ApJ* , **461**, 812

[27] **Ray, P.S.** *et al.* **1996**, *ApJ* , **470** , 1103

[28] **Foster, R.S., Wolszczan, A. & Caldwell, B.J. 1995**, in *Millisecond Pulsars: A Decade of Surprise*, eds. Fruchter, Tavani, Backer, ASP Conf.Ser., 24

[29] **Camilo, F., Nice, D., Shrauner, J.A., Taylor, J.H. 1996**, *ApJ*, **469** , 819

[30] **Foster, R.S., Caldwell, Wolszczan, A. & Anderson, S.B. 1995**, *ApJ*, **454** , 862

[31] **Ray, P.S.** *et al.* **1995**, *ApJ*, **443**, 265

[32] **Somer, A. 2000**, in *Pulsar Astronomy - 2000 and beyond*, Proc. of IAU Colloquium 177, ASP Conf.Series, in press

[33] **Fruchter, A. 1995**, unpublished work

[34] **Xilouris, K., Fruchter, A., Lorimer, D.R., Eder, J., Vasquez, A. 2000** in *Pulsar Astronomy - 2000 and beyond*, Proc. of IAU Colloquium 177, ASP Conf.Series, in press

[35] **Johnston, S.** *et al.* **1992**, *ApJ*, **387**, L37

[36] **Segelstein, D.J., Rawley, L.A., Stinebring D.R., Fruchter A.S., Taylor J.H. 1986**, *Nature*, **322**, 714

[37] **Fruchter, A.S., Stinebring, D.R. & Taylor, J.H. 1988**, *Nature*, **333**, 237

[38] **Nicastro L., Lyne, A.G., Lorimer, D.R., Harrison, P.A., Bailes, M., Skidmore, B.D. 1995**, *MNRAS*, **273**, L98

[39] **Sayer, R.W., Nice, D., Taylor, J.H. 1997**, *ApJ*, **474**

[40] **Johnston, S.** *et al.* **1993**, *Nature*, **361**, 613

[41] **Stappers, B.W.** *et al.* **1996**, *ApJ*, **465**, L119

[42] **Gorham, P.W.,** *et al.* **1996**, *ApJ* , **458**, 257

[43] **Wolszczan, A., Cordes, J.M., Dewey, R.J. 1991**, *ApJ*, **372**, L99

[44] **Biggs, J.D. & Lyne, A.G. 1996**, *MNRAS*

[45] **Kaspi, V.M.** *et al.* **1996**, *AJ*, **111**, 2028

[46] **Philp, C.J., Evans, C.R., Leonard, P.J.T., Frail, D.A. 1996**, *AJ*, **111**, 1220

[47] **Sayer, R.W., Nice, D. & Kaspi, V.M. 1996**, *ApJ*, **461**, 357

[48] **Kaspi, V.M., Manchester, R.N. & D'Amico 1996**, *ApJ*

[49] **Lundgren, S.C., Zepka A.F., Cordes J.M. 1995**, *ApJ*, **453**, 419

[50] **Nice, D. & Sayer, R.W. 1997**, *ApJ*, **476**

[51] **Kulkarni S.R., Anderson, S.B., Prince, T.A., Wolszczan, A. 1991**, *Nature*, **349**, 47

[52] **Deich, W.T.S** *et al.* **1993**, *ApJ*, **410**, L95

[53] **Anderson, S.B., Kulkarni S., Prince, T., Wolszczan A. 1990**, *IUA Circ.*, **5013**,

[54] **Anderson, S.B.** *et al.* **1990**, *Nature*, **300** , 615

[55] **Manchester R.N., Lyne, A.G., Robinson, C., D'Amico N., Bailes, M., Lim, J. 1991**, *Nature*, **352**, 219

[56] **Manchester R.N., Lyne, D'Amico N., Johnston, S., Lim, J., Kniffen, D.A. 1990**, *Nature*, **345**, 598

[57] **Lyne, A.G., Manchester, R.N. & D'Amico, N. 1996**, *ApJ*, **460**, L41

[58] **Lyne, A.G.** *et al.* **1990**, *IAU Circ.*, **4974**

[59] **D'Amico, N.** *et al.* **1993**, *MNRAS*, **260**, L7

[60] **Thorsett, S.E.** *et al.* **1993**, *ApJ*, **416**, 182

[61] **Clifton, T.R.** *et al.* **1991**, *MNRAS*, **254**, 177

[62] **D'Amico, N.** *el al.* **1988**, *MNRAS*, **234**, 437

[63] **Wolszczan, A., Anderson, S.B., Kulkarni, S.R., Prijce, T. 1989**, *IAU Circ.*, **4880**,

[64] **Lyne, A.G. 1988**, *Nature*, **332**, 45

[65] **Anderson, S.B.** *et al.* **1990**, *Bull.Am.Phyis.Soc.*, **22**, 1285

[66] **Biggs, J.D., Lyne, A.G. & Johnston, S. 1989**, in *X-ray Binaries*, proc. 23d ESLAB Symp. , eds ESA, Paris, 293

[67] **Lyne, A.G. 1990**, *Nature*, **347**, 650

[68] **Biggs, J.D.** *et al.* **1994**, *MNRAS*, **267**, 125

[69] **Middleditch, J.** *et al.* **1991**, *Bull.Am.Phys.Soc.*, **23**, 1348

Appendix B

Current surveys

The theoretical calculation of this *Thesis* was prompted by the results of the observations performed up to 1998. They have been discussed in Appendix A. During the development of this work, new experiments were undertaken and in this Appendix B we will report on their preliminary results (section [B.1]), in particular focusing on the surveys and the targeted searches aimed at the detection of ultra rapidly spinning objects (section [B.2]).

B.1 Major current surveys

The more important completed surveys had poor sensitivity in the ultra rapid pulsations range as a consequence of the adopted large total bandwidths and integration times (see Appendix A for an extended discussion). This choice allowed the experiments to span a wide space of parameters (either P and DM) of the pulsars population and paid back with the detection of a large sample of ordinary pulsars in addition to a few millisecond ones. Such an approach is still valid and followed, for instance, in the main pulsar survey currently running, the *PM-Survey*. It uses a bandwidth of 288 Mhz and an integration time of 35 minutes. The high frequency and low noise of the adopted receiver (1374 MHz, $T_{sys} \simeq 23$ K) allow to reduce the effect of the scattering, increasing the sensitivity to distant sources located in the galactic plane. Moreover the 13 beams available at the 64-m dish at Parkes compensate for the narrow field of view, permitting the galactic disk to be covered in a reasonable number of pointings ($\simeq 2670$) [1]. At about half of the experiment lifetime, the *PM-Survey* has detected $N_{psr} = 703$ pulsars with $N_{new} = 513$ new discoveries [2], among which 3 millisecond pulsars. In principle, the frequency resolution, the sampling time and the intrinsic sensitivity (see Table B.1 for a summary) would allow to detect pulsation periods down to 1 ms in a sphere of 1 kpc-radius around the Sun (see equation (A.8)), but only a tiny slice of this sphere is planned to be effectively scanned (that between the galactic latitudes $b = +5^o \longrightarrow b = -5^o$). Indeed, the survey was mainly designed for probing the inner regions of the Galaxy, where the bulk of the population of young pulsars should reside (8 new sources with $\tau_c \leq 10^5$ yrs have been already discovered), whereas the observation of new millisecond pulsars will be a by-product of the experiments. As far as the ultra short periods range is concerned, the P_{65}(DM) parameter for the *PM-Survey* is equal to $\simeq$ 0.9 ms; taking into account the extremely small galactic volume explored, it turns out that even this sophisticated experiment is not effective in searching periods $P \lesssim 1$ ms.

The *Swinburne Intermediate Latitude* survey [5] appears more promising. It uses the same instrumental apparatus as the *PM-Survey*, but adopting a faster sampling time and a shorter integration time (Table B.1 reports on the details of this experiment). Hence, it suffers a decrease of the sensitivity to the long period pulsars (about a factor 2.5 ÷ 3), but can more easily resolve short pulsations periods. It is probing the galactic regions just outside the strip investigated by the *PM-Survey*. When about 90% of the survey area has been observed and processed, 58 new pulsars have been confirmed, among which 8 recycled objects with periods in the typical range of the millisecond pulsars [6].

No object showing pulsations at periods below 1 ms has been detected so far. Since this has been the first medium-scale survey ($\simeq$ 12% of the entire sky covered) having good sensitivity at spin frequencies $\simeq$ 1000 Hz, its negative result deserves speculations with which we will deal in Appendix C.

Table B.1: Major current surveys

Experiment name	δt (ms)	$\delta\nu$ (MHz)	ν (MHz)	Δt (s)	$\Delta\nu$ (MHz)	S_0 (mJy)	P_{65}(DM) (ms)	DM_{ref} (pc cm^{-3})
PMSurvey	0.250	3.0	1374	2100	288	0.15	0.9	26
Swinburne	0.125	3.0	1374	265	288	0.45	0.55	26

Experiment name	Sky coverage	N_{psr}	N_{new}	Ref.
PMSurvey	$\lvert b\rvert \leq 5^o$	703	513	[1]
Swinburne	$5^o < \lvert b\rvert \leq 15^o$	??	58	[6]

Table B.1: Labels as described in the caption of Tables A.3 and A.5.

B.2 Current searches for ultra rapid pulsations

The very interesting physics involved in the existence (or not) of ultra fast rotating neutron stars prompted many researchers to design experiments entirely dedicated to the discovery of extremely rapid pulsations.

The only way to improve the sensibility in the *sub*-millisecond range, without exacerbating the data storage requirements and the processing times **is to sacrifice the total bandwidth and the integration time**. In fact, each individual observation produces

$$N_{ch}\ N_{sampl}\ \frac{N_{bit}}{8}\ \text{Bytes} = \frac{\Delta\nu_{MHZ}}{\delta\nu_{MHZ}}\ \frac{\Delta t}{\delta t}\ \frac{N_{bit}}{8}\ \text{Bytes} \tag{B.1}$$

of data, where N_{sampl} is the number of time-samples in the observation and N_{bit} is the number of bit used in digitising the signal. As an example, each beam in the *PMSurvey* allocates $\simeq 130$ MBy of data. To fulfill the requirement of decreasing δt (and in turn $\delta\nu_{MHZ}$, see equation (A.7)) one must accept a reduction in Δt and $\Delta\nu_{MHZ}$.

Which is the best observing frequency? For the typical ν_{GHZ}-values of the low and high frequency surveys, the equation (A.9) predicts the minimum number of spectral channels needed to successfully recover a signal of period P_{-3} (in ms) up to a distance of a 1 kpc:

$$N_{ch} \gtrsim \begin{cases} 1563\ d_{max}(\text{kpc})\ \frac{\Delta\nu_{100MHZ}}{P_{-3}} & \text{if } \nu_{GHZ} = 0.400 \\ 37\ d_{max}(\text{kpc})\ \frac{\Delta\nu_{100MHZ}}{P_{-3}} & \text{if } \nu_{GHZ} = 1.400 \end{cases} \tag{B.2}$$

accordingly, one would select a high frequency. But such a choice would imply the need of about 4 times more pointings to cover the sky isotropically, each with a duration about 8 times longer to reach the same minimum flux density of a low frequency survey (we assumed a typical pulsar spectral index of 1.6 [7]). In summary **the completion of an high frequency survey would take at least 30 times more time than a low frequency one** (other parameters unchanged). If the galactic distribution and luminosity of the *sub*-millisecond pulsars is similar to that of the millisecond pulsars, we expect to find them also at high latitudes and therefore low frequencies should be preferred (even more favoured by the low sky background temperature away from the galactic disk). Of course, the bandwidth must be strongly narrowed, that is in equation (B.2) one has to choose $\Delta\nu_{100MHZ} \ll 1$. We will deal with some experiments of this kind in the next sections [B.2.1] and [B.4.2].

When looking at a small number of selected and perhaps distant targets (*i.e.* the globular clusters [3] where the scattering becomes a threat) one could exploit the advantages of higher frequencies. We will report on an ongoing directed search at high frequencies in section [B.2.1].

Finally, high frequencies would be necessary if the population of *sub*-millisecond pulsars were extremely sparse, and hence the average distances of these sources were high. In this case one should perform a sensitive devoted deep search in the entire galactic plane: a task beyond the technical, economical and computational capabilities of the current instruments and research groups.

B.2.1 *Targeted searches*

Crawford, Kaspi and Bell [8] searched for rapid radio pulsations in 92 unidentified point-like sources extracted from the FIRST and the NVSS catalogs. Both these catalogs result from VLA radio surveys of the Northern Sky at 1400 MHz. In particular in the FIRST catalog, positions and fluxes of about 140000 discrete sources are complete to $\simeq 1$ mJy [9]. The NVSS catalog lists $\gtrsim 1.8 \times 10^6$ sources complete up to a flux of $\simeq 2.5$ mJy, and it preserves information about the polarization [10]. Crawford, Kaspi and Bell used the following selection criteria:

1. unidentified sources;
2. point-like sources;
3. bright sources with minimum flux density of 15 mJy @ 1.4 GHz;
4. linear polarization higher than 5%.

The choice of 5% as threshold linear polarization allows to exclude a strong contamination of extra galactic radio sources: the authors claim that $\simeq 90\%$ of the non-pulsar population should show a polarization degree smaller than the one chosen. Moreover, a statical comparison between the NVSS catalog and the on-line pulsar catalog [11] suggests that $\simeq 90\%$ of the identified pulsars in the NVSS survey possess a linear polarization higher than 5%. So at most a small fraction of objects could escape the selection.

The observation took place at the Lovell 76-m radiotelescope, using a center frequency of 610 MHz. In order to fulfill the requirements discussed in the previous section [B.2], the signal was split in 32 channels covering a narrow bandwidth of only 1 MHz. The enhancement of the time resolution (50μs) dictated a short integration time of 7 minutes. The time-series were digitized at $N_{bit} = 1$. Assuming a duty cycle of 5%, the intrinsic sensitivity S_0 of the experiment was $\simeq 8$ mJy @ 600 MHz. The parameter $P_{65}(\mathrm{DM} = 26)$, calculated for the reference DM as in Table A.5, is equal to 0.16 ms. Since all but two of the targets reside at galactic latitudes greater than 5^o, the role of the interstellar scattering is negligible and the dispersion measures should not exceed $\simeq 100$ cm^{-3}pc. At these DMs, the experiment could detect pulsations from the selected sources at any period $P \gtrsim 0.25$ ms (with the assumption of a spectral index $\alpha = 1.6$ [7]).

The search ended up with **no detection of pulsations from the 92 target sources**.

In the same framework of the Crawford, Kaspi & Bell's experiment, Han, Manchester, Lyne & Qiao has recently undertaken a targeted search at the Parkes 64-m radiotelescope, adopting 1.4 GHz as observing frequency [12]. In this case, the selection criteria applied to the sources of the NVSS catalog are:

1. unresolved sources between declination $-40^o \longrightarrow +20^o$;
2. linear polarization L/S higher than 25%;
3. uncertainty in L/S smaller than 10%

resulting in 246 sources, comprising 5 known pulsars. The higher selected frequency allows (see equation (B.2)) for an extremely wider bandwidth of 256 MHz, divided into 512 0.5-MHz wide spectral channels. The sampling and the integration time are 80 μs and 320 seconds and the parameter $P_{65}(\mathrm{DM} = 26)$ is 0.26 ms. The experiment is still running at January 2000.

B.2.2 *The Bologna survey*

Since 1997, a large scale survey with high sensitivity in the very short period range is in progress at the Northern Cross radiotelescope, near Bologna, in Italy [2]. It uses the East-West arm of the antenna, taking advantage from the very large collecting area available (600 $\times$ 30 meters), implying a remarkable gain $G = 2.5$ K/Jy. The temperature of the system varies in the interval $T_{sys} = 100 \div 120$ K. It is a transit instrument operating at 408 MHz with a narrow beam in Right Ascension (4 arcmin) and a much larger beam in declination (2^o). An electrical phase shift between different subsections of the antenna allows to track a source for more than 1 min ($\gtrsim$ 4 times the nominal transit time: 16 sec). The other parameters of the experiment are summarized in Table B.2.

Table B.2: Bologna sub-millisecond pulsar search parameters

Experiment name	δt (ms)	$\delta\nu$ (MHz)	ν (MHz)	Δt (s)	$\Delta\nu$ (MHz)	S_0 (mJy)	P_{65}(DM) (ms)	DM_{ref} (pc cm^{-3})
Bologna	0.064	0.032	408	67	4	9	0.25	26

Table B.2: Labels as described in the caption of Table A.5.

The low operational frequency suggests a narrow bandwidth of 4 MHz (see equation (B.2)), limited also by the local pattern of the interferences. After being preamplified, downconverted (at 30 MHz) and suitably amplified, the RF signal enters a filterbank where it is split in 128 spectral channels, each 32 kHz wide. Then it is detected and digitized at $N_{bit} = 1$. A very fast sampling time $\delta t = 64\mu$s

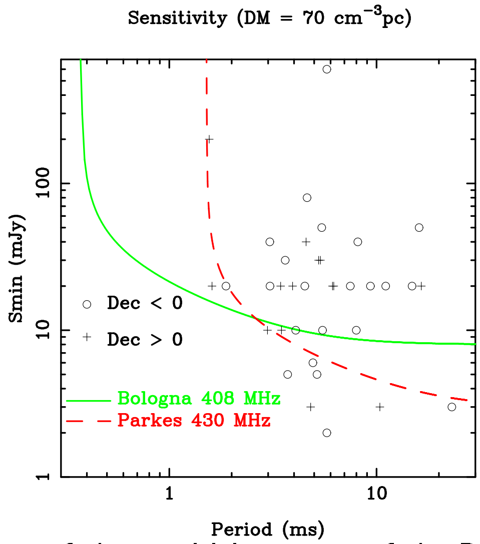

Figure B.1: Comparison of the sensitivity curves of the Bologna experiment and of the *Parkes 70 cm* survey [13]. A reference DM=70cm^{-3}pc is used. The *crosses* indicate the known millisecond pulsars in the Northern sky, whereas the *empty dots* those in the Southern sky [14].

allows an high time resolution, whilst the integration time is limited at $\Delta t = 67$ sec by the short transit time of the targets at their culmination. Due to the small values of both $\Delta\nu_{MHZ}$ and Δt, **the intrinsic sensitivity of the experiment in not very high** (nominally $\simeq 9$ mJy), **but it is capable of exploring the whole Northern sky in a period range unprobed by other completed or current surveys**.

No new normal pulsars are expected to be found by the Bologna survey, but, nevertheless, its nominal sensitivity allows to detect most of the known visible millisecond pulsars and to search sources pulsating well below 1 ms; in particular, the $P_{65}(\mathrm{DM} = 26)$ parameter is equal to 0.25 ms. At DM $= 100$ cm^{-3}pc, the P_{65} parameters is still 0.62 ms, in principle permitting to recover dispersed *sub*-millisecond signals coming from sources located inside a sphere with centre in the Sun and radius of at least 2.5 kpc.

The entire survey calls for the observation of about 150000 beams, each producing $128 \times 10^6 \times 1/8 \ = \ $16MBytes of data, for a total amount of 2.4 TBytes. The data processing takes place on-line.

The raw data of each pointing are stored in a dedicated hardware device, namely a 16 MBytes buffer memory addressed at 1 bit (instead of the usual 8 bit) in order to improve the i/o operations. Hereafter, a 80486-cpu based PC orchestrates the work of a cluster of CPUs (Alpha 288 and i860). A block diagram of this part of the data processing is reported in Figure B.2. Each of the CPUs

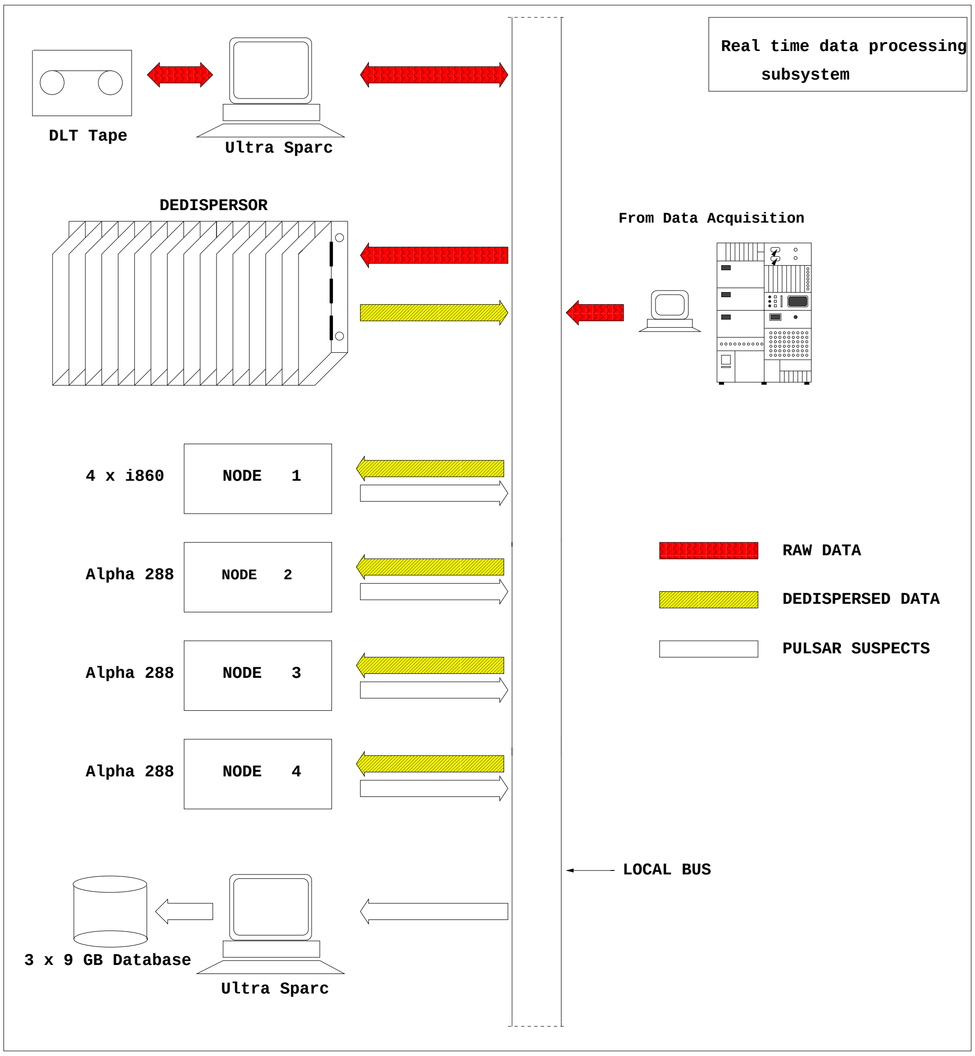

Figure B.2: Block diagram of the pipeline for data processing subsystem of the Bologna experiment [2].

performs the following jobs:

1. assignation of the i-th value of dispersion DM_i to the *DEDISPERSOR unit*; this device performs the dedispersion of the raw data [in less than 200 ms for 16 MBytes of data] and returns the i-th time series to the CPU;

2. calculation of the power spectrum of the i-th time series related to the frequency interval $[0;\mathrm{N}_q]$, where N_q is the Nyquist frequency;

3. normalization of the i-th power spectrum;

4. calculation and normalization of the i-th power spectra related to 4 upper harmonics, namely the power spectra related to the frequency ranges $[0;\mathrm{N}_q/2]$, $[0;\mathrm{N}_q/4]$, $[0;\mathrm{N}_q/8]$, $[0;\mathrm{N}_q/16]$;

5. search of the 32 most significant peaks in each of the 5 i-th power spectra;

6. storing of the used DM_i and of the related 32×5 period values and 32×5 power spectrum normalized amplitudes in a RAM Buffer available on the local bus.

The next stage of the experiment pipeline is run by an external Sun workstation. It collects all the results stored for the 160 explored values of DM (spanning the interval $0 \longrightarrow 100\mathrm{cm}^{-3}\mathrm{pc}$). Then it sorts the $32 \times 5 \times 160$ periods according to their amplitudes in the power spectrum and eventually selects the first 6. The last step includes a fine-tuning of the best values of period and dispersion measure for each of the six selected suspects: this task is performed by a suitable code which dedisperds the raw data using eight spectral sub-bands and folds them in many sub-intervals in time. The period P, the dispersion measure DM and the signal-to-noise S/N for the six suspects are displayed using a graphic interface, which summarizes other useful information for inspecting the quality of the observation and the reliability of the suspect. The only duty for the researcher is to scan, one by one, these automatically selected suspects and classify them as interferences or interesting candidates for a reobservation.

At January 2000, about a 2/5 of the planned pointings have been completed, covering 80% of the declination strips between -4^o and 42^o (about 29% of the whole celestial sphere). 35 known long period pulsars have been detected, and 5 millisecond pulsars. In particular the original millisecond pulsar, PSR 1939+2134, is usually detected in survey mode at signal-to-noise $S/N \simeq 90 \div 100$. One new millisecond pulsar, namely PSR 0030+0454, has been discovered [2] (it was independently detected also by Somer *el al.* during an *Arecibo drift scan search* at 430 MHz [15]). It has a period of 4.86 ms and a dispersion measure of 4.3 $\mathrm{cm}^{-3}\mathrm{pc}$, thus being the second closer millisecond pulsar (at $\simeq 230$ pc using the ISM-model of Taylor & Cordes [16]).

As far as faster rotating objects, up to now **no pulsar with period less than 1.56 ms has been detected**.

Bibliography

[1] **Camilo, F.** *et al.* **2000**, in *Pulsar Astronomy - 2000 and beyond*, Proc. of IAU Colloquium 177, ASP Conf.Series, in press

[2] **D'Amico, N. 2000**, in *Pulsar Astronomy - 2000 and beyond*, Proc. of IAU Colloquium 177, ASP Conf.Series, in press

[3] **D'Amico, N., Possenti, A.** *et al.* **2000**, in preparation

[4] **Backer, D.C., Kulkarni, S.R., Heiles, C., Davis, M.M., Goss, W.M. 1982**, *Nature*,**300**, 615

[5] **Edwards, R.T.** *el al.* **2000**, *ApJ*, in preparation

[6] **Edwards, R.T. 2000**, *Pulsar Astronomy - 2000 and beyond*, Proc. of IAU Colloquium 177, ASP Conf.Series, in press

[7] **Lorimer, D., Yates, J., Lyne, A. & Gould, D. 1995**, *MNRAS*, **273**, 411

[8] **Crawford, F., Kaspi, V.M. & Bell, J.F. 2000**, in *Pulsar Astronomy - 2000 and beyond*, Proc. of IAU Colloquium 177, ASP Conf.Series, in press

[9] **White, R.L., Becker, R.H., Helfand, D.J. & Gregg, M.D. 1997**, *ApJ*, **475**, 479

[10] **Condon, J.J.** *et al.* **1998**, *AJ*, **115**, 1693

[11] **Han, J.L. & Tian, W.W 1999**, *A&A*, **136**, 571

[12] **Han, J.L., Manchester, R.N, Lyne, A.G. & Qiao, G.J. 2000**, private communication

[13] **Manchester, R.N.** *et al.* **1996**, *MNRAS*, **279**, 1235

[14] **D'Amico, N. 1996**, in *Nato-ASI workshop*, Lipari, Italy

[15] **Somer, A. 2000**, in *Pulsar Astronomy - 2000 and beyond*, Proc. of IAU Colloquium 177, ASP Conf.Series, in press

[16] **Taylor, J.H. & Cordes, J.M. 1993**, *ApJ*, **411**, 674

Appendix C

Difficulties in observing *sub*-millisecond pulsars

The *Swinburne intermediate latitude* survey [1], and the Crawford, Kaspi and Bell's targeted search [2] showed no evidence for ultra fast pulsating radio sources. Up to now similar outcomes emerge from the on-going Bologna survey [3] and from the directed searches in progress at Parkes [4]. Indeed, only a part of the sky and an even smaller fraction of the volume of the Galaxy has been probed with enough sensitivity to submillisecond pulsations; therefore a **complete analysis is not yet possibile**.

In Chapter 3 we noticed that no known physical law prevents a neutron star to rotate at a period $P < 1.56$ ms. In Chapter 6 we calculated that highly spinning neutron stars could be generated within quite general parameters for the recycling and they should have a lifetime as long as to appear as a significant fraction of the population of the millisecond pulsars. Of course, choosing all the most unfavourable parameters, the formation of a *sub*-millisecond pulsar could become extremely rare.

In the following we will introduce some preliminary options suggested by the current observations and possibly suggestive for the next experiments.

- ⋈ ***Sub*-millisecond pulsations have a large duty cycle**. The opening angle of the emission beam of the millisecond pulsars is usually narrower than predicted by the simple scaling law $\propto P^{-1/2}$ observed in the normal pulsar population [5], but nevertheless the millisecond pulsars show intrinsic pulse widths W which are, in average, wider than in the normal pulsar population and can reach $\simeq 1/4$ of the period. Should the duty cycle increase even more for faster spin rates, the signal could assume the typical shape of the interferences and the canonical detection algorithms could fail. In principle this problem affects all the completed and the on-going experiments; however the directed searches could get rid of it more easily than the surveys, due to the possibility of a more extended visual inspection of the suspects selected by the automatic processing. The extremely narrow beam of the first discovered and fastest millisecond pulsar, PSR J1939+2134, [6], could be either a counterexample for the widening trend of the pulse profiles or a clue for an existing bias in the observations: among a substantial population of wide profile fast rotating pulsars we could be able to detect only the very few having extremely narrow pulses.

⋈ *Sub*-**millisecond pulsars are dim**. The millisecond pulsars seem to be slightly less luminous and less efficient radio emitters compared to the normal pulsars [5]. In particular the luminosity distribution goes down abruptly towards higher intensities, therefore lacking the tail of the brightest and thus easiest to detect objects. If this trend would enhance at shorter periods, an experiment like that of Crawford, Kaspi & Bell should investigate a sample chosen in the low luminosity tail of the unidentified NVSS sources, instead of pointing more luminous objects. In addition, the observations suggest that the isolated MSPs are less luminous than the millisecond pulsars in binaries. But the latter (especially if in tight systems) could be more difficult to discover, due to the smearing of the folded signal produced by the orbital acceleration in the binary system. Thus, short integration times (as that used in the Bologna survey, see Table B.2) would be preferred, but it would need also an intrinsic sensitivity much better than that of the Northern Cross apparatus.

⋈ *Sub*-**millisecond signals suffer strong scintillation**. Since the known millisecond pulsars are a nearby low dispersed population, scintillation due to the inhomogeneities in the interstellar medium can affect their observability. In effect, unless using a wide bandwidth, the flux density of the millisecond pulsars can be highly variable over typical timescales [7] $\tau_s \simeq 10 \div 15$ min at 400 MHz ($\tau_s \propto \nu^{1.2}$). In principle this effect should half the detection efficiency for sources having mean flux density comparable with the sensitivity limit S_{min} of the experiment; in fact in average the scintillation decreases the signal of an half of the pulsars (pushing their apparent flux density below the detection threshold) while enhancing the luminosity of the other half of the objects. Crawford, Kaspi & Bell [2] remarked that the flux densities at 1.4 GHz of their selected sources are still compatible with the hypothesis that they are *sub*-millisecond pulsars at a distance smaller than 2 kpc, just where the scintillation could deeply affect the observations. However, taking into account the previous considerations, it seems unlikely [2] that the scintillation could have suppressed the detection of pulsations in the whole set of 92 sources investigated by these authors. Similar statements will be applied to the results of the on-going directed search at Parkes by Han, Manchester, Lyne & Qiao [4] and to the current large scale surveys. In summary, if an experiment scans the sky only one time (like is the usual case for the surveys), the scintillation should not decrease the number of the detected *sub*-millisecond spinning objects more than a factor ~ 2, at the nominal sensitivity limits of the instrumental apparatus.

In principle the brightening effect produced by the scintillation could even favour the detection of sources whose mean flux density is below S_{min}: but this statement must be cautiously investigated. A very dim pulsar (under the nominal detection threshold) could be visible just only at its scintillation peak and then never seen during many other pointings (when scintillation is less effective in brightening the signal). This could severely limit the success of confirmations for a survey as the one in *Bologna*, whose integration time (67 sec) could make a source detectable just at the short maximum of scintillation. The high frequency *Swinburne Intermediate Latitude Survey* could be also slightly affected by this confirmation problem, despite the use of a much larger bandwidth.

⋈ ***Sub*-millisecond pulsar are very rare**. No one can predict the absolute number or the distribution of the *sub*-millisecond pulsar population: if they were significantly sparser than the millisecond pulsars, their mean distance could be much higher than that of the millisecond sources and one should look for candidates along the galactic plane instead than at high or intermediate galactic latitudes. We have already discussed in section [B.2] why such a search cannot be nowadays undertaken.

Bibliography

[1] **Edwards, R.T.** *el al.* **2000**, *ApJ*, in preparation

[2] **Crawford, F., Kaspi, V.M. & Bell, J.F. 2000**, in *Pulsar Astronomy - 2000 and beyond*, Proc. of IAU Colloquium 177, ASP Conf.Series, in press

[3] **D'Amico, N.** *et al.* **2000**, *ApJ*, in preparation

[4] **Han, J.L., Manchester, R.N, Lyne, A.G. & Qiao, G.J. 2000**, private communication

[5] **Kramer M.** *et al.* **1998**, *ApJ*, **501**, 270

[6] **Backer, D.C., Kulkarni, S.R., Heiles, C., Davis, M.M., Goss, W.M. 1982**, *Nature*,**300**, 615

[7] **Johnston, S., Nicastro, L,, Koribalski, B. 1998**, *MNRAS*, **297**, 108

Related papers

The following refereed papers and proceedings have been written during the development of this *Thesis*:

Possenti, A., Colpi, M., D'Amico, N., Burderi, L. 1998, *ApJL*, **497**, L97

Colpi, M., Possenti, A., D'Amico, N. & Burderi, L. 1998, Proc. Symp. *Neutron Stars and Pulsars*, Tokyo, Japan, Ed. N. Shibazaki, N. Kawai, S. Shibata, T. Kifune, Universal Academy Press, Inc., 39

D'Amico, N., Pronti, S., Grueff, G., Burderi, L., Possenti, A., Fauci, F. & Maccaferri, A. 1998, Proc. Symp. *Neutron Stars and Pulsars*, Tokyo, Japan, Ed. N. Shibazaki, N. Kawai, S. Shibata, T. Kifune, Universal Academy Press, Inc., 235

Burderi, L., Possenti, A., Colpi, M., Di Salvo, T., D'Amico, N. 1999, *ApJ*, **519**, 285

Possenti, A., Colpi, M., Geppert, U., Burderi, L., D'Amico, N. 1999, *ApJS*, **125**, 463

Possenti, A., Colpi, M., Geppert, U., Burderi, L., D'Amico, N. 2000, in *Pulsar Astronomy - 2000 and beyond*, Proc. of IAU Colloquium 177, ASP Conf.Series, in press

Acknowledgments

My *Ph.D. Thesis* would not be ever ended up unless for

Nichi D'Amico
Monica Colpi
Gavril Grueff
Tiziana Di Salvo
Luciano Burderi
Ulrich Geppert
Aldo Treves
the Ph.Ds and the staff of the Astronomy Department in Bologna
the persons of the Astronomical Observatory of Bologna
the members of the KfA at the Physics Department in Milano
the people of the PM-Survey at Parkes

My *Ph.D. Thesis* would not have been so a funny job unless for

Vincenzo Vagnoni
Leda Zanet
Marino Lagalla
Maurice Toscano
Sarah Tommasetti
Chiara Pardi
Agnese Mandrino
Anna Maria Lombardi
Antonella Testa
Davide Cenadelli
Luca Reduzzi

My *Ph.D. Thesis* would not be at all unless for

mamma
papà

Det bästa som vi äga,
det kan man inte giva,
det kan man inte säga
och inte heller skriva.

[*Karin Boye*]

The best things we have,
none of us can give,
none of us can tell
or write as well.